

EC PROJECT
EVG1-CT-2002-00069



REL. I. E. F.



RELIable Information on Earthquake Faulting

Large Earthquake Faulting and Implications for the Seismic
Hazard Assessment in Europe:
The Izmit-Duzce earthquake sequence of August-November 1999
(Turkey, Mw 7.4, 7.1)

ANNUAL REPORT

Third year

January 2006

WP 6: Integration of multidisciplinary data for seismic hazard assessment

WP 9: Multidisciplinary seismic hazard assessment

Prepared by K. Atakan and M. B. Sørensen

PARTNER 6: Department of Earth Science, University of Bergen



List of Contents

1. Introduction
2. Project participation from UiB and external collaboration
3. WP6: Integration of multidisciplinary data for Seismic Hazard Assessment
 - 3.1. Earthquake catalogues
 - 3.2. Ground motion scaling and attenuation
 - 3.3. Local site effects: A detailed study in Ataköy
4. WP9: Multidisciplinary Seismic Hazard Assessment (SHA)
 - 4.1. Ground motion simulations based on earthquake scenarios
 - 4.2. Sensitivity analysis for the ground motion simulations
 - 4.3. Seismic risk: Damage estimation based on ground motion simulations for the RRS
5. WP10: Dissemination of the results
 - 5.1. Dissemination of the results (publications, conference presentations etc.)

Acknowledgements

References

- Appendix I The historical earthquake catalogue for the Marmara Region (by N.N. Ambraseys)
- Appendix II Akinci A., Malagnini, L., Herrmann, R.B., Gok, R. and Sørensen, M.B. (in press). Ground Motion Scaling in the Marmara Region. *Geophys. J. Int.*, Jan.2006.
- Appendix III Sørensen, M.B., Oprsal, I., Bonnefoy-Claudet, S., Atakan, K., Mai, P.M., Pulido, N., and Yalciner, C. (in review). Local site effects in Ataköy, Istanbul, Turkey, due to a future large earthquake in the Marmara Sea. *Geophys. J. Int.*, Jan. 2006.

1. Introduction

Department of Earth Science (Institutt for geovitenskap), University of Bergen (hereafter called UiB), is mainly responsible of the work packages WP6 (Integration of multidisciplinary datasets to seismic hazard assessment) and WP9 (Multidisciplinary seismic hazard assessment). In accordance with the project proposal, during the period December 2004 to November 2005, activities of the UiB were concentrated around these two work packages. Main focus has been on finalizing the work on site effect estimation and the sensitivity analysis on ground motion simulations for various scenario earthquakes. In addition, UiB's contribution to workpackage WP10 is given separately. Activities that are associated with the UiB contributions in 2005 are described in the following sections.

2. Project participation from UiB and external collaboration

Main participants from the UiB are: Kuvvet Atakan and Mathilde Bøttger Sørensen. In addition, Odd Johann Berland and Knut Andre Furuløkken have been involved partially in software maintenance. Close collaboration with scientists from other institutions is also continued with Nelson Pulido (NIED, Japan) in ground motion simulations, as well as with several colleagues at the Kandilli Observatory and Earthquake Research Institute of Bogazici University, Istanbul (Mustafa Erdik, Atilla Ansal, Eser Durukal, Gülüm Birgören, Oguz Özel and Yasin Fahjan) in different aspects of ground motion simulations. Several contributions from these individuals as well as the collaborations with participants from the RELIEF Partner institutions provide the basis for the present report.

3. WP6: Integration of multidisciplinary data for seismic hazard assessment

3.1. Earthquake catalogues

As part of WP06, a revised catalogue of earthquakes including both historical and instrumental events is prepared. The sub-contractor N. Ambraseys, IC London, has delivered a revised historical catalogue of earthquakes in the Marmara region. This catalogue covers the period 1500-2000 and is complementary to the catalogue covering the instrumental period (1900 – present) compiled earlier (see RELIEF-UiB annual report for year 1). Here only the list of earthquakes ($M \geq 7.0$) from this

revised catalogue is given in Appendix I. The complete report is given in RELIEF Deliverable 25 – Appendix I.

3.2. Ground motion scaling and attenuation

As described in the RELIEF 1st annual report from UiB in 2003, a separate study was initiated in collaboration between UiB and INGV, Rome, on establishing an attenuation relationship for the Marmara Sea region. This was conducted using ground motion scaling on small earthquakes (see RELIEF deliverable no. 18 for details). By the end of 2003, the technique had been applied to a small dataset, which was insufficient to constrain the regressions, and it was concluded that more data are needed in order to obtain reliable results. Such a new dataset became available, and work is now completed and a paper is being published on this topic (See Appendix II; Akinci et al., in press).

3.3. Local site effects: A detailed study in Ataköy

During 2004, intensive work was conducted on estimating local site effects for a pilot area in Istanbul. As described in the previous annual reports from UiB, microtremor data were collected at 30 sites in Ataköy, western Istanbul, and have been analyzed in detail (Figure 3.3.1). The results were combined with a number of other approaches to estimate the site effects. The work on site effect estimation was divided into four separate studies; microtremor analysis, 1D-modeling, weak motion analysis on records from temporary broadband stations and 3D-modeling. These studies are now finalized and most of the results are presented in a paper which is submitted for publication (See Appendix III; Sørensen et al., in review). For details the reader is referred to the UiB-Annual Report for 2004.

Results obtained in this study indicate significant site effects associated with the unconsolidated sediments within the alluvial deposits which may have significant consequences in the Ataköy area in case of future large earthquakes in the Marmara Sea (Figure 3.3.2). However, other factors such as construction practices, density of building stock and proximity to alluvial sediments will play an important role, especially when taking into account the frequency variations of the site effects. These results are naturally valid only for Ataköy area, however the similarity of the geological formations in the neighboring Bakirköy and Zeytinburnu districts provide an insight to possible consequences in these highly populated areas in Istanbul.

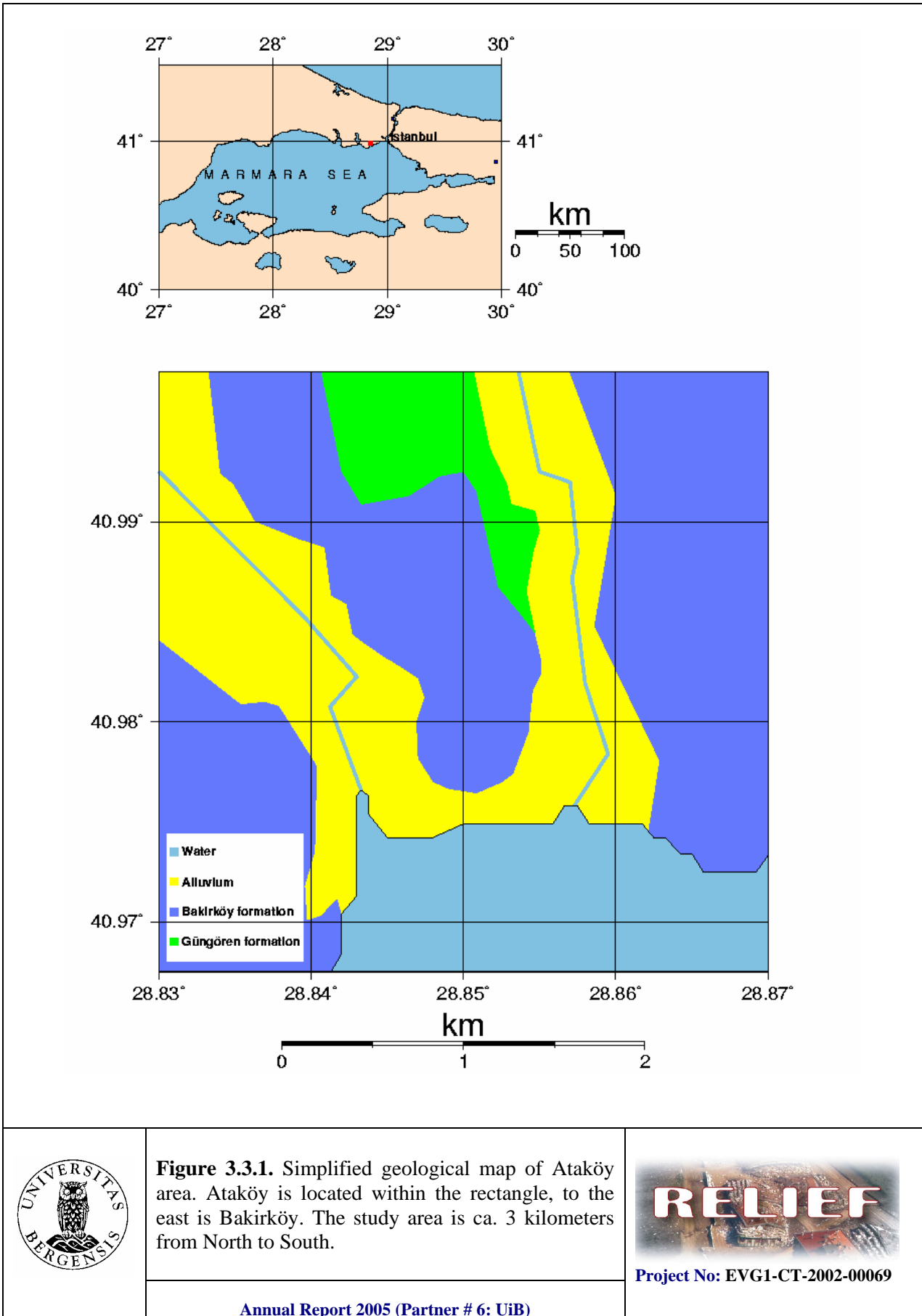


Figure 3.3.1. Simplified geological map of Ataköy area. Ataköy is located within the rectangle, to the east is Bakirköy. The study area is ca. 3 kilometers from North to South.



Project No: EVG1-CT-2002-00069

Annual Report 2005 (Partner # 6: UiB)

Spectral-acceleration amplification in Istanbul area

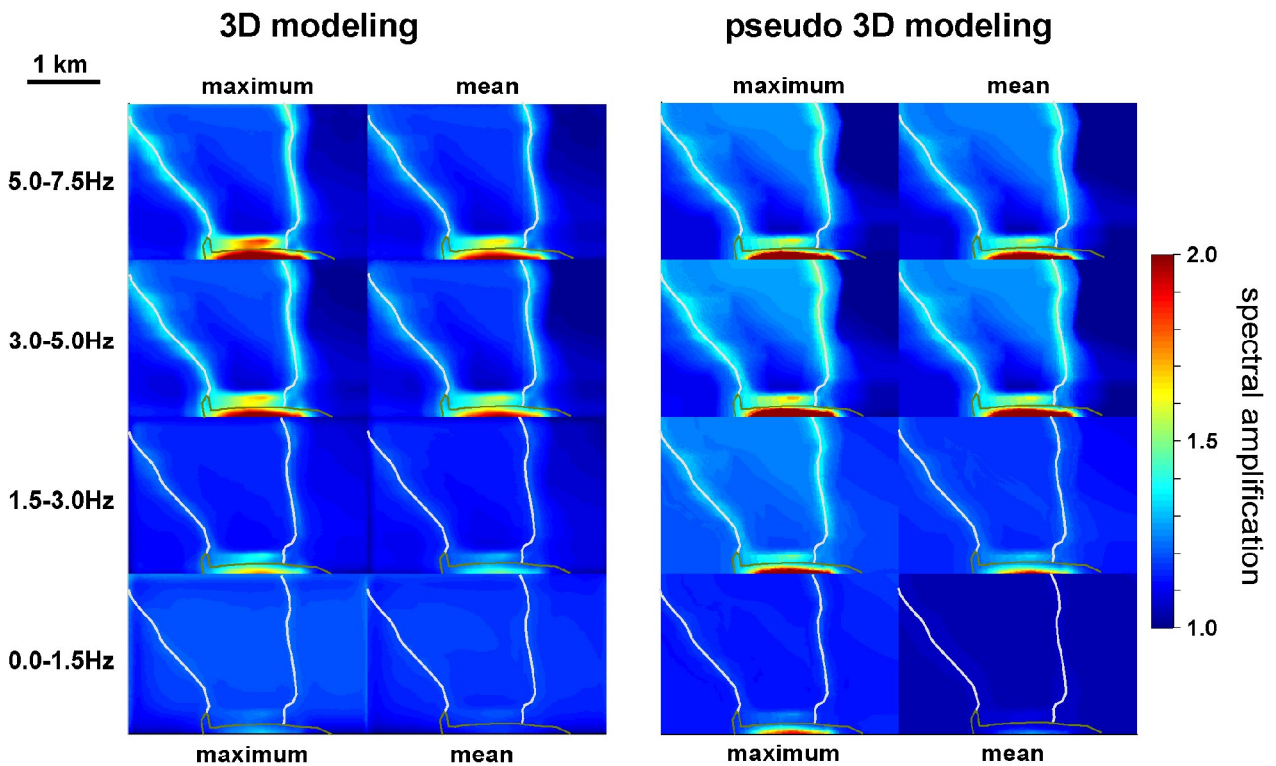


Figure 3.3.2. The spectral amplifications in the Ataköy area, shown in various frequency bands. The color code indicates the absolute level amplification factors. The maps shown on the left are the results from the 3D-modeling. The maps on the right are from pseudo 3D-modeling.



Project No: EVG1-CT-2002-00069

Annual Report 2005 (Partner # 6: UiB)

4. WP9: Multidisciplinary Seismic Hazard Assessment

In terms of the seismic hazard assessment of the region, we have followed three separate approaches. These are: (i) Probabilistic seismic hazard assessment (PSHA) based on “poissonian” earthquake occurrence, (ii) Time-dependant seismic hazard assessment (TDSHA) based on “renewal” models and (iii) Ground motion simulations based on earthquake scenarios. These approaches were all described in some detail in the previous UiB-Annual Reports for 2003 and 2004. In 2005 substantial work has been done with regard to the parameter sensitivity of the ground motion simulations, and this is described in detail below.

Seismic hazard in Istanbul has previously been estimated using probabilistic methods (Atakan et al., 2002; Erdik et al., 2004). Within the framework of the RELIEF project new set of probabilistic seismic hazard computations were conducted and the results were presented in previous UiB-Annual Reports. During the project it became clear that the earthquake posed by the NAFZ within the Marmara Sea requires other techniques to be employed. Recently, increased knowledge on the NAF within the Marmara Sea allowed other methods to be applied. In the present project, the bedrock ground motions due to a finite extent scenario earthquake source ($M=7.5$) in the Marmara Sea were modeled using a hybrid broadband simulation technique, and hereby gave a first insight to the complexity of ground shaking to be expected in a future earthquake (Pulido et al., 2004). Such results are important due to their direct engineering implications. However, the uncertainties related to defining the source parameters of a scenario earthquake influence the scenario result in a way which is until now not well resolved. Our main objective was therefore to study and quantify the effect of these uncertainties.

4.1. Ground Motion Simulations based on earthquake scenarios

One of the approaches followed in seismic hazard assessment for the Marmara Sea region is the ground motion simulations for a $M = 7.5$ scenario earthquake in the Marmara Sea. This work is done in collaboration with Nelson Pulido from Earthquake Disaster Mitigation Research Center EDM, NIED, Kobe, Japan, Martin Mai from ETH, Zurich, Switzerland, Anibal Ojeda from INGEOMINAS, Colombia, and a number of people from the Kandilli Observatory and Earthquake Research Institute (KOERI), Istanbul, Turkey.

We follow the approach of Pulido et al. (2004), using a hybrid method for modeling the ground motion. This method combines deterministic calculations for low frequencies (0.1-1Hz) with a semi-stochastic procedure for high frequencies (1-10 Hz). The basic idea of the method is to determine the ground motion radiated from a finite-fault source model composed of asperities, embedded in a flat-layered velocity structure. Each asperity is divided into a number of subfaults, which are considered point sources, and the ground motion at a given receiver is then calculated by summing the contributions from each sub-fault. For the low frequencies, the sub-fault contributions are calculated using discrete wave number theory (Bouchon, 1981), and summation is performed assuming a given rupture velocity. At high frequencies the ground motions are calculated using the stochastic method of Boore (1983) and the empirical Green's function (EGF) method of Irikura (1986). A frequency dependent radiation pattern is introduced in the calculations (Pulido et al., 2004), which provides a smooth transition from a theoretical double couple radiation pattern at $f=1$ Hz to an isotropic radiation pattern at $f=3$ Hz.

The first part of the work was conducted by Pulido et al. (2004) who performed calculations on a regular grid, testing the effects of different rupture initiation points. In this study a $M = 7.5$ scenario earthquake was used rupturing a 150 km long segment of the North Anatolian Fault (NAF) in the Marmara Sea. The study showed that the worst-case earthquake scenario for the city of Istanbul is the case where the rupture initiates in the western end of the rupturing fault. This causes substantial forward directivity towards the city. With this scenario the predicted ground accelerations reach up to 0.5g in the southern part of Istanbul.

4.2. Sensitivity analysis for the ground motion simulations

Ground motions were simulated due to a number of earthquake scenarios in the Marmara Sea and were compared to a 'standard' scenario. The various scenarios (16 in total) are defined by changing the critical source parameters one at a time to see their influence on the simulated ground motions. This provides important information about the sensitivity of the ground motions to the different source parameters and reveals the most critical ones. In the standard scenario, the location and dimensions of the rupturing fault are defined by considering the local tectonics and seismicity. We assume a combined rupture of the Central Marmara Fault (CMF) and North Boundary Fault (NBF) segments of the North Anatolian Fault (NAF). A total fault length of 130 km is used, which is confined to the area between the 1999 Izmit rupture to the east and the 1912 Ganos rupture to the west. We assume a fault width of 20 km in agreement with the depth of the seismogenic zone as

indicated by the depth distribution of seismicity (Gurbuz et al., 2000). The fault plane solution used is the one of Pulido et al. (2004) with pure right-lateral strike-slip faulting along the CMF and an oblique-normal mechanism along the NBF. Two asperities are defined covering 22% of the fault plane following the empirical results of Somerville et al. (1999). These are located near the intersection of the CMF and NBF segments. This area has previously been suggested to be a seismic gap (Gurbuz et al., 2000), characterized by its low seismicity. The seismic moment released by the scenario earthquake is 2.0×10^{20} Nm, which is an average value of the seismic moments estimated by different authors for the 1999 Izmit earthquake (Pulido et al., 2004). The velocity model used in the modelling is the one used for routine location of earthquakes in the region. For the cut-off frequency f_{\max} we use a value of 10 Hz, which is also the upper frequency limit of the calculations. In practice this implies that the high-frequency decay of the ground motion is mainly controlled by attenuation.

For the standard scenario, the rupture initiation point is located in the westernmost edge of asperity 1 (Figure 4.2.1). This is believed to be a likely location since the boarder regions of asperities represent significant changes in physical properties of the fault and thereby zones of weakness. Based on seismic moment, fault area and asperity area, the stress drop is calculated based on the relations of Das and Kostrov (1986) and Brune (1970) following Pulido et al. (2004). Rupture velocity and rise time are taken from Pulido et al. (2004) for the standard scenario. The regional attenuation is defined in terms of Q. For the standard scenario we have used the “Low Attenuation Model” of Pulido et al. (2004). The source parameters of the standard scenario are summarized in Table 1. It should be noted that the standard scenario is considered as a conservative approximation.

Table 1: Source parameters for the standard scenario.

| | |
|-----------------------------------|------------------------------|
| Seismic moment | $M_0 = 2.0 \cdot 10^{20}$ Nm |
| Strike / Dip / Slip - CMF segment | 81.5 / 90 / 180 |
| Strike / Dip / Slip - NBF segment | 110 / 90 / -135 |
| Average stress drop | 5.0 MPa |
| Asperity stress drop | 10 MPa |
| Rise time | 3.0 s |
| Rupture velocity | 3.0 km/s |
| f_{\max} | 10 Hz |
| Q | $100 \cdot f^{1.5}$ |

Based on the standard scenario, we have changed source parameters one by one in order to test the effect on the ground motions. The parameters, which have been tested, are: low-frequency attenuation (Q_p and Q_s), high-frequency attenuation (Q), rise time, rupture velocity, rupture initiation point and stress drop. In total, 16 “test scenarios” have been investigated, which are listed in Table 2.

Table 2: Scenarios which have been tested in this study.

Only the parameter differing from the standard scenario is listed.

| | |
|-------------|---|
| Scenario 1a | Q_p and Q_s reduced by 50% |
| Scenario 1b | $Q = 100 \cdot f^{0.5}$ |
| Scenario 1c | $Q = 250 \cdot f^{1.5}$ |
| Scenario 1d | $Q = 250 \cdot f^{0.5}$ |
| Scenario 2a | Rise time 2.0 s |
| Scenario 2b | Rise time 4.0 s |
| Scenario 2c | Rise time random 3 ± 1 s |
| Scenario 3a | Rupture velocity 2.5 km/s |
| Scenario 3b | Rupture velocity 3.5 km/s |
| Scenario 3c | Rupture velocity random 3 ± 0.5 km/s |
| Scenario 4a | Rupture initiation at western edge of CMF |
| Scenario 4b | Rupture initiation at intersection of CMF and NBF |
| Scenario 4c | Rupture initiation at eastern edge of asperity 2 |
| Scenario 4d | Rupture initiation at eastern edge of NBF |
| Scenario 5a | Stress drop asperity: 5 MPa, background: 2.5 Mpa |
| Scenario 5b | Stress drop asperity: 15 MPa, background: 7.5 Mpa |

The results of this study reveal that the simulated ground motions are influenced by a number of critical parameters which depend on the details of the source complexity in the input model. The uncertainties associated with the parameter sensitivity should be taken into account when the results are going to be implemented. In any case the results gave an insight to the upper and lower limits of the expected ground motions.

The most important parameters for the ground motion modeling, in terms of ground shaking levels, are the location of the rupture initiation, rupture velocity, rise time, stress drop and the high-frequency attenuation relation used for the studied region. Examples of these are given in Figures (4.2.1 – 4.2.4). However, the impact of these parameters in frequency bands of engineering interest

varies. From an engineering perspective, the most important parameters are the stress drop and the location of rupture initiation.

The following conclusions can be drawn from the ground motion simulation results:

- The effect of a M=7.5 earthquake in the Marmara Sea on the city of Istanbul is found significant with the largest ground motions occurring in the southern and southeastern parts of the city. Here, ground accelerations at the level of 0.5g can be expected at bedrock level.
- The level and distribution of modeled ground motions is highly dependent on the input source parameters and these uncertainties should be taken into account when applying modeling results.
- Rise time, rupture velocity, rupture initiation point and stress drop are the most significant parameters in terms of variations in ground shaking levels. However these parameters have their effect in different frequency bands and the engineering significance therefore varies.
- From an engineering point of view, stress drop and rupture initiation point are the most important input parameters since these have a large effect on the ground shaking level at frequencies of engineering interest.
- Even though the level, distribution and spectral values of the ground motions differ significantly, the response spectra are consistent, revealing the strength of ground motion modeling in estimating a realistic hazard for Istanbul and hence in risk mitigation efforts despite the large uncertainties involved.

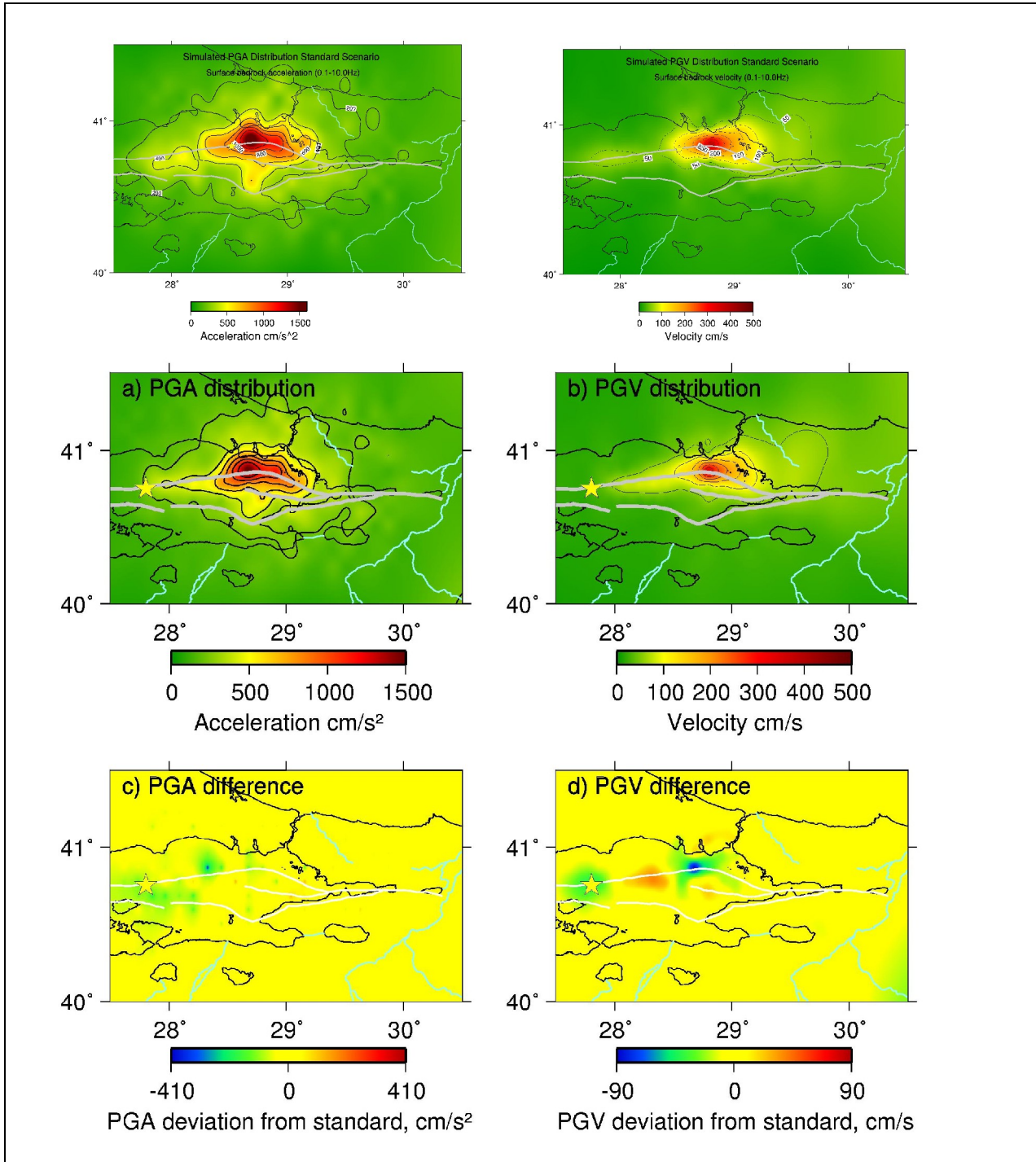


Figure 4.2.1. (a) Comparison of the ground motion simulation results associated with the rupture initiation point. Note that rupture initiation point is moved to the western end of the CMF (Scenario 4a). In the standard scenario it is in the western corner of the asperity 1. The top two plots are for the standard scenario. The middle two plots are for the test scenario and the two plots in the bottom are for the difference between the standard and the test scenario.



Project No: EVG1-CT-2002-00069

Annual Report 2005 (Partner # 6: UiB)

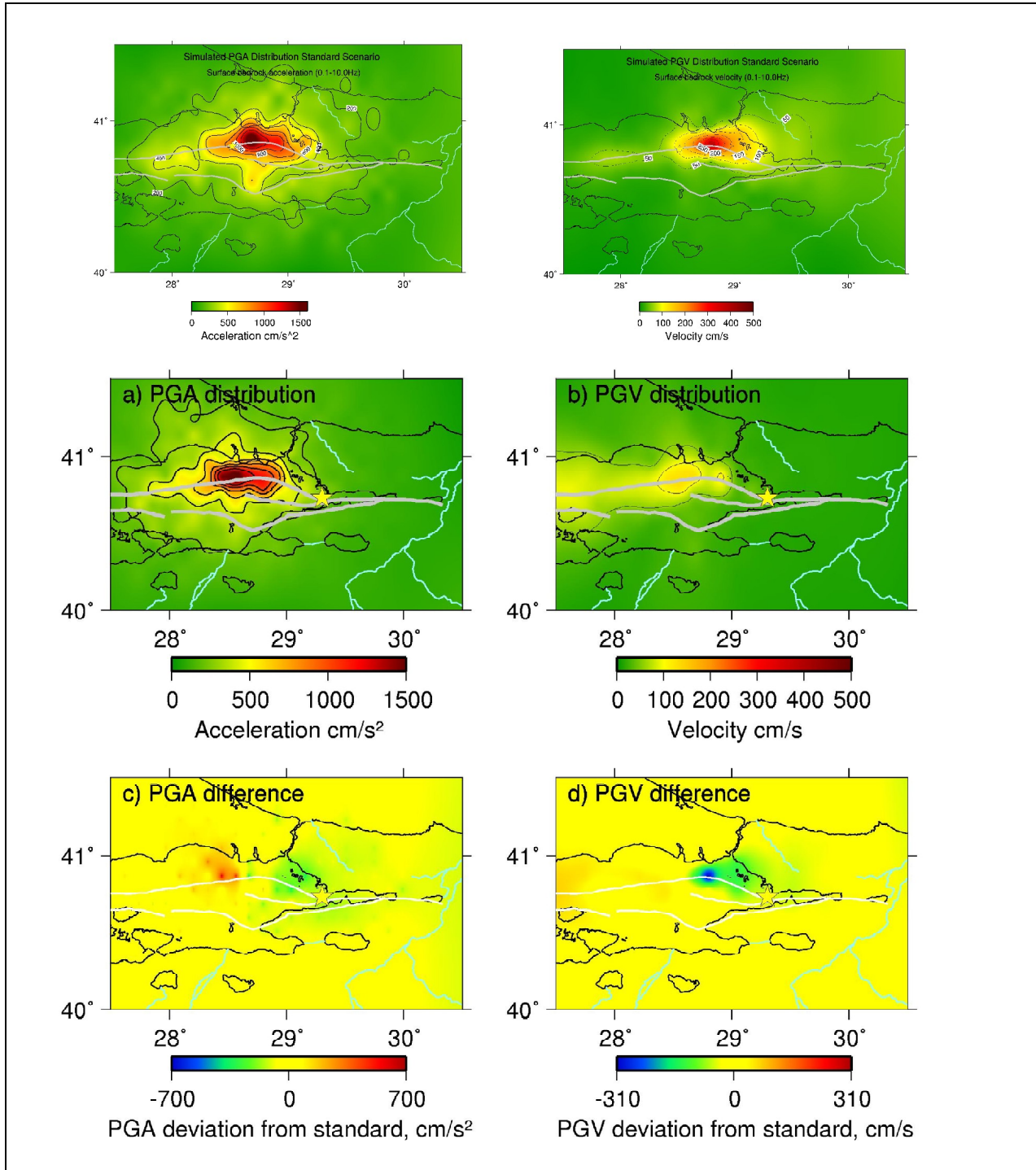


Figure 4.2.1. (b) Comparison of the ground motion simulation results associated with the rupture initiation point. Note that rupture initiation point is moved to the eastern end of the NBF (Scenario 4d). In the standard scenario it is in the western corner of the asperity 1. The top two plots are for the standard scenario. The middle two plots are for the test scenario and the two plots in the bottom are for the difference between the standard and the test scenario.



Project No: EVG1-CT-2002-00069

Annual Report 2005 (Partner # 6: UiB)

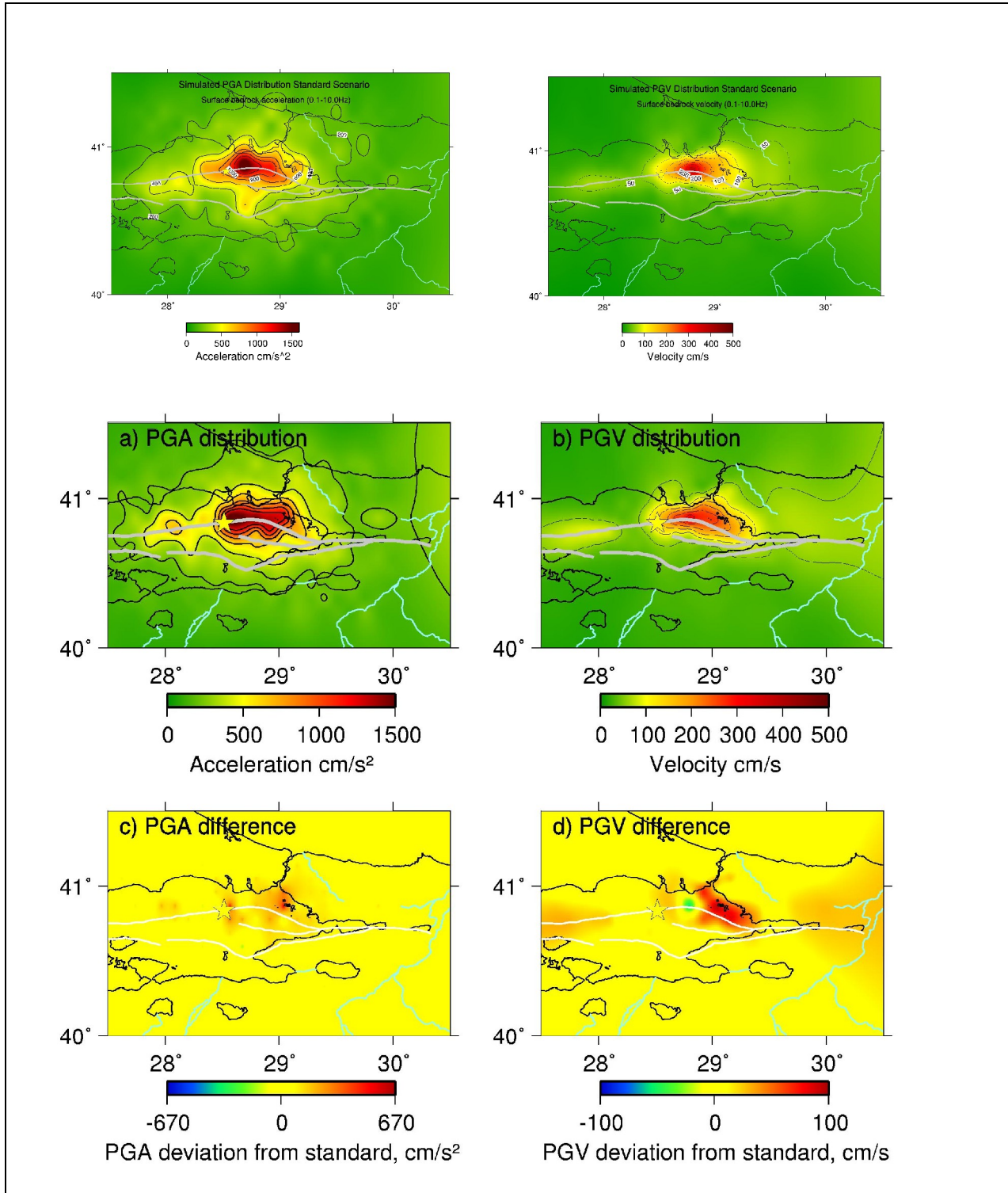


Figure 4.2.2. Comparison of the ground motion simulation results associated with increased rupture velocity (Scenario 3b). (Arrangement of plots follows the same convention as Figure 4.2.1: top: standard scenario; middle: test scenario; bottom: difference maps).



Annual Report 2005 (Partner # 6: UiB)



Project No: EVG1-CT-2002-00069

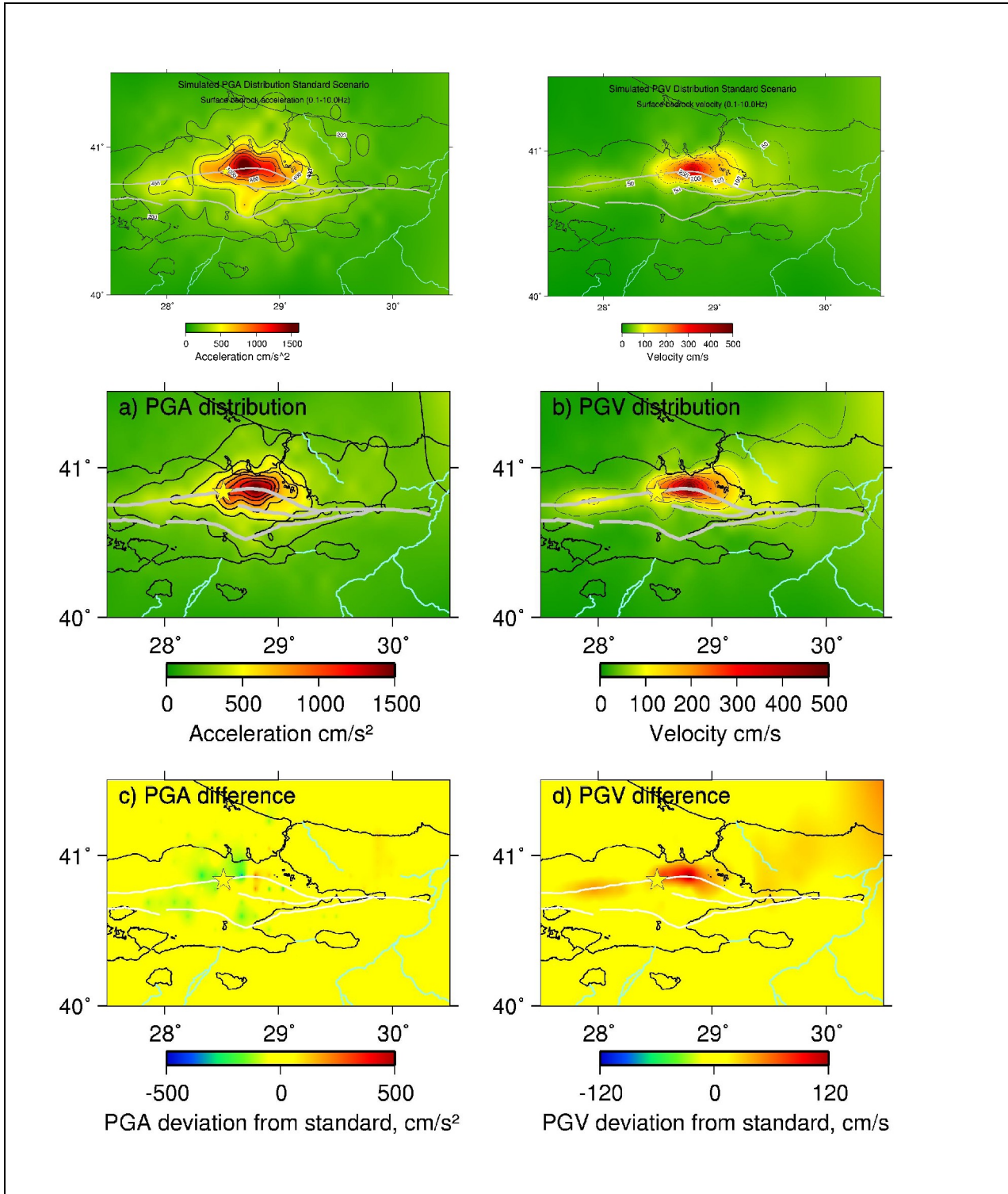


Figure 4.2.3. Comparison of the ground motion simulation results associated with the reduced rise time (Scenario 2a). (Arrangement of plots follows the same convention as Figure 4.2.1: top: standard scenario; middle: test scenario; bottom: difference maps).



Annual Report 2005 (Partner # 6: UiB)



Project No: EVG1-CT-2002-00069

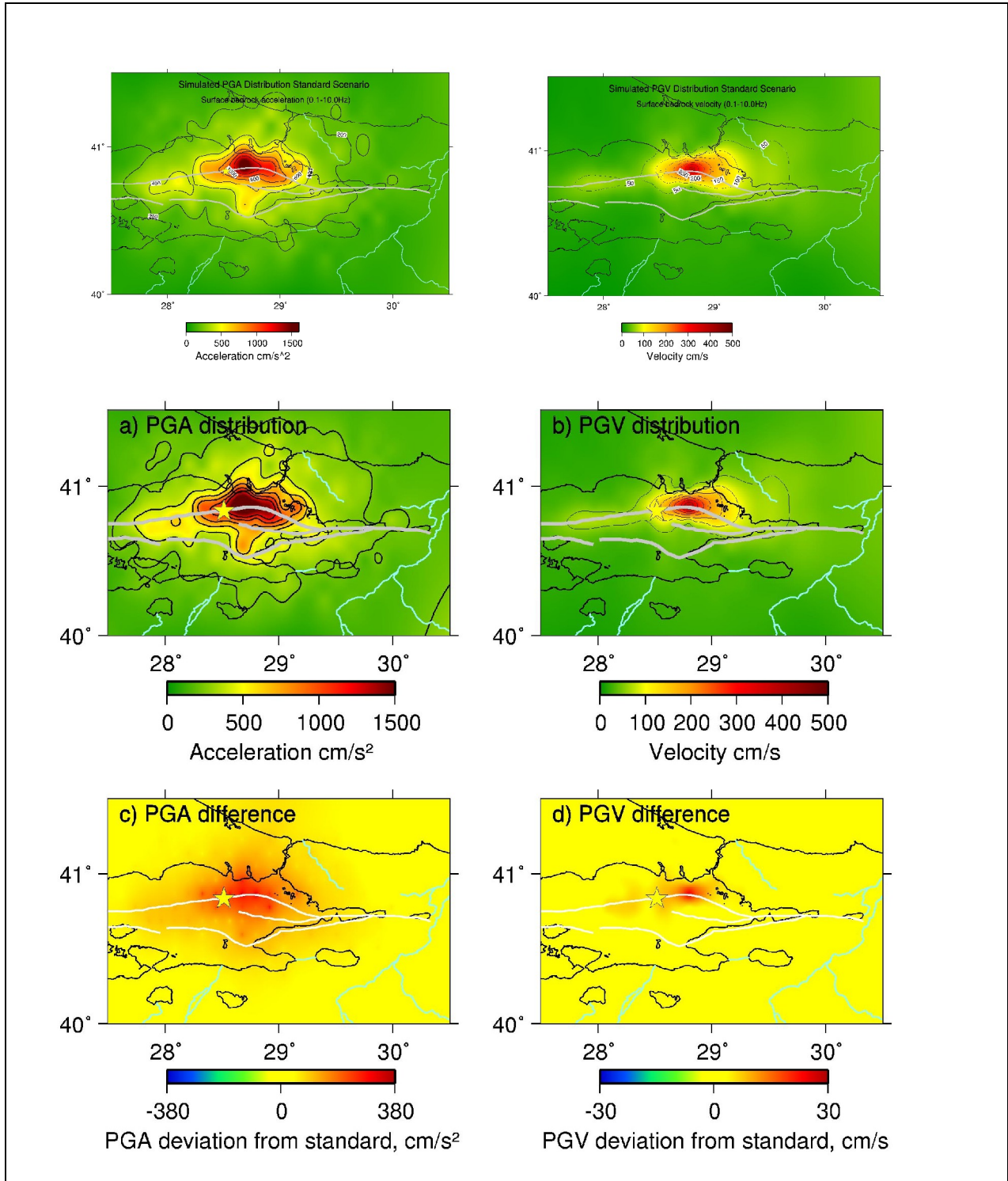


Figure 4.2.4. Comparison of the ground motion simulation results associated with the increased stress drop (Scenario 5b). (Arrangement of plots follows the same convention as Figure 4.2.1: top: standard scenario; middle: test scenario; bottom: difference maps).



Annual Report 2005 (Partner # 6: UiB)



Project No: EVG1-CT-2002-00069

4.3. Seismic risk: Damage estimation based on ground motion simulations for the RRS

The next step in this study has been to perform calculations for a scenario earthquake corresponding to the standard scenario described in the previous section at the recording sites of the Istanbul Earthquake Early Warning and Rapid Response System (IEEWRR) of KOERI (Erdik et al., 2003). IEEWRRS is a recently installed system of 110 accelerometer stations issuing early warnings and rapid response to possible earthquake damage. The early warning system consists of 10 stations located close to the NAF, recording online. When several stations trigger, an alarm level is set depending on the number of triggering stations and the recorded peak ground motions. This alarm level is sent directly to critical facilities (such as power stations, computer centers and telephone systems), which then have a chance to close down before the earthquake strikes. The rapid response system consists of 100 stations located in densely populated areas of Istanbul with an average station spacing of 2-3 km (black dots in Figure 4.3.1). These stations are run in dial-up mode with a trigger system. When a station triggers, it calculates spectral acceleration at a number of frequencies together with 12 Hz filtered PGA and PGV values and sends these data to a main data center as an sms message every 20 s. The main data center combines data from all stations to produce shake, damage maps which are passed on to the end users where they are available within 5 min after the earthquake. This makes it possible to respond rapidly to a large earthquake and provides a great help in distributing the emergency aid.

Since the IEEWRR system is recently installed, there has not yet been any significant earthquakes recorded by the system, except for two moderate sized earthquakes ($M=4.2$) on May 16, 2004 and ($M=4.1$) September 29, 2004 (Birgören et al., 2004). By performing our ground motion calculations at these stations, we were able to provide a realistic earthquake scenario input to the system. The results are aimed at calibrating the system and for calculating realistic shake and damage maps for a large earthquake scenario.

Figures 4.3.1 and 4.3.2 show the calculated PGV and PGA values interpolated over the whole Istanbul area. The most striking feature of the results is the strong forward directivity towards the city of Istanbul. The largest ground motions are predicted in the southern part of the city in agreement with the results of Pulido et al. (2004). Due to the irregular grid, artifacts are introduced in the interpolation, and the results from calculating with a regular grid (Pulido et al., 2004) should be used if a general overview of the peak ground motions in the city is wanted. However, the most

important output from these calculations is the single station waveforms at the individual recording sites. An example of such a waveform is shown in Figure 4.3.3. This waveform is for a station in Avcilar in the western part of Istanbul, which suffered great damage during the 1999 Izmit earthquake due to strong local site effects and is therefore a place of interest for the present study. It is important here to note that the above described calculations are performed for a bedrock site, meaning that no local site effects are taken into account. The waveforms show that even without taking local site effects into account, relatively strong accelerations can be expected, up to 449 cm/s^2 . In the velocity waveforms, a clear forward directivity pulse is seen with a period of 5-7 s.

Recently, the simulation results have been applied in estimating a damage scenario based on the routines established at the IEEWRRS operated by the KOERI. This gave for the first time a realistic picture of the expected effects of a large earthquake based on the input of simulated ground motions for Istanbul. The simulation results in spectral displacements for different building categories and in terms of estimated collapsed buildings are given in Figures 4.3.4 – 4.3.6. In this study we follow the building categories as defined by Dept. Earthquake Engineering, BU-KOERI (2003). These are: low-rise (1-4 stories); mid-rise (5-8 stories) and high-rise (>8 stories). It should be noted that shown scenarios are based on bedrock ground motions and do not take local site effects into account. Further work is already initiated which aims to integrate the local site effects to the ground motion simulation results for the entire Istanbul metropolitan area. In order to take local site effects into account the main approach followed is to attach an amplification factor to each simulation site by using information on the local geology and empirical Green's functions (EGF).

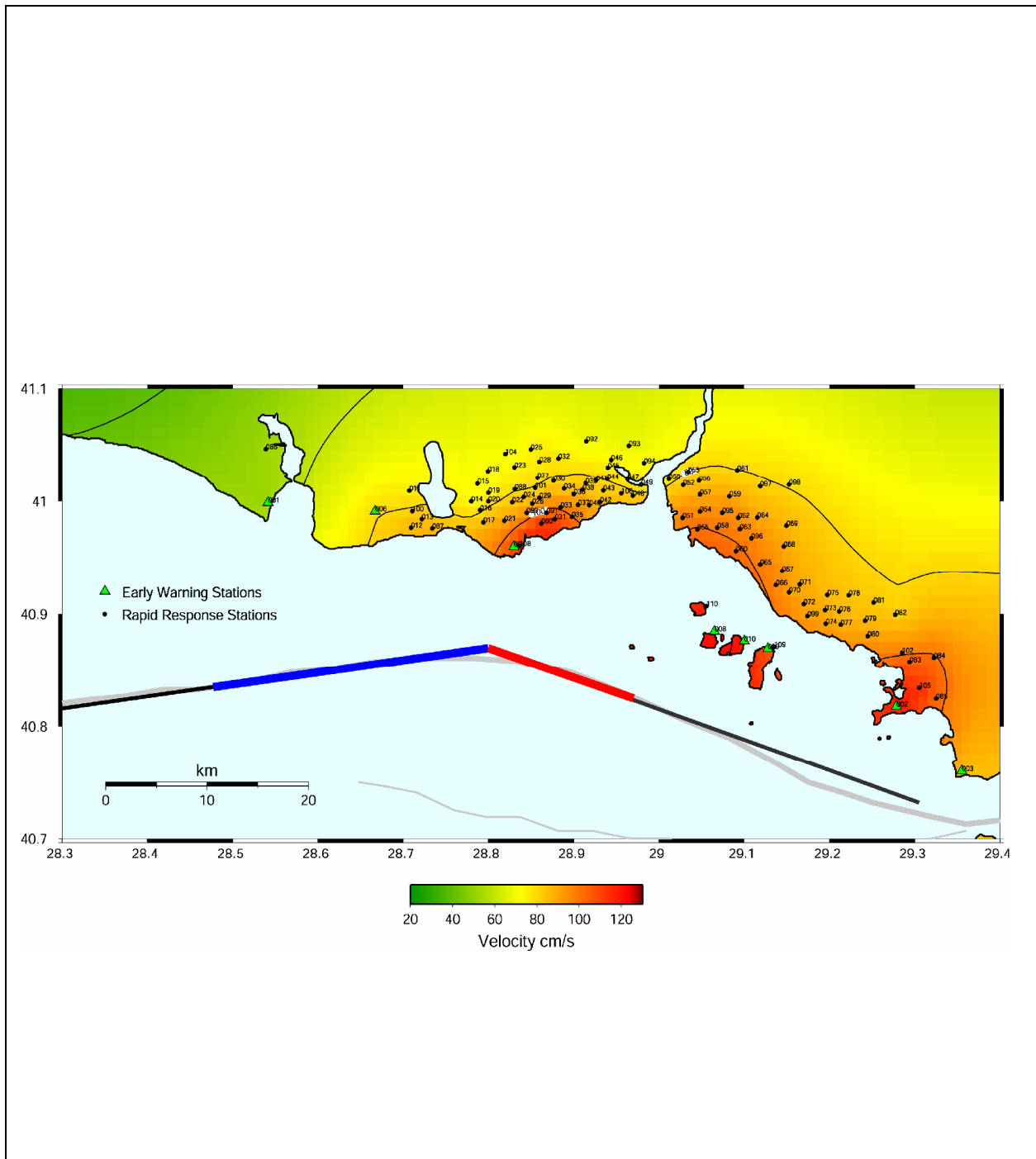


Figure 4.3.1. PGV results of ground motion simulations for a scenario earthquake (marked as black line) in the Marmara Sea, calculated on the irregular grid of the IEEWRR system. Red and blue lines are fault asperities used in the model. Numbers indicate the IEEWRR stations.



Project No: EVG1-CT-2002-00069

Annual Report 2005 (Partner # 6: UiB)

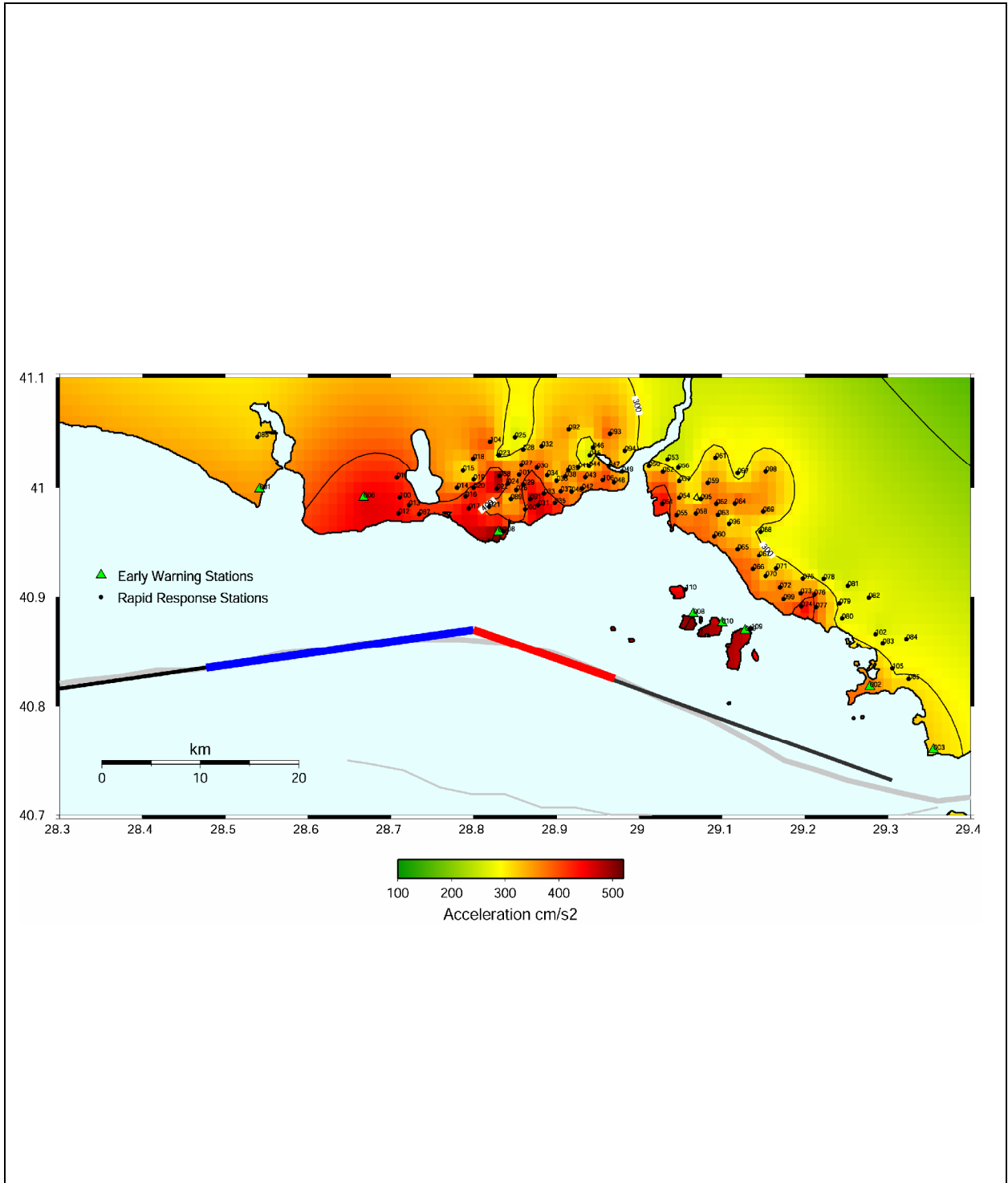


Figure 4.3.2. PGA results of ground motion simulations for a scenario earthquake (marked as black line) in the Marmara Sea, calculated on the irregular grid of the IEEWRR system. Red and blue lines are fault asperities used in the model. Numbers indicate the IEEWRR stations.



Project No: EVG1-CT-2002-00069

Annual Report 2005 (Partner # 6: UiB)

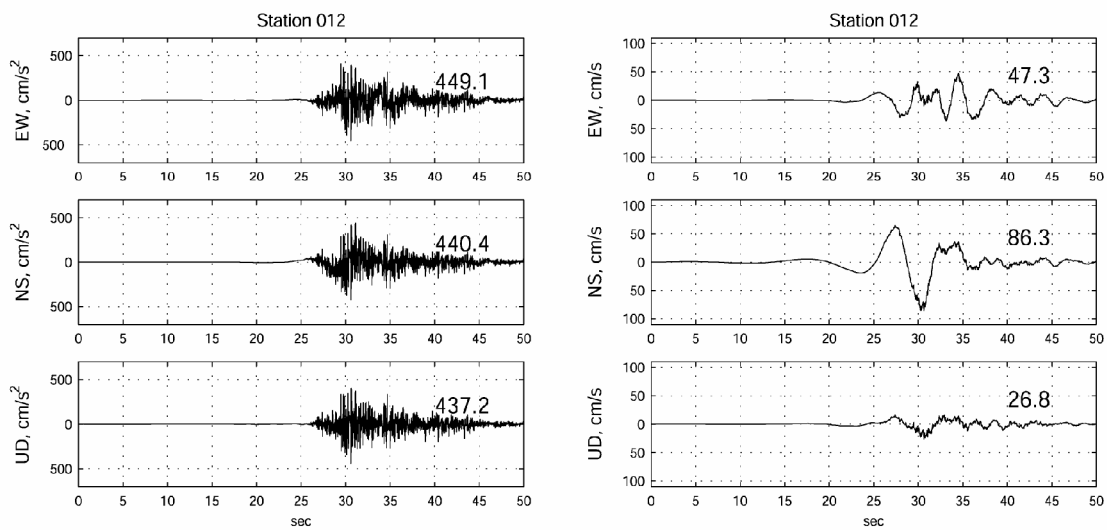


Figure 4.3.3. Waveforms simulated for a site in Avcilar, western Istanbul. To the left is 3-component ground acceleration, to the right are velocity traces. Peak values are shown above each seismogram to the right.



Project No: EVG1-CT-2002-00069

Annual Report 2005 (Partner # 6: UiB)

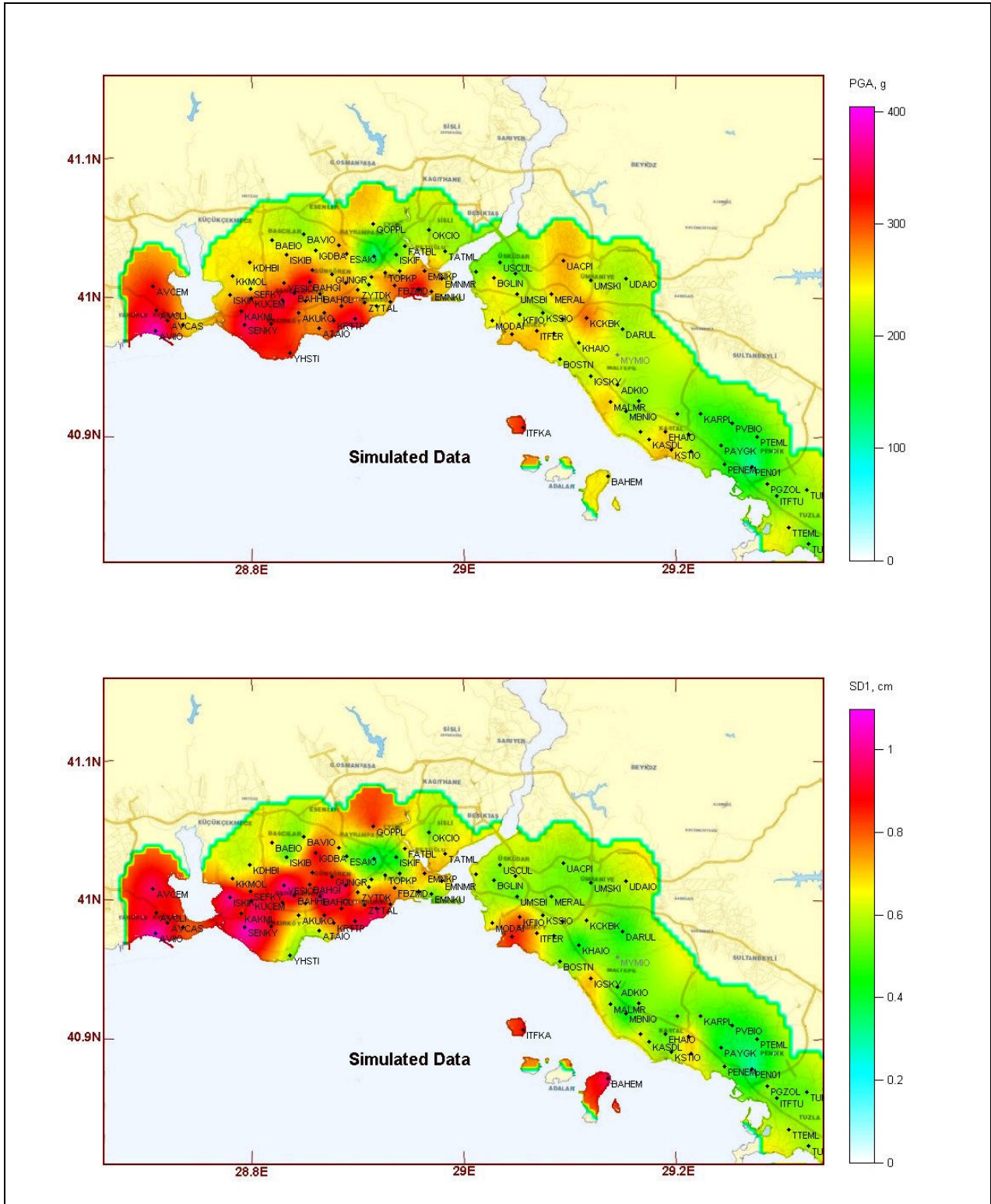


Figure 4.3.4. Top: Distribution of simulated ground motions in PGA in Istanbul (in cm/sec^2). Bottom: Spectral displacements in Istanbul (in cm) for building category 1 (low-rise).



Project No: EVG1-CT-2002-00069

Annual Report 2005 (Partner # 6: UiB)

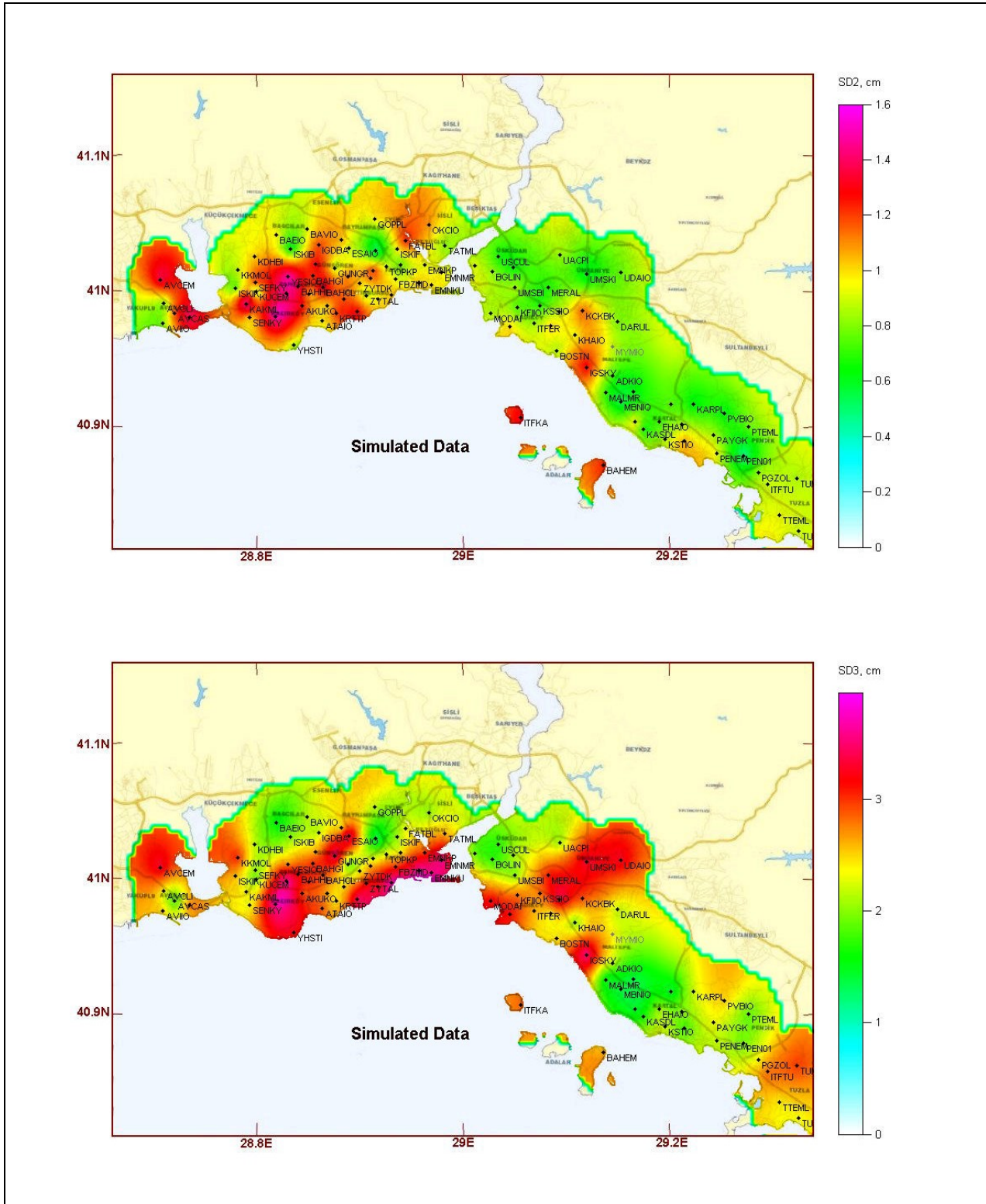


Figure 4.3.5. Top: Distribution of simulated ground motions in spectral displacements in Istanbul (in cm) for building category 2 (medium-rise). Bottom: Spectral displacements in Istanbul (in cm) for building category 3 (high-rise).



Annual Report 2005 (Partner # 6: UiB)



Project No: EVG1-CT-2002-00069

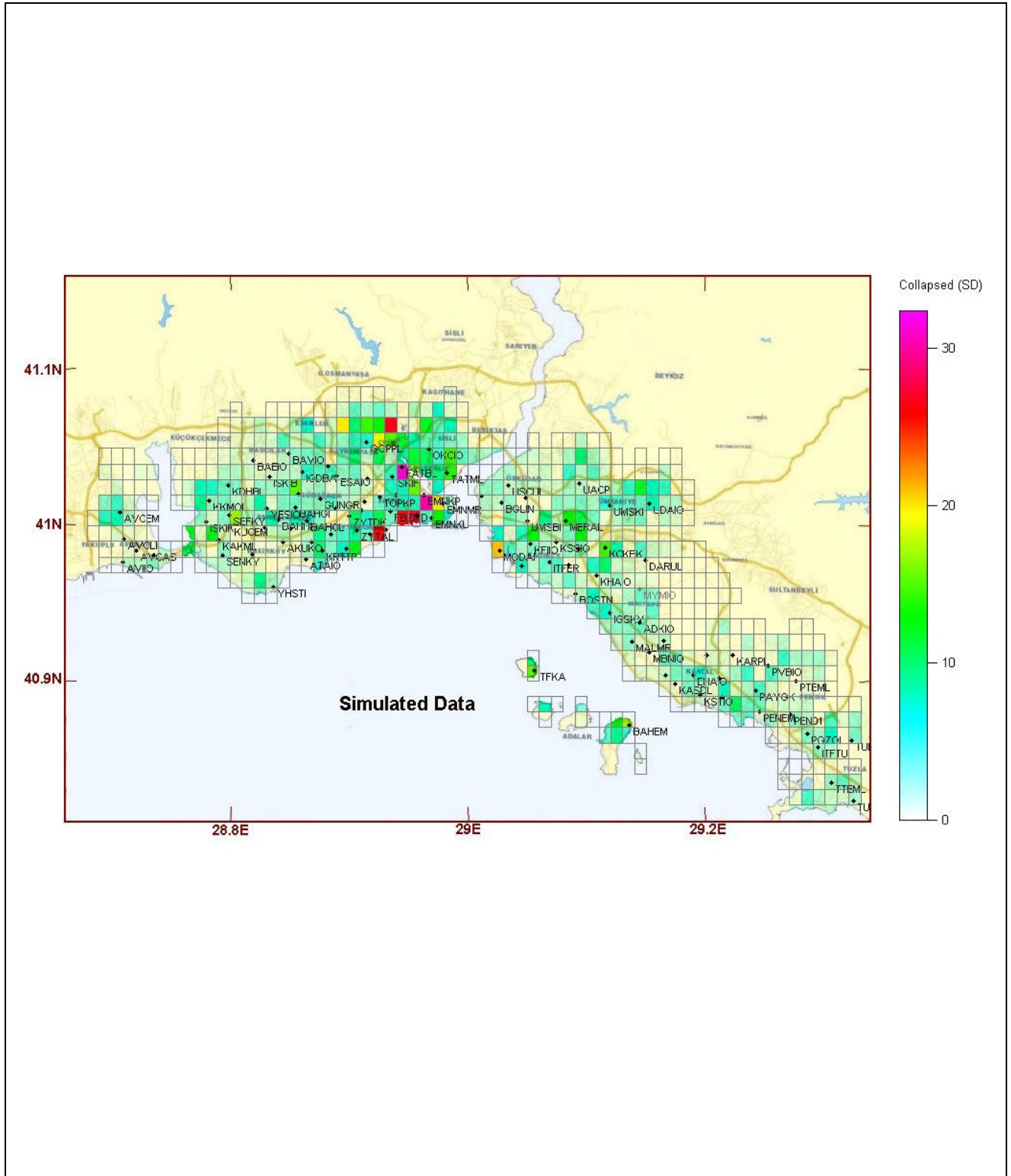


Figure 4.3.6. Distribution of damage in Istanbul due to a scenario earthquake in the Marmara Sea calculated at bedrock level in terms of collapsed buildings. Color code indicates the number of collapsed buildings.



Project No: EVG1-CT-2002-00069

Annual Report 2005 (Partner # 6: UiB)

5. WP10: Dissemination of the results

5.1. Dissemination of the results (publications, conference presentations etc.)

Following is a summary of the dissemination of the results during 2005:

Publications:

- Akinci A., Malagnini, L., Herrmann, R.B., Gok, R. and Sørensen, M.B. (in press). Ground Motion Scaling in the Marmara Region. *Geophys. J. Int.*, Jan.2006.
- Sørensen, M. B., Oprsal, I., Bonnefoy-Claudet, S., Atakan, K., Pulido, N., Mai, M. M, and Yalciner, C. (in review.): Local site effects in Ataköy area, Istanbul, Turkey, due to future large earthquake in the Marmara Sea. Submitted to the *Geophysical Journal International*.
- Sørensen, M.B., Pulido, N., and Atakan, K. (in review). Sensitivity of ground motion simulations to earthquake source parameters: A case study for Istanbul, Turkey. Submitted to the *Bulletin of the Seismological Society of America*.

Conference presentations:

- Meghraoui, M., Pantosti, D., Akyuz, S., Leroy, S., Mai, M., Atakan, K. 2005. The RELIEF Project: Large earthquake faulting and implications for the seismic hazard assessment in Europe, the 1999 Izmit-Duzce earthquake sequence (MW 7.3 – 7.1, Turkey). Hokudan Symposium on Active Faulting, 17-24 January 2005, Hokudan, Japan.
- Meghraoui, M., Pantosti, D., Akyuz, S., Leroy, S., Mai, M., Atakan, K. 2005. The RELIEF Project: Large earthquake faulting and implications for the seismic hazard assessment in Europe, the 1999 Izmit-Duzce earthquake sequence (MW 7.3 – 7.1, Turkey). Seismological Society of America, Eastern Section Meeting, April 2005.
- Meghraoui, M., Pantosti, D., Akyuz, S., Leroy, S., Mai, M., Atakan, K., RELIEF Working Group. 2005. The RELIEF Project: large earthquake faulting and implications for the seismic hazard assessment in Europe, the 1999 Izmit-Duzce earthquake sequence (MW 7.3-7.1, Turkey). European Geosciences Union General Assembly 2005, Vienna, Austria, 24-29 April 2005. (Poster presentation).
- Sørensen, M.B., Oprsal, I., Bonnefoy-Claudet, S., Atakan, K., Mai, M., Pulido, N., Yalciner, C. 2005. Local site effects in Ataköy, Istanbul, Turkey: empirical data vs. synthetics from hybrid modelling. European Geosciences Union General Assembly 2005, Vienna, Austria, 24-29 April 2005.

- Sørensen, M. B., Pulido, N., Atakan, K., Ojeda, A., Erdik, M. 2005. Ground motion simulations for a M=7.5 scenario earthquake in the Marmara Sea and implications for the city of Istanbul, Turkey. European Geosciences Union General Assembly 2005, Vienna, Austria, 24-29 April 2005. (Poster presentation).
- Sørensen, M.B., Pulido, N., Atakan, K., Ojeda, A. and Erdik, M. 2005. Ground motion simulations for a M=7.5 scenario earthquake in the Marmara Sea and implications for the city of Istanbul, Turkey. 36th Nordic Seminar on Detection Seismology, Copenhagen, Denmark, June 8-10, 2005.
- Atakan, K. 2005 (invited). Seismic hazard in Istanbul: Six years after the disastrous earthquakes in 1999. Keynote lecture at the International Symposium on the Geodynamics of the Eastern Mediterranean: Active Tectonics of the Aegean”, Istanbul, Turkey, June 15-18, 2005.
- Atakan, K. (invited). 2005. İstanbul'daki deprem tehlikesi ve yer hareketi simülasyonları. (in Turkish). Middle East Technical University, Ankara, Turkey, 23 September 2005.
- Sørensen, M.B., Oprsal, I., Bonnefoy-Claudet, S., Atakan, K., Mai, M., Pulido, N., and Yalciner, C. 2005. Local site effects in Ataköy, Istanbul, Turkey: empirical data vs. synthetics from hybrid modeling. IASPEI General Assembly, Santiago, Chile, 2-8 October 2005. (Poster presentation).
- Sørensen, M.B., Pulido, N., Atakan, K., Ojeda, A., and Erdik, M. 2005. Ground motion simulations for a M=7.5 scenario earthquake in the Marmara Sea and implications for the city of Istanbul, Turkey. IASPEI General Assembly, Santiago, Chile, 2-8 October 2005.
- Atakan, K. (invited). 2005. İstanbul'daki deprem tehlikesi hakkında bilmek istediklerimiz. (in Turkish). Dokuz Eylül University, Izmir, Turkey, 1 November 2005.
- Atakan, K., and Sørensen, M.B. 2005. Earthquake hazard in Istanbul: general overview. RELIEF Project Final Meeting, Istanbul, Turkey, 24-25 November 2005.
- Sørensen, M.B., Atakan, K., and Pulido, N. 2005. Ground motion simulations for Istanbul: a parameter sensitivity study. RELIEF Project Final Meeting, Istanbul, Turkey, 24-25 November 2005.
- Atakan, K., Sørensen, M.B., Pulido, N., Erdik, M., Ojeda, A., Durukal, E., Oprsal, I., Bonnefoy-Claudet, S., Mai, P.M., Birgören, G., Özel, O., Fahjan, Y., Meghraoui, M., Pantosti, D., Akyüz, H.S., Leroy, S., Pucci, S., Yalciner, C.C. and the RELIEF-Team. 2005. Earthquake hazard in Istanbul: synthesis and implications for the end-users. RELIEF Project Final Meeting, Istanbul, Turkey, 24-25 November 2005.
- Atakan, K. 2005. Paleosismik verilerin deprem tehlikesi degerlendirmesindeki önemi ve uygulanması (in Turkish). RELIEF Project Final Meeting, Istanbul, Turkey, 24-25 November 2005.
- Oglesby, D.D., Mai, P.M., Atakan, K., Pantosti, D., and Pucci, S. 2005. Dynamic rupture in the presence of fault discontinuities: An application to the faults in the Marmara Sea. AGU Fall Meeting, San Francisco, USA, Dec.5-9, 2005.
- Atakan, K. (invited) 2005. İstanbul'daki deprem tehlikesi hakkında bilmek istediklerimiz: Kapsamlı araştırmalardan istenilen uygulamaya geçişteki zorluklar (in Turkish). İstanbul Büyükşehir Belediyesi (İBB, İstanbul Metropolitan Municipality), Istanbul, Turkey, Dec. 14, 2005.

Acknowledgements

In addition to the persons that are listed in the list of contributors, the work presented in this report has benefited largely from the other project participants. We thank all of them for their enthusiasm and help throughout this time.

References

- Akinci A., Malagnini, L., Herrmann, R.B., Gok, R. and Sørensen, M.B. (in press): Ground Motion Scaling in the Marmara Region. *Geophys. J. Int.*, Jan.2006.
- Atakan, K., Ojeda, A., Meghraoui, M., Barka, A.A., Erdik, M. and Bodare, A., (2002): Seismic Hazard in Istanbul following the 17 August 1999 Izmit and 12 November 1999 Düzce Earthquakes, *Bulletin of the Seismological Society of America*, 92, 466-482.
- Birgören, G., Özel, O., Fahjan, Y. and Erdik, M.(2004): Determination of site effects in Istanbul area using a small earthquake record of the dense strong ground motion network, Poster at 29th general assembly of the European Seismological Commission, Potsdam, Germany 12-17 September 2004.
- Boore, D. M. (1983): Stochastic simulation of high frequency ground motions based on seismological models of the radiated spectra, *Bull. Seism. Soc. Am.*, 73, 1865-1894
- Bouchon, M. (1981): A simple method to calculate Green's functions for elastic layered media, *Bull. Seism. Soc. Am.*, 71, 959-971.
- Brune, J., (1970): Tectonic stress and the spectra of seismic shear waves from earthquakes. *J. Geophys. Res.*, 75, 4997-5009.
- Das, S., and Kostrov, B.V., (1986): Fracture of a single asperity on a finite fault: a model for weak earthquakes? In: Das, S., Boatwright, J., Scholz, C. (Eds.). *Earthquake source mechanism*. American Geophysical Union, Washington, pp.91-96.
- Dept. Earthquake Engineering, BU-KOERI (2003): *Earthquake Risk Assessment for the Istanbul Metropolitan Area*. Final Report. Department of Earthquake Engineering, Bogazici University, Kandilli Observatory and Earthquake Research Institute, Bogazici University Press., 300p.
- Erdik, M., Fahjan, Y., Ozel, O., Alcik, H., Mert, A. and Gul, M. (2003): Istanbul Earthquake Rapid Response and the Early Warning System, *Bulletin of Earthquake Engineering*, 1, 157-163.
- Erdik, M., Demircioglu, M., Sesetyan, K., Durukal, E. And Siyahi, B., (2004): Earthquake hazard in Marmara Region, Turkey, *Soil Dynamics and Earthquake Engineering*, 24, 605-631.
- Gurbuz, C., Aktar, M., Eyidogan, H., Cisternas, A., Haessler, H., Barka, A., Ergin, M., Turkelli, N., Polat, O., Ucer, S.B., Kuleli, S., Baris, S., Kaypak, B., Bekler, T., Zor, E., Bicmen, F., and Yoruk, A.,

(2000): The seismotectonics of the Marmara region (Turkey): results from a microseismic experiment. *Tectonophysics*, 316, 1-17.

Irikura, K. (1986): Prediction of strong acceleration motion using empirical Green's function, *Proceedings of the 7th Japan. Earthq. Eng. Symp.*, 151-156

Pulido, N., Ojeda, A., Atakan, K. and Kubo, T. (2004): Strong ground motion estimation in the Sea of Marmara region (Turkey) based on a scenario earthquake, *Tectonophysics*, 391, 357-374.

Somerville, P., Irikura, K., Graves, R., Sawada, S., Wald, D., Abrahamson, N., Iwasaki, Y., Kagawa, T., Smith, N., and Kowada, A., (1999): Characterizing crustal earthquake slip models for the prediction of strong ground motion. *Seismol. Res. Lett.*, 70, 59-80.

Sørensen, M. B., Oprsal, I., Bonnefoy-Claudet, S., Atakan, K., Pulido, N., Mai, M. M, and Yalciner, C. (in review.): Local site effects in Ataköy area, Istanbul, Turkey, due to future large earthquake in the Marmara Sea. Submitted to the *Geophysical Journal International*.

APPENDIX I

The List of Historical Earthquakes ($M_s \geq 7.0$) in the Greater Marmara Region for the period 1500 – 2000

by

N. N. Ambraseys

The list of historical earthquakes ($M_s \geq 7.0$)
in the greater Marmara Region for the period 1500-2000.

| Y | M | D | OT | N | E | Ms |
|----------|----------|----------|-----------|----------|----------|-----------|
| 1509 | 09 | 10 | 2200 | 40.9 | 28.7 | 7.2 |
| 1556 | 05 | 10 | 2400 | 40.6 | 28.0 | 7.2 |
| 1625 | 05 | 18 | 2400 | 40.3 | 26.0 | 7.1 |
| 1653 | 02 | 22 | 0000 | 37.9 | 28.5 | 7.0 |
| 1659 | 02 | 17 | 1900 | 40.5 | 26.4 | 7.2 |
| 1672 | 02 | 14 | 0000 | 39.5 | 26.0 | 7.0 |
| 1719 | 05 | 25 | 1200 | 40.7 | 29.8 | 7.4 |
| 1737 | 03 | 06 | 0730 | 40.0 | 27.0 | 7.0 |
| 1766 | 05 | 22 | 0500 | 40.8 | 29.0 | 7.1 |
| 1766 | 08 | 05 | 0530 | 40.6 | 27.0 | 7.4 |
| 1829 | 05 | 05 | 1500 | 41.2 | 25.4 | 7.1 |
| 1855 | 02 | 28 | 0230 | 40.1 | 28.6 | 7.1 |
| 1894 | 07 | 10 | 1224 | 40.7 | 29.6 | 7.3 |
| 1912 | 08 | 09 | 0129 | 40.8 | 27.2 | 7.3 |
| 1928 | 04 | 18 | 1922 | 42.3 | 25.0 | 7.0 |
| 1944 | 02 | 01 | 0323 | 41.1 | 32.2 | 7.4 |
| 1953 | 03 | 18 | 1906 | 39.9 | 27.4 | 7.1 |
| 1957 | 05 | 26 | 0633 | 40.7 | 31.0 | 7.2 |
| 1967 | 07 | 22 | 1657 | 40.7 | 30.7 | 7.2 |
| 1999 | 08 | 17 | 0001 | 40.8 | 30.0 | 7.4 |
| 1999 | 11 | 12 | 1657 | 40.8 | 31.2 | 7.1 |

APPENDIX II

Akinci A., Malagnini, L., Herrmann, R.B., Gok, R. and Sørensen, M.B. (in press). Ground Motion Scaling in the Marmara Region. *Geophysical Journal International*, Jan.2006.

GROUND MOTION SCALING IN THE MARMARA REGION, TURKEY

(1) Akinci, A., (1) Malagnini, L., (2) Herrmann, R.B., (3) Gok, R and (4) Sørensen, M. B.

(1) Istituto Nazionale di Geofisica e Vulcanologia, Via di Vigna Murata 605, 00143 Roma, Italy

(2) Department of Earth and Atmospheric Sciences, Saint Louis University, 3507 Laclede Ave. St. Louis, MO 63103 USA

(3) Lawrence Livermore National Laboratory, Earth Sciences Division L-206 7000 East Ave Livermore, California, USA

(4) Department of Earth Science, University of Bergen, Allegaten 41, 5007 Bergen, Norway

Geophysical Journal International
January 2006

Summary

Predictive relationships for the ground motion in the Marmara region (north-western Turkey) are parameterized after regressing three-component waveforms from regional earthquakes, in the frequency range: 0.4-15.0 Hz, and in the distance range: 10 - 200 km. The data set consists of 2400 three-component recordings from 462 earthquakes, recorded at 53 stations. Moment magnitudes, M_w , range between 2.5 and 7.2. The largest event for which we have waveforms available (M_w 7.2) occurred in Duzce on November 12, 1999. The aftershocks of that earthquake, together with the aftershocks of the August 17, 1999 Izmit event ($M_w = 7.4$), are included in the dataset. Regressions are performed, independently, on Fourier velocity spectra and on peak ground velocities, for a large number of sampling frequencies. A simple model is used to relate the logarithm of the measured ground motion to excitation, site, and propagation terms. Results obtained for peak velocities are used to define a piecewise continuous geometrical spreading function, $g(r)$, a frequency-dependent $Q(f)$, and a distancedependent duration function. The latter is used, through random vibration theory (RVT), in order to predict time-domain characteristics (i.e., peak values) of the ground motion. The complete model obtained for the peak ground motion was used to match the results of the regressions on the Fourier amplitudes. Fourier velocity spectra for the combined horizontal motion are best fit by a hinged quadri-linear geometrical spreading function for observations in the 10 – 200 km hypocentral distances range as a function of frequency: $f < 1.0 \text{ Hz}$, $r^{-1.2}$ for $r \leq 30 \text{ km}$; $r^{-0.7}$ for $30 < r \leq 60 \text{ km}$; $r^{-1.4}$ for $60 < r \leq 100 \text{ km}$; $r^{-0.1}$ for $r > 100$, $f \geq 1.0 \text{ Hz}$, $r^{-1.0}$ for $r \leq 30 \text{ km}$; $r^{0.6}$ for $30 < r \leq 60 \text{ km}$; $r^{-0.9}$ for $60 < r \leq 100 \text{ km}$; $r^{-0.1}$ for $r > 100 \text{ km}$. The frequency dependent crustal shear-wave quality factor $Q(f)$ coefficient $Q(f) = 180 f^{0.45}$. The $T(5-75\%)$ duration window provides good agreement between observed and predicted peak values. By modeling the behavior of the small earthquakes at high frequency, we also quantified a regional parameter $\kappa = 0.055 \text{ sec}$. Spectral models with one single-corner frequency (Brune), and with two corner frequencies (Atkinson and Silva, 2000) fit the observed high frequency excitation levels equally well, whereas the model by Atkinson and Silva (2000) fits the low frequency observations slightly better than the Brune's one. Random Vibration Theory (RVT) is used to predict the absolute levels of ground shaking, following Boore's (1996) implementation of the stochastic ground motion model (Boore's

SMSIM codes). Our regional empirical predictive relationships are compared to the ones adopted in several regions of the world, from California to Western United States (U.S.).

Keywords: Marmara Region, Turkey, Attenuation, Ground Motion Scaling.

Introduction

A significant proportion of Turkey is subjected to frequent and damaging earthquakes. Turkey is located on the relatively small Anatolian plate, which is being squeezed between three other major tectonic plates, the north-moving African and Arabian plates, which are both colliding with the Eurasian plate. As a consequence of the complex tectonics, the Anatolian plate is forced to move westward, into the Aegean Sea, through relatively simple fault systems located at the boundaries between plates. The most important of these systems is the North Anatolian Fault Zone (NAFZ, Sengor et al., 1985).

The NAFZ is a relatively simple, narrow, right-lateral strike-slip fault zone. It is defined quite obviously by surface ruptures, along almost its entire length (over 1000 km). Most of the length of the NAFZ was broken by a series of large earthquakes between 1939 and 1967 (Fig.1). In the vicinity of the Sea of Marmara, the NAFZ splits into several fault strands, and the deformation becomes distributed over a broad zone, ~120 km wide. The two largest event ($M_w=7.4$ and $M_w=7.2$) occurred on the northern branch of the NAFZ on August 17 and November 12, 1999, respectively. Along the northern shoreline of the Gulf of Izmit is a major industrial area, whereas the adjacent area to the south is predominantly residential and heavily populated. The damage caused by the 17 August 1999 earthquake was extensive. According to official data, this catastrophic event resulted in 17,127 casualties, 43,953 injuries and nearly 600,000 homeless. 77,342 buildings collapsed, including residential buildings and 77,169 buildings were moderately damaged, including residential buildings. Apart from the casualties, economic losses were substantial. Estimates of property loss, according to the World Bank report, Sept. 14, 1999, range from \$3 billion to \$6.5 billion, equivalent to 1.5 to 3.3 percent of the annual Gross National Product of Turkey. Because of the real earthquake threat in the Marmara region, the need for seismic hazard studies has become progressively more important for earthquake engineering applications. A fundamental requirement for these studies is the determination of predictive relationships for the ground motion (Kramer, 1996). A number of such relationships have been developed for many regions of the world (Ambraseys et al., 1996; Boore and Joyner, 1991; Boore, 1983; Toro and McGuire, 1987; Atkinson and Boore, 1995; Atkinson and Silva, 1987; Campell, 1997; Sadigh, 1997), mainly by regressing strong-motion data. These studies have shown that the ground motion levels can differ significantly in different tectonic regimes, for example depending on whether stresses are extensional or compressional.

However, in many parts of the world there are too few, or no, strong-motion recordings, and no strong-motion predictive relationships can be derived specifically for these regions. In these cases, it is necessary to adopt results obtained elsewhere, and use relationships from regions with comparable geology, tectonics, and seismicity. As an alternative, a number of papers have been published recently (e.g., Malagnini *et al.*, 2002; Akinci *et al.*, 2001; Bodin *et al.*, 2004) on the determination of some aspects of ground motion scaling in various regions of the world by exploiting large amounts of data from the background seismicity. These studies have used weak- and strong-motion recordings for deriving predictive relationships.

Until recently the predictive relationships adopted for Turkey (mainly, for the Marmara region) were taken from the Western U.S. and California because of the similarities of the tectonic environments. In order to obtain regionalized attenuation relationships for the Marmara region, Ozbey *et al.* (2004)

used the strong motion records from stations recently operated by Kandilli Observatory and Earthquake Research Institute (KOERI), Bogazici University, Istanbul Technical University (ITU), and Earthquake Research Department (ERD), General Directorate of Disaster Affairs. They used 195 strong motion records from 17 earthquakes, including the Izmit (M_w 7.4) and Duzce (M_w 7.2) earthquakes and their aftershocks, as well as other events with magnitude $M > 5.0$. They compared their proposed model to predictions based on Western US empirical attenuation models for shallow crustal zones, and pointed out that the Western US models overpredict ground motions: in some cases, the Western US based predictions differed more than one standard deviation from those of their Marmara model.

The objective of this study is to characterize ground motion observations in the Marmara region, using data from the network deployed after the 17 August 1999, Izmit earthquake. Predictive relationships are obtained through Random Vibration Theory (RVT) (Boore, 1983), which requires signal duration and amplitude spectra to estimate peak motions. Thus, we use seismograms from the large amount of aftershock data recorded by the micro-seismic networks instead of trying to reproduce the details of the high-frequency ground motion in the time domain, we use a source model and a regional scaling law to predict spectral shape and amplitude of ground motion at various source-receiver distances. At a set of sampling frequencies, we regress the peak values of narrow bandpass-filtered ground velocity time histories, as well as RMS-average Fourier spectral amplitudes, and define a regional predictive relationship characterized by a piece-wise linear geometric spreading (in a log-log space), a frequency-dependent crustal $Q(f)$, and a function describing the effective duration of the ground motion in the region. The excitation spectral model contains the competing effects of an effective stress parameter, $\Delta\sigma$, of Brune's single-corner source model and a high-frequency attenuation term $\exp(-\pi\kappa f)$. Using all the described information, then we obtain estimates of pseudo spectral acceleration (PSA), using the SMSIM (Stochastic Model SIMulation) codes of Boore (1996).

Seismological and Geological Background

The Marmara region is located at the western end of the NAFZ. The NAFZ extends for about 1500 km from Karliova, in the east, to the Aegean Sea at its western end. The NAFZ is a transitional structure: transpressional in its eastern part, it borders the Northern Anatolian Block, in a transtensional regime and reaches the extensional region of the Aegean Sea.

The NAFZ is an intercontinental dextral strike-slip fault, which comprises the boundary between Eurasia to the north and the Anatolian block to the south. Comparable in length and seismicity with the San Andreas Fault in California, it accommodates the westward extrusion of the Anatolian plate caused by the collision between the Arabian and the Eurasian plates in Eastern Anatolia (e.g. McKenzie 1972). The cumulative displacement along the fault is estimated to be about 40 km in the eastern section of the fault zone, and 20–30 km in its western end (e.g. Barka 1992). Recently, displacement rates of 22 ± 3 mm yr^{-1} are obtained from GPS data (Straub and Kahle, 1997). East of longitude 32°E , the deformation is related to the extrusion process, and the deformation is localized on a fault system that is several km wide. West of 32°E , the fault splits into several branches, and deformation is rather distributed (e.g. Michel 1994). A major structural feature in the western part of the fault system is a tensional bend, displacing the main fault by about 25 km to the north (Fig. 1). At about $30.40 - 30.60^\circ\text{E}$, the bending trace of the main fault intersects two ENE-striking strands of the fault system. The junction area is seismically active and characterized by a mixture of earthquake mechanisms (Neugebauer *et al.* 1997).

The westernmost section of the NAFZ in the Sea of Marmara, is a large pull-apart basin, which appears to have been a geometrical/mechanical obstacle encountered by the NAFZ during its

propagation. An outstandingly clear submarine morphology reveals a segmented fault system, including pull-apart features at a range of scales, indicating a dominant transtensional tectonic regime. Moreover, it has been observed that the NAF is continuous beneath the Sea of Marmara (Okay et al., 2000; Le Pichon et al., 2001), so it has no significant fault offsets that could stop a fault rupture. This result is critical for understanding the seismic behavior of this region of the NAFZ, close to Istanbul. A series of strong earthquakes broke the NAFZ from east to west, starting with the destructive $M_s = 7.4$, Erzincan earthquake of 1939, and ending with the 1999 Izmit and Duzce individual events. Even if we include the 1912 Galipoli earthquake, $M_w=7.2$, which occurred west of the Marmara Sea, there is still a gap corresponding to the branch of the NAF which crosses the northern border of the Marmara Sea (Ambraseys, 1970, 1975; Stein *et al.*, 1997; Barka 1992). This gap has a length of 150 km and is therefore capable of generating an earthquake with magnitude similar to that of the Izmit earthquake (Hubert-Ferrari *et al.*, 2000; Parsons *et al.*, 2000). The return period for large earthquakes south of Istanbul varies between 100-1000 years depending on the magnitude of earthquakes. The last major large earthquake on this segment was probably in 1509AD, (intensity, IX), (Barka, 1992, 1997-poly-project). The westward sequential progression of $M_w > 6.7$ earthquakes along the NAFZ during the 20th century was studied by Stein *et al.*, (1997) and by Nalbant *et al.*, (1998). Stein *et al.* (1997) showed the earthquake-induced Coulomb stress changes on adjacent fault segments. Application of this technique to evaluate the effect of the Izmit earthquake on neighboring faults, shows an area of increased stress to the east, including the Düzce fault which ruptured just after the Izmit earthquake (12 November, 1999, $M_w=7.2$). To the west, both the 80 km-long Yalova segment, southeast of Istanbul, and the Northern Boundary fault, immediately south of Istanbul, may be close to failure (Hubert-Ferrari *et al.*, 2000).

Data

Following the destructive 1999 earthquakes, permanent regional earthquake monitoring was augmented through the temporary deployed instruments by United States Geological Survey (USGS), Lamont Doherty Earth Observatory-USA (LDEO), the permanent and temporary deployments of Earthquake Research Directorate, Ministry of Public Works and Reconstruction - Turkey (ERD), as well as the permanent deployed broadband stations of Bogazici University, Kandilli Observatory and Earthquake Research Institute (KOERI), among others. In this study, we used data recorded by 53 three-component digital stations after the 17 August 1999, Izmit earthquake ($M_w=7.4$). The digital waveform data from these deployments was assembled and made available in the CDROM distributed by the USGS and at web page http://geopubs.wr.usgs.gov/openfile/of_01-163/ (Celebi et al., 2001). The data sampling frequency of strong motion records are 100 SPS (USGS Golden and Menlo Park, LDEO, ERD) as well as the broadband stations of KOERI. Magnitude and location calculation plays an important role in KOERI's activities and currently they report duration magnitude (M_d), local magnitude (M_L), and moment magnitude (M_w). The details about the data set and network is given by Celebi *et al.*, (2001) in detail and is briefly discussed here. Gok and Hutchings (2006) have uniformed the data correcting with instrumental responses and converting the whole dataset into a single unit (cm/sec²). The locations of the seismic stations and of selected events used at epicentral distances between 5 and 250 km are shown in Fig. 2. The 462 events in the data set span a magnitude range from 2.5 to 7.2 (Fig. 3). We only used unclipped and high signal/noise ratio data recorded in the time window 17 August 1999 - 30 November 2000. Fig. 4 displays the spatial distribution of the recordings at each station, as a function of hypocentral distance. We note that the spatial sampling of the available recordings is extremely dense and well distributed, at least out to a 200-km hypocentral distances. This characteristic leads to excellent regression results. The large amount of the data used in this study, recorded by LDEO, ERD and Geological and Earthquake Hazard Team of USGS. The data quality is confirmed with the existing M_w obtained from waveform inversion by Orgulu *et al* (2001) and with the coda method estimations by Mayeda *et al* (2005). Locations and the source

parameters of the 30 aftershocks of the August 17, 1999 Izmit earthquake, $4.0 < M_w < 5.9$ are given by Orgulu and Aktar (2001).

Due to the heterogeneity of the surface geology in the region, the stations were deployed on different kinds of geologic outcrops. They are mostly deployed on unconsolidated sediments or in a building where the man made noise level was high. More information related with the stations site can be found in the distributed CD. The S/N of the KOERI broadband stations is better than the others since they were buried in few meters below the surface.

Ground Motion Regression

Regression analysis for both peak motion and Fourier velocity spectra are performed using a simple model. Assuming that the observed spectra can be described as a convolution of source, regional propagation, and site transfer functions, the logarithm of the spectral amplitude of the ground motion observed on the k -th waveform (the RMSaverage taken within a frequency band logarithmically centered at the sampling frequency), relative to the i -th source and recorded at the j -th site, can be written as follows:

$$\text{AMP}_{kij}(f) = \log \text{amp}_{kij}(f) = \text{EXC}_i(f) + D(r_{ij}, r_{ref}, f) + \text{SITE}_j(f) \quad (1)$$

where EXC_i is an excitation term, referred to a suitable reference distance from the source, SITE_j is a site term (relative to an average site, see below), and $D(r_{ij}, r_{ref}, f)$ is the crustal propagation term, expressing the combined effect of geometrical spreading $g(r)$ and the anelastic attenuation, $Q(f)$. The propagation term is normalized to a null value at a reference hypocentral distance r_{ref} (see below).

With the implicit use of RVT, and of the Parseval's theorem, one can also write the logarithm of the peak amplitude of a relatively narrow bandpass-filtered time history around the frequency f , as the sum of source, propagation, and site terms:

$$\text{PEAK}_{kij}(f) = \log \text{peak}_{kij} = \text{EXC}_i(f) + D(r_{ij}, r_{ref}, f) + \text{SITE}_j(f) \quad (2)$$

Although equations (1 and 2) are simple in appearance, the true separation of these terms is difficult to achieve because of hidden trade-offs. For example, special care must be taken to select recording sites at a large range of hypocentral distances, so that undesirable trade-offs between an event source term and the distance function are avoided. Constraints must also be applied to reduce the number of degrees of freedom of the system, and to permit a stable inversion:

- $D(r=r_{ref}, f) = 0$ at some reference distance. The reference distance, r_{ref} , used in the constraint is chosen such that errors in source depth at that distance would make little difference. Moreover, convenience suggests that supercritical reflections from the Moho in the continental crust should not appear in the chosen distance range.
- An additional reduction of the degrees of freedom of the system is achieved by forcing the summation of some (at least one), or all, the site terms to a null value: $\sum_i \text{SITE}_i = 0$. A side effect of this constraint is that anytime the absolute average would be nonzero, its value is automatically forced into all individual excitation terms. Site terms thus represent relative responses to the (sub) network average. Once again, we emphasize the fact that we are not defining the earthquake source spectra; we are in fact parameterizing the observed ground motions.

Investigations by Atkinson (1993), Atkinson and Boore (1995) in eastern North America and by Atkinson and Silva (1997) in California indicate that the distance dependence of geometrical spreading may not have a simple functional form. However, in a log log space, the geometrical spreading may be expressed as a hinged, piecewise continuous, linear relation. Some requirements are forced on the geometrical spreading function, $g(r)$, which should not differ significantly from r^{-1} at short distances (body-wave-like spreading), and should be close to $r^{-1/2}$ at larger distances (surface-wave-like spreading). Anderson and Lei (1994) and Harmsen (1997) extended the concept of describing a complex geometrical spreading function by fitting their data with many linear segments (in a linear space), hinged and tied together with a smoothness constraint. With such an approach, the definitions of the geometrical spreading function, and of the frequency dependent Q is deferred to a later stage. At any given frequency, we parameterize the crustal propagation function as piecewise linear:

$$D(r, r_{ref}, f) = L_i(r) + \sum_{i=0}^n D_i \quad (3)$$

$D_{i=i_{ref}} = 0$

where $L_i(r)$ is a linear interpolation function, and the D_i are node values such that $D(r_i) = D_i$. A smoothness constraint can be applied by requiring

$$D_{i-1} - 2D_i + D_{i+1} = 0 \quad (4)$$

A constraint to minimize roughness is easily incorporated in the system. If the nodes are evenly spaced, the constraint is effectively a minimum roughness one.

Given the level of ground motion at $r_{ref}=40$ km, $D(r, r_{ref}, f)$ propagates the motion to the desired distance, r , and the site term adjusts the motion to a particular physical location (station). Other aspects of the parameterization that must be understood are the tradeoffs between excitation, site, and distance terms. Two cases illustrate the problem. First, if one event dominates a distance range, then there will be a tradeoff between the excitation for that event and the adjacent distance terms at that specific distance. This scenario may occur when an event is separated by a network dimension from a neighboring event, and if the distribution of distance nodes is too dense. A second case occurs if only one station dominates in a narrow range of distances, with an anomalous response. In this case, $D(r, r_{ref}, f)$ will be distorted by this station, and a bias will be introduced in all other site terms by the site term constrains (Herrmann, 2000).

Data Analysis

The following procedure was followed in order to study the excitation and propagation of the ground motion:

1. Each waveform was first bandpass-filtered about a center frequency, f_c , by an 8-pole high-pass causal Butterworth filter with corner frequency at $(f_c/\sqrt{2})$ Hz, followed by an 8-pole low-pass Butterworth filter with corner frequency at $\sqrt{2} f_c$ Hz. The set of central frequencies was {0.5, 1, 2, 3, 4, 6, 8, 10, 12, 14, 16} Hz. The peak filtered ground velocity was saved.

2. In addition, a duration window was computed for each filtered time history. We used the 5% and 75% bounds of the normalized integral of the squared signal, following the S-wave arrival. For each central frequency, for each waveform, the unfiltered signal within this time window was Fourier

transformed, and an rms average of the Fourier velocity spectra was made between the two corners of the bandpass filter.

3. For each filter frequency, the peak filtered motion, Fourier velocity spectrum, duration and amplitudes of signal envelopes, were tabulated for use in later processing. The reason for saving this information for subsequent use of RVT (Boore, 1983), which relates rms-averaged spectral amplitudes and duration to peak motion.

4. The crustal propagation function, $D(r) = \log_{10}(r, r_{ref}, f)$ was parameterized as a piecewise linear function with 14 nodes between 10 and 200 km. For our regression, we chose $r_{ref} = 40$ km. For each central frequency, there were 462 event terms, 159 site terms for the 53 three-component stations, and 14 nodes in the distance function. The source-receiver distance distribution for the whole dataset is shown in Fig. 4. The range hypocentral distances spanned by our data set is evenly sampled by our observations, a characteristic that allows a stable inversion. The 14 nodal distances were chosen after looking at the data distribution.

5. A hybrid approach was used to perform the regressions: because of the presence of significant outliers, an L_1 -norm inversion scheme (Bartels and Conn, 1980) was used to obtain the regression parameters. An L_2 -norm regression scheme (SVD) was then used to obtain estimates of the standard errors. Given the large amount of data used, even though the hybrid approach is not rigorously correct (no assumptions are made on the statistical distribution of the residuals prior to the computation of the parameters), for any practical purposes, at least in the cases described in this study, the L_1 - and the L_2 -norm solutions (mean and median values) coincide when the distribution of the residuals is well-behaved. The L_1 - norm procedure, however, protects us against severe individual deviations from the average behavior due to noisy individual data (for the time-domain quantities: spikes in the original time histories, and glitches induced by the action of the filters; for the frequency-domain quantities: wrong estimates of the rms-averaged Fourier spectral amplitudes due to substantial miscalculations of the 5-75% time window lengths. The standard errors associated to each parameter, although the distribution of the residuals is not perfectly Gaussian, may give idea of their scatter around the medians.

Results and Ground Motion Parameterization

Fig. 5 shows durations computed over all the available recordings, plots are shown for 6 of the central frequencies. An empirical function is calculated by using the L_1 -norm inversion procedure, where the summation of the absolute values of residuals is minimized. We note significant scatter at 1.0 Hz, which substantially decreases at higher frequencies. Error bars are estimated using the L_2 norm. At higher frequencies, low signals due to attenuation did not permit a reliable estimation of duration at large distance.

The duration function is parameterized as a piecewise linear function of distance: $T(r) = \sum T_i N_i(r)$. No constraints are forced to the duration function, except $T(r=0\text{km}) = 0$, which is appropriate for small earthquakes. To determine the $T(r)$ duration function, we assume the measured duration is practically insensitive to the event size for small earthquakes. RVT predictions depend on the assumed signal duration: $T_s + T(r)$, where T_s is the source contribution and $T(r)$ is the distance dependent wave propagation contribution (dispersion) to total duration. Predictions for larger earthquakes need extended source durations, T_s , to overcome the null duration constraint at short distance (Herrmann, 1985). The least squares fits are also plotted in Fig. 5. The last stage of the processing entails the specification of a simpler parametric model to describe the observations. The Fourier velocity spectra, $a(f,r)$, given the frequency and the hypocentral distance, are modeled as:

$$A(f, r) = s(f) g(r) \exp(-\pi f r / Q(f) \beta) \langle v(f) \exp(-\pi \kappa_0 f) \rangle_{\text{avg}} \quad (5)$$

where $s(f)$ is the source spectrum term to generate ground velocity, $g(r)$ is geometrical spreading, $Q(f) = Q_0 (f / f_{\text{ref}})^n$ is the frequency-dependent propagation Q , β is the velocity of the S-waves, and the $\langle v(f) \exp(-\pi \kappa_0 f) \rangle_{\text{avg}}$ term controls the average site modification of the signal spectrum. $v(f)$ represents the site amplification term relative to generic “rock”, similar to that of Atkinson and Silva (2000) for California. It can be computed from the shallow shear-wave velocity structure near the site (Boore, 1986). κ_0 describes the depletion of high-frequency motion at the site, which may be due to the local $Q(z)$ structure.

Figs 6a,b and 7a,b (colored lines) show the $D(r)$ functions, empirically determined in the inversion as a function of frequency, for PGVs and Fourier amplitudes, together with the difference between the observed and predicted $D(r)$ as a function of distance, respectively. As seen in Figs 6b and 7b, we successfully parameterize the distance effect, within $\pm 0.1 \log_{10}$ units in the first 100 km distance range. To enhance presentation, these figures show the deviation from an r^{-1} trend. Black lines in the background represent theoretical, RVT-based, predictions, obtained after a trial-and-error modeling obtained through the functional form:

$$10^{D(r_{ij}, r_{\text{ref}}, f)} = [g(r_{ij}) / g(r_{\text{ref}})] \exp[-\pi f (r_{ij} - r_{\text{ref}}) / Q(f) \beta] \quad (6)$$

The functions (6) are deduced from the data through a trial-and error modeling procedure, where the Fourier amplitudes are produced in the entire distance range using an arbitrary source spectral model, and the geometrical/anelastic attenuation model described in (6). The forward model is solved at each frequency, after fixing the corresponding duration function to the values obtained from the regressions. All frequencies are simultaneously fitted by the frequency-dependent attenuation/duration model. Normalization to the arbitrary reference distance removes the effects of the specific source model and parameters used.

This is done by assuming $Q(f) = Q_0 f^n$ and a simple piecewise linear geometrical spreading function. In our case, the functional form $g(r)$ used to fit the empirical results is:

$$\begin{aligned} f < 1 \text{ Hz, } g(r) &= r^{-1.2} \text{ for } r \leq 30 \text{ km} \\ &= r^{-0.7} \text{ for } 30 < r \leq 60 \text{ km} \\ &= r^{-1.4} \text{ for } 60 < r \leq 100 \text{ km} \\ &= r^{-0.1} \text{ for } r > 100 \text{ km} \\ f \geq 1 \text{ Hz, } g(r) &= r^{-1.0} \text{ for } r \leq 30 \text{ km} \\ &= r^{-0.6} \text{ for } 30 < r \leq 60 \text{ km} \\ &= r^{-0.9} \text{ for } 60 < r \leq 90 \text{ km} \\ &= r^{-0.1} \text{ for } r > 100 \text{ km} \end{aligned}$$

The effect of anelastic attenuation is to reduce amplitude with distance by a factor of $\exp(-\pi f r / Q(f) \beta)$ where $\beta = 3.5$ km/sec. For the set of attenuation parameters Q_0 , n and $g(r)$, theoretical Fourier spectra were estimated at each of the distances used in the regression for $D(r)$. Results were normalized to the reference distance of 40 km, and the logarithms were taken for direct comparison with the regression results. As a check, we also compared the $D(r)$ values obtained from the time domain regression by making random vibration theory estimates of peak filtered ground velocities. In doing so, we used the observed durations and random vibration theory (Boore, 1983). We accounted for the time domain response of the filters in the manner of Boore and Joyner (1984) for lightly damped single degree of freedom oscillators by stating that the RMS duration is the sum of the source duration, the propagation duration and twice the filter period. In addition, the duration

used for determining the number of random peaks is the sum of the source duration, the propagation duration, and filter period. This exercise yielded $r_{ref} = 40$ km, $Q_o = 180$ and $n = 0.45$.

Figs 8 and 9 show the site terms from the regression on filtered peak amplitudes and Fourier velocity spectra. In general, the site terms for the radial and the transverse components overlay. Because the constraint of null average was applied to the horizontal component site terms at the sites of the broadband stations, we may interpret the excitation terms of equation (2) as the horizontal ground motion that would be observed at the average network site, 40 km away from the hypocenter. Because of the averaging action introduction by regressing data from different azimuths, only the average source radiation pattern would be included.

The site terms are similar for the regressions in both the time and the frequency domains. Each term may be written as follows:

$$10_{SITEi}(f) = [v_i(f) \exp(-\pi \kappa_i f)] / \langle v(f) \exp(-\pi \kappa_o f) \rangle_{avg} \quad (7)$$

where the subscript i indicates the i -th site; $\langle v(f) \exp(-\pi \kappa_o f) \rangle_{avg}$ is the average network site effect and $v(f)$ is the generic site amplification factor relative to generic “rock” site. Finally, we compared the observed excitation levels of the horizontal motion for both data sets (peak values and Fourier spectra) at 40 km to model based predictions as a function of moment magnitude. Since there are data for $M_w > 5.0$ in our dataset, we felt confident in defining a source excitation model. The excitation spectra of especially larger events were modeled by using the regional propagation, together with the 2-corner equivalent-point-source model of Atkinson and Silva (2000) and a single-corner frequency Brune spectral model. The model for the horizontal velocity spectra is given by:

$$10_{EXC(ref, f)} \approx C (2\pi f) M_o s(f) g(r_{ref}) \exp(-\pi f r_{ref} / Q(f) \beta) \exp(-\pi \kappa_{eff} f) \quad (8)$$

where:

$$\exp(-\pi \kappa_{eff} f) \square \langle v_i(f) \exp(-\pi \kappa_o f) \rangle_{avg}$$

is the average high-frequency attenuation term due to the shallow geology,

$$C = (0.55) (0.707) (2.0) / 4 \pi \rho \beta^3$$

and for the single-corner Brune model, the functional form for $s(f)$ is given:

$$s(f) = 1 / (1 + (f / f_c)) \quad (9)$$

where $f_c = 4.9 * 10^6 \beta (\Delta\sigma / M_o)^{1/3}$, corner frequency and the 0.55 represents the S-wave average radiation pattern, 2.0 is the amplification at the free surface, 0.707 is the reduction factor that accounts for the partitioning of energy into two horizontal components (Boore, 1983), $\rho=2.8$ g/cm³ and $\beta=3.5$ km/sec are the density and the shearwave velocity. The seismic moment is M_o .

Atkinson and Silva (2000) described their two-corner source spectral model as:

$$s(f) = [(1-\epsilon) / [1 + (f / f_a)^2] + \epsilon / [1 + (f / f_b)^2]] \quad (10)$$

where $\log f_a = 2.181 - 0.496 M$ is the lower corner frequency, and $\log f_b = 2.41 - 0.408 M$ is the higher corner frequency, is the frequency at which the spectrum attains $1/2$ of the high-frequency

amplitude level. The remaining parameter, $\log \varepsilon = 0.605 - 0.255 M$, is a relative weighting parameter whose value lies between 0 and 1. Figs 10 and 11 compare the excitation terms at 40 km from our regressions for both the peak values and the Fourier spectral amplitudes with the predictions based on the Atkinson and Silva (2000), two corner source model combined with our crustal attenuation model and duration functions between 0.4 - 15 Hz. The gray curves in Figs 10 and 11 represent the theoretical excitation terms that are computed by using the parameters of Table 1.

In order to improve the presentation we first only plot error bars for the nine large events for which we have the seismic moments (M_w 's), with the predictions based on the two source models (one-corner Brune, 1970 and two-corner, Atkinson and Silva, 2000, source model), respectively, in Figures 12a,b. The excitation spectra of larger events were modeled by using the regional propagation, a single-corner frequency Brune spectral model (Brune, 1970, 1971) characterized by an effective stress parameter, $\Delta\sigma=80$ bar (Fig 12a), and by a regional estimate of the near-surface, distance independent, network averaged attenuation parameter, $\kappa_0=0.055$ sec that was estimated from the roll-off the empirical source spectra obtained from the regressions (Table 2). The model fits the observation of the large earthquakes, the $M_w=6$ fits close to the mean of the M_w 5.7-5.9 events, some adjustment at high frequencies may be required for $M_w=5.0$ events, but this adjustment is not that important if one is really interested in the big earthquake motions. The predicted shapes and levels are within the error bounds for the $M_w \sim 5.0$ earthquakes. The fit for larger earthquakes is excellent for frequencies greater than or equal to 2 Hz. The fit at high frequencies means that we would have confidence in using this model to predict peak accelerations. Concerning the fit at M_w 5.7-5.9, we have two earthquakes that are fitted very well with the Atkinson and Silva (2000) source model. The $M_w=6.0$ prediction at frequencies greater than 5 Hz goes through the mean of the levels of the M_w 5.7 and 5.9. Even though we have many stations that should average over the radiation pattern, these events behave very differently at high frequencies, which reinforces the idea that earthquake of the same size can radiate energy in different fashions. Fits to the $M_w=7.2$ are very similar for both models, the Atkinson and Silva (2000) one is slightly better at the low frequencies. Both models do not work well for the $M_w=6.0$ and underestimate high frequency levels for $M_w = 5.0$. Fig. 13 shows the residuals in fitting the $\log a(f, r)$ with equation (2); the scatter is typical of such regressions.

Empirical Predictive Attenuation relationships

Stochastic point-source simulations using the two-corner source spectrum of Atkinson and Silva (2000) were used to predict the absolute levels of ground shaking. In doing so, we followed Boore's (1996) implementation (Boore's SMSIM code), and used the attenuation parameters and the empirical duration function, obtained in this study. We compare these values to the peak ground acceleration observations of the 17 August 1999, Izmit earthquake and several attenuation relationships for the California and the Western U. S. The reason for using this earthquake, instead of main-shock of the 12 November, 1999, $M_w=7.2$ Duzce earthquake, is that there were many more observations at the closest distance. The fact permits us to test our predicted relationships. Fig. 14 shows a comparison between the attenuation relations by Ozbey *et al.*, (2004, OZB04), Boore *et al.*, (1997, BJF97), Atkinson and Silva, (2000, AS2000) and our results obtained for the BC site conditions (soil classification of the U.S. National Earthquake Hazard Research Program, NEHRP), (Boore and Joyner, 1997) for PSA at frequencies of 1 Hz, 3 Hz and 5 Hz. This site condition is the boundary between NEHRP classes B and C, (i.e, a site with an average shear wave velocity - V_s - of 760 m/sec in the top 30m). This refers to site as "firm rock," differentiating it from "hard rock" with shear-wave velocities near 3.0 km/sec at the surface.

The OZB04 attenuation relationship was obtained from strong motion records, from stations operated by the Bogazici University, the Kandilli Observatory and the Earthquake Research

Institute (KOERI), by Istanbul Technical University (ITU), and by the General Directorate of Disaster Affairs' Earthquake Research Department (ERD). Their cumulative data set consisted of 195 records from 17 earthquakes with $M_w \geq 5.0$. The BJF97 relationship was calibrated using strong motion records for shallow earthquakes in western North America, and cannot be used to predict ground motions at distances greater than 80 km, or for magnitudes less than 5.5 or greater than 7.5. The AS2000 attenuation relationships have been developed for California based on a stochastic model, which combines the main advantages of both point-source and finite fault modeling approaches. The stochastic ground motion relationships are underpinned by a source model that has been validated for earthquakes from magnitudes 4 through 8. Their attenuation model is derived from regional seismographic data over distances of hundreds of km (Raof et al., 1999).

The predicted spectral accelerations of this study are very similar to those by BJF97, over the entire distance range at 3 and 5 Hz, but there are significant differences at short distances. With respect to our predictive relationships, AS2000 and OZB04 show higher and lower amplitudes, respectively, over almost the entire distance range and especially at 3 and 5 Hz. Our predicted results are in good agreement with BJF9's and AS2000's ones, in the distance range 10-200 km, at frequencies of 1.0 Hz, and they are always higher than OZB04's ones. Even though we used $g(r) = r^{-0.1}$, which is different from $g(r) = r^{-0.5}$, used for existing strong-motion predictive relationships (for Europe, California, Western U.S and other active tectonic regions) beyond 100 km, our empirical relationship is in good agreement with BJF9's, AS2000's and OZB04's ones.

Conclusions and Discussion

Using ground velocities from three-component recordings from the Marmara region, we have characterized the ground velocity distance scaling in the range 10 - 200 km. Results of this study indicate that low frequency signals have longer durations than high frequency ones, and that duration increases significantly with distance. The low frequency duration data exhibit much scatter up to 1.0 Hz. Duration results indicate that both the degree of distance dependence and scatter increase with decreasing frequency.

The empirical distance and site terms obtained from the Fourier amplitude and from the time domain data are similar. Random Vibration Theory (RVT) has been used to model the observed peak ground motion. Peak velocities are controlled by a combination of source characteristics, duration of the signal, geometrical spreading, and anelastic attenuation. Results from the application of RVT indicate that our data are well fitted with a hinged, quadri-linear geometrical spreading function. We propose a frequency dependent quality factor $Q(f) = 180 f^{0.45}$ for the combined three-component data set. We find that the amplitude of high-frequency ground motion in the Marmara region decreases rapidly $g(r) = r^{-1.2}$ at short distances ($r < 30$) and low frequencies ($f < 2$ Hz). The observed decay is stronger than what is observed in other settings studied using the same technique: Central Europe (Malagnini *et al.*, 2000a), the Apennines region of Italy (Malagnini *et al.*, 2000b), the Friuli region of northeastern Italy (Malagnini *et al.*, 2002), southern California (Raof *et al.*, 1999) and Utah (Jeon, 2000). This rapid decrease has implications for ground motion predictions for large earthquakes. For longer distances (beyond 60-70 km) the interaction between seismic waves and propagation medium is more complex, as suggested by a geometrical spreading coefficient $r^{-0.9}$ for 60-100 km distances and $r^{-0.1}$ for distances $R > 100$ km. Researchers often pre-define the functional dependence of $g(r)$ for the region of interest, requiring $r^{-1.0}$ at short distances for body waves and $r^{-0.5}$ at larger distances for surface waves. The exponents of the geometrical spreading function describe the geometry of the wave-front (e.g., spherical or cylindrical propagation, or even the appearance of supercritical reflections in the transitional distance ranges), which strongly depends on the velocity structure of the medium (Aki and Richards, 2002). It is clear that if we fix the geometrical spreading function to $1/r$, we hypothesize a spherical wave front, and

hence, implicitly, a uniform crust. For a detailed estimate of the nature of the geometrical spreading, we need to take into account possible crustal heterogeneities and the existence of a strongly layered structure (e.g., the existence of a strong discontinuity, the Moho). Our $g(r)$ results differ from $r^{-0.5}$ at relatively long distances. This could be caused by the boundary between the falloff of direct wave, the emergence of lower crustal or Moho reflections and the contribution of the SmS phases. The overall behavior depends on several factors, such as: focal depth, crustal thickness, crustal velocity gradient, etc. Differences are seen in the geometrical spreading functions in our study at low and high frequencies might be also responsible for a laminated lower crust or a thick crust-mantle transition zone. In fact, Boztepe- Guney and Horasan (2002) observed the large amplitude SmS phases arrive 2 to 3 sec after direct S-waves in the distance range between 120 and 160 km. The amplitude of SmS arrivals is 3-6 times larger than the amplitude of the direct S-waves. These results suggest that the crust may not have a simple structure in the Marmara Sea, and that the effect of the large-amplitude SmS phases on the ground motion should be taken into consideration in the studies related with the seismic hazard in the region (Boztepe-Guney and Horasan, 2002).

This study improves the estimate of the frequency-dependent crustal attenuation of the region over what was previously available. Gunduz et al. (1998) estimated $Q_c(f)=41f^{1.08}$ and $Q_s(f)=50f^{1.09}$ in the Marmara region, in the distance range between 20 and 110 km, and in the frequency range between 1.5 and 24 Hz. Akyol et al, (2002) found $Q_s(f)=47f^{0.67}$ around the Bursa area (eastern part of the Marmara region). The frequency dependence suggested by Gunduz et al, (1998) seems to be extremely high when compared with other results from Mediterranean regions, California, or the western United States. Raouf et al., (1999) determined that the California attenuation can be modeled by geometrical spreading of r^{-1} to a distance of 40 km, with $r^{-0.5}$ spreading for r greater than 40 km. The anelastic attenuation associated with this spreading model is presented by a frequency-dependent regional quality factor given by $Q_s(f)=180f^{0.42}$. Jeon (2000) estimated the attenuation function to be between $Q_s(f)=145f^{0.65}$ and $Q_s(f)=180f^{0.60}$ for Utah (Basin and Range Province). Baskoutas et al, (2000) found $Q_s(f)=108f^{0.65}$ for 40 s lapse time window at the Erythres station, in the central Greece.

The fact that a single functional form for $Q(f)$ is used for all distances is somehow inappropriate because the direct radiation recorded at short distances mainly samples the crust above the hypocenter, whereas at large distances the seismic waves sample the entire crust. Therefore, the used method loses any azimuthal or depth information contained in each recording, yielding a picture of the statistical characteristics of the crustal-wave propagation in the region.

The estimated $\kappa_{\text{eff}} = 0.055$ sec value is consistent with the average value of $\kappa=0.056$ sec found by Durukal and Catalyurekli (2004) in the northwestern Turkey for the sites belonging to class D of the NEHRP soil classification (Boore and Joyner, 1997). A comparison of the Fourier domain excitation terms (Fig. 10) and the time domain terms (Fig. 11) shows the same relative pattern between data and predictions. This supports the internal consistency of our parameterization of the data in terms of anelastic attenuation, geometrical spreading and duration. Especially at the low frequencies, a spectral model characterized by two corner frequencies fits better the observed excitation terms for large events in Marmara than does a single-corner frequency Brune spectrum (Fig 12a, b). As an exercise in ground motion prediction, we used the model parameters of Table 1 and a set of programs called SMSIM (Stochastic Model SIMulation, Boore, 1966), to predict expected peak spectral accelerations (PSA). Since we have more PGA observations than for the 7.2, Duzce earthquake for closest distances, we compare our predicted values to the PGA's observed during the August 17, 1999 ($M_w = 7.4$) event, and used the predictions of the OZB97, AS2000 and BJF97 models. Compared to their predicted PSA's, our model is in good agreement with BJF97, and it yields higher and lower values than, respectively, the AS2000's and OZB97's ones, between a distance range of 10-100 km. This is especially true at 3 and 5 Hz.

We have shown the value of using aftershock recordings to describe the characteristics of the high-frequency ground motions as a function of hypocentral distance. When calibrated over large aftershocks with known seismic moment, the technique can provide excellent estimates of expected high frequency ground motion from large earthquakes.

References

- Ambraseys, N. N., 1970. Some characteristic features of the Anatolian fault zone. *Tectonophysics*, 9, 65-143.
- Ambraseys, N. N., 1975. Studies in historical seismicity and tectonics, *Geodynamics Today*, Royal Soc. Publ., London.
- Ambraseys, N. N., K. A. Simpson and J. J. Bommer, 1996 Prediction of Horizontal Response Spectra in Europe. *Earthquake Engineering and Structural Dynamics*, 25, 371-400.
- Anderson, J. G., and Y. Lei 1994. Nonparametric description of peak acceleration as a function of magnitude, distance, and site in Guerrero, Mexico, *Bull. Seis. Soc. Am.* 84, 1003-1017.
- Aki, K., Richards, P., 2002. Quantitative Seismology, 2nd ed. University Science Books, Sausalito, CA. 700 pp.
- Akinci, A., Malagnini, L., Herrmann, R.B, Pino, N.A., Scognamiglio, L., Eyidogan, H., 2001. High-Frequency Ground Motion in the Erzincan Region, Turkey: Inferences from Small Earthquakes, *Bull. Seis. Soc. Am.*, 91, 6, 1446-1455.
- Akyol, N., Akinci, A., Eyidogan, H, 2002. Separation of Source, Propagation and Site Effects from Observed S-wave of Bursa City and Its Vicinity in the North-western Anatolian Fault Zone, Turkey, *Pure and Applied Geophysics*, Volume 159, Number 6, pp 1253-1269.
- Atkinson, G. M. 1993. Earthquake source spectra and attenuation in southeastern Canada, University of Western Ontario, London, Ontario, *Ph.D. thesis*.
- Atkinson, G. M., and D. M. Boore 1995. Ground-motion relations for eastern North America, *Bull. Seism. Soc. Am.*, 85, 17-30.
- Atkinson, G. M., and W. Silva 1997. An Empirical study of earthquake source spectra for California earthquakes, *Bull. Seism. Soc. Am.*, 87, 97-113.
- Atkinson, G. M., and W. Silva, 2000. Stochastic Modeling of California Ground Motion. *Bull. Seism. Soc. Am.*, 90, 255-274.
- Barka, A., 1992. The North Anatolian Fault Zone. *Annales Tetonicae, Suppl.* To Vol. VI: 164-195.
- Barka, A. A., 1996. Slip distribution along the North Anatolian fault associated with the large earthquakes of the period 1939- to 1967. *BSSA*, 86, 5, 1238-1254.
- Barka, A. A., 1997. Neotectonics of the Marmara Region. *Active tectonics of Northwestern Anatolia-The Marmara Project*. Ed., C. Schindler and M. Pfister. VDF, ETH Zurich. 55-88.
- Bartels, R.H. and Conn, A. R., 1980. Linearly constrained discrete L_1 problems, *Transactions of the ACM on Mathematical Software*, vol. 6(4), pp. 594-608.
- Baskoutas I., G. Panopoulou and Th. Rontoyanni, 2000. The seismic attenuation in two regions with different geological aspect. *Boll. Geof. Theor. Appl.*, Vol 41, No3 pp233- 242.
- Bodin, P., L. Malagnini, and A. Akinci, 2004. Ground-Motion Scaling in the Kachchh Basin, India, Deduced from Aftershocks of the 2001 Mw 7.6 Bhuj Earthquake, *Bull. Seism. Soc. Am.*, 94, 5, 1658-1669.
- Boore, D. M. 1983. Stochastic simulation of high-frequency ground motions based on seismological models of the radiated spectra, *Bull. Seism. Soc. Am.*, 73, 1865-1894.
- Boore, D. M., and W. B. Joyner 1984. A Note on the Use of Random Vibration Theory to predict peak amplitudes of transient signals, Letter to the Editor, *Bull. Seism. Soc. Am.*, 74, 2035-2039.
- Boore, D. M. 1986. Short-period P- and S-wave radiation from large earthquakes: implications for spectral scaling relations. *Bull. Seism. Soc. Am.*, 76, 43-64.
- Boore, D. M., and W. B. Joyner 1991. Estimation of ground motion at deep-soil sites in eastern North America, *Bull. Seism. Soc. Am.*, 81, 2167-2185.
- Boore, D. M., 1996. SMSIM-Fortran programs for simulating ground motion from earthquakes: version 1.0, *U. S. Geological Survey open-file report 96-80-A*, 73 p.

- Boore, D. M. and W. B. Joyner, 1997. Site amplifications for generic rock sites. *Bull. Seism. Soc. Am.*, 87, 327-341.
- Boore, D. M., W. B. Joyner and T. E. Fumal, 1997. Equations for Estimating Horizontal Response Spectra and Peak Acceleration from Western North American Earthquakes: A summary of Recent Work. *Seism. Res. Lett.*, 68, 1, 128-153.
- Boztepe-Güney, A., Horasan, G., 2002. Enhanced ground motions due to large-amplitude critical reflections (SmS) in the Sea of Marmara, *Geophysical Research Letters*, 29, 9- 1/9-4.
- Brune, J., 1970. Tectonic stress and the spectra of seismic shear waves from earthquakes. *J. Geophys. Res.* 75, 4997– 5009.
- Campell, W., K., 1997. Empirical near-source attenuation relationships for horizontal and vertical components of peak ground acceleration, peak ground velocity, and pseudoabsolute acceleration response spectra. *Seis. Res. Lett.*, 68,1, pp.128-154.
- Celebi M., S. Akkar, U. Gulerce, A.Sanlı, H. Bundock, A. Salkin, 2001. Main shock and aftershock records of the 1999 Izmit and Duzce, Turkey earthquakes. USGS/OFDA project [USGS project no: 1-7460-63170]. <http://geopubs.wr.usgs.gov/open-file/of01-163/>
- Durukal E., Y.Çatalyürekli, 2004. Spectral Analysis of Source Parameters of the 1999 Kocaeli and Düzce Earthquake Aftershock Sequences, *proceeding of the 13th World Conference on Earthquake Engineering*, Vancouver, Canada, 1-6 August 2004.
- Gok, R. and L. Hutchings, 2006. Source Parameters and Scaling Relations for 1999 North Anatolian Fault Zone Aftershocks, in preparation.
- Gunduz, H., K. Ayse, B. Aysun and T. Niyazi, 1998. S-wave attenuation in the Marmara region, northwestern Turkey, *Geophysical Research Letters*, 25, 2733-2736.
- Harmsen, S. 1997. Estimating the Diminution of Shear-Wave Amplitude with Distance: Application to the Los Angeles, California, Urban Area. *Bull. Seism. Soc. Am.*, 87, 888- 903.
- Herrmann, R. B. 2000. Comparative ground motion studies, USGS Award Number: 1434-HQ-97-GR03090. 80
- Herrmann, R. B., 1985. An extension of Random Vibration Theory estimates of strong ground motion to large earthquakes, *Bull. Seis. Soc.Am.*, 75, 1447-1453.
- Hubert-Ferrari, A., A. Barka, E. Jacques, S. S. Nalbant, B. Meyer, R. Armijo, P. Tapponier, and G.C.P. King, 2000. Seismic hazard in the Sea of Marmara following the Izmit earthquake. *Nature*, 404, 269-272.
- Jeon, Y. S., 2000. High frequency earthquake ground motion scaling in Utah, *M.S. Thesis*, Saint Louis University.
- Kramer, S. L., 1996. Geotechnical Earthquake Engineering, Prentice Hall.
- Le Pichon, X., Sengor, A.M.C., Demirbag , E., Ragin, C., Imren, C., Armijo, R., Gorur, N., Catagay, N., Mercier de Lepinay, B., Meyer, B., Saatçilar, R., Tok, B., 2001. The active Main Marmara Fault. *Earth Planet. Sci. Lett.* 192, 595– 616.
- McKenzie, D., 1972. Active tectonics of the Mediterranean region, *Geophys J. R. Astr. Soc.* 30, no. 2, 109–185.
- Malagnini, L., R.B. Herrmann and K. Koch 2000a. Regional ground motion in scaling in Central Europe, *Bull. Seism. Soc. Am.* 90, 1052-1061.
- Malagnini L., R. B. Herrmann and M. Di Bona 2000b. Ground motion scaling in the Apennines (Italy), *Bull. Seism. Soc. Am.*, 90, 1062-1081.
- Malagnini, L., Akinci, A., Herrmann, R. B., Pino, N.A., Scognamiglio, L., 2002. Characteristics of the ground motion in Northeastern Italy, *Bull. Seism. Soc. Am.*, 26, 2186-2204 .
- Mayeda K., R. Gök, W. R. Walter, and A. Hofstetter, 2005. Evidence for Non-Constant Energy/Moment Scaling From Coda-Derived Source Spectra, *Geophysical Research Letter*, Vol. 32, L10306, doi:10.1029/2005GL022405.
- Michel, G., 1994. Neo-kinematics along the North-Anatolian Fault (Turkey), PhD thesis, Tu`binger geowiss. Arb., Reihe A 16.
- Nalbant, S., Hubert, A. and King, G. C. P., 1998. Stress coupling between earthquakes in northwest Turkey and the north Aegean Sea., *Journal of Geophys. Res.*, 103, B10, 24,469- 24,486.
- Neugebauer, J., Loffler, M., Berckhemer, H. and Yatman, A., 1997. Seismic observations at an overstep of the western North-Anatolian Fault (Abant-Sapanca region, Turkey), *Geol. Rund.*, 86, 93–102.

- Okay, A. I., Ozcan, A. K., Imren, C., Guney, A. B., Demirbag, E., Kuscu, I., 2000. Active faults and evolving strike-slip basins in the Marmara Sea, northwest Turkey: a multi channel seismic reflection study. *Tectonophysics* 321, 189–218.
- Orgulu, G., Aktar, M. 2001. Regional Moment Tensor Inversion for Strong Aftershocks of the August 17, 1999 Izmit Earthquake (Mw=7.4), *Geophysical Research Letters*, 28, No. 2, 371-374.
- Ozbey, C., Sari, A., Manuel, L., Erdik, M. Fahjan, Y., 2004. An empirical attenuation relationship for Northwestern Turkey ground motion using a random effects approach. *Soil Dynamics and Earthquake Engineering*, 24, 115–125
- Parsons, T., 2000. Heightened odds of large earthquakes near Istanbul: An interaction based probability calculation, *Science*, 288, 661–665.
- Raoof, M., R. B. Herrmann, and Malagnini, L. 1999. Attenuation and excitation of three component ground motion in Southern California, *Bull. Seism. Soc. Am.* 89, 888-902.
- Sadigh, K. 1997. Attenuation relationships for shallow crustal earthquakes based on California strong motion data, *Seism. Res. Lett.*, 68, No. 1, 180-189.
- Stein, R. S., Barka, A. A. and Dietrich J. H., 1997. Progressive failure on the North Anatolian Fault since 1939 by earthquake stress triggering. *Geophys. J. Int.*, 128, 594-604.
- Straub, C., and Kahle, H. G., 1995. Active crustal deformation in the Marmara sea region, N. W. Anatolia, inferred from GPS measurements. *Geophys. Res. Lett.*, 22, 18, 2'533-2'536.
- Toro, G. R. and R. K. McGuire 1987. An investigation into earthquake ground motion characteristics in eastern north America, *Bull. Seism. Soc. Am.* 77, 468-489.
- Sengor, A.M.C., Gorur, N. and Saroglu, F., 1985. Strike-slip faulting and related basin formation in zones of tectonic escape: Turkey as a case study. In: *Strike- Slip Faulting and Basin Formation* (K.T. Biddke and N. Christie-Blick, eds). Spec. Publ. Soc. Econ. Paleont. Miner., Tulsa, 37, 227–264.
- The World Bank, Turkey, 1999. Marmara Earthquake Assessment, from the World Wide Web <http://www.worldbank.org>, September 14, 1999 and <http://www.imf.org/external/NP/LOI/1999/092999.HTM>.

Figure Captions

Figure 1. Strip map showing the 1500-km-long North Anatolian fault. Relatively straight, the fault has several short, minor strands associated with it along its eastern half and breaks into three strands to the west. The section of the fault that ruptured to the surface during the 1999 Izmit and Duzce earthquakes are shown with the dashed line. In 1999, the fault ruptured along the northernmost, generally east-west main strand, as well as along a northerly strand called the Düzce fault. Modified from Barka (1996).

Figure 2. Location of stations (solid triangles) and earthquakes (open circles) used for this study. The size of the circles indicates relative earthquake magnitudes.

Figure 3. Moment magnitude distribution of the records used for the regression analysis.

Figure 4. Source-receiver hypocentral distance distribution of data used for the regression analysis. The horizontal axis refers to hypocentral distance (km), whereas on the vertical axis shows the names of the seismic stations. Each small square corresponds to a single horizontal-component recording

Figure 5. Distance dependence of duration for 0.25, 0.40, 1.0, 3.0 and 5.0 Hz filtered data.

Figure 6. a) Colored curves show attenuation functional $D(r, r_{ref}, f)$ obtained from the regression the filtered velocities together with b) the difference between the observed and predicted $D(r)$ as a function of distance at frequencies of 1.0, 2.0, 3.0, 4.0, 5.0, 6.0, 8.0, 10.0, 12.0, 14.0 and 16.0 Hz.

Black lines in the background represent theoretical predictions obtained after a trial-and-error modeling of the empirical (color) curves. The reference hypocentral distance is 40 km. Frequency dependence of filtered time domain $D(r)$ corrected for r^{-1} geometrical spreading coefficient.

Figure 7. a) Colored curves show attenuation functional $D(r, r_{ref}, f)$ obtained from the regression the Fourier amplitudes together with b) the difference between the observed and predicted $D(r)$ as a function of distance at frequencies of 1.0, 2.0, 3.0, 4.0, 5.0, 6.0, 8.0, 10.0, 12.0, 14.0 and 16.0 Hz. Black lines in the background represent theoretical predictions obtained using trial-and-error modeling of the empirical (color) curves. The reference hypocentral distance is 40 km. Frequency dependence of Fourier velocity spectra $D(r)$ corrected for r^{-1} geometrical spreading coefficient. b)

Figure 8. The site terms obtained from regression of Fourier velocity spectra.

Figure 9. The site terms obtained from regression horizontal peak filtered velocities.

Figure 10. Excitation of peak filtered velocity at a reference hypocentral distance $r_{ref}=40$ km. Excitation terms for all events used in this study with magnitude between $M_w=2.5$ and 7.2 are compared to predictions obtained by using RVT. The gray curves representing the theoretical source terms are computed for magnitudes of 3.0, 4.0 5.0, 6.0 and 7.2 by using the parameters of Table 1.

Figure 11. Excitation of Fourier velocity spectra at a reference hypocentral distance $r_{ref}=40$ km. Excitation terms for all events used in this study with magnitude between $M_w=2.5$ and 7.2 are compared to predictions. The gray curves representing the theoretical source terms are computed for magnitudes of 3.0, 4.0 5.0, 6.0 and 7.2 by using the parameters of Table 1.

Figure 12. Excitation of peak filtered velocity at a reference hypocentral distance $r_{ref}=40$ km. Excitation terms for nine large events with the predictions based on the two source models, a) one-corner Brune, 1970 and b) two-corner, Atkinson and Silva, 2000, source model, for which we have the seismic moments, indicated with boxes (showing M_w) and arrows to the excitation, respectively. The gray curves representing the theoretical source terms are computed for magnitudes of 5.0, 6.0, 7.2 by using the parameters of Table 1 and Table 2.

Figure 13. The residuals of the regressions, for six of the sampling frequencies (1.0, 2.0, 4.0, 5.0, 10.0 and 16.0 Hz).

Figure 14. Comparison of different estimates of PSA (g) at frequencies of 1.0, 3.0 and 5.0 Hz in the Marmara region as obtained by using the empirical relationships by Ozbey *et al.*, (2004, dotted), Boore *et al.*, (1997, gray line) and Atkinson and Silva (2000, short dashed); dark solid line indicate PSA computed by Boore's program SMSIM (Boore, 1996) using the crustal attenuation and excitation parameters shown in Table 1. Curves are computed for M_w 7.4 and compared to the observed values of PGA (at soft, stiff and rock sites) during the 17 August 1999, $M_w =7.4$, Izmit earthquake.

Table 1.

High frequency ground motion model parameters
(two corner frequency source model)

$\rho = 2.8 \text{ g/cm}^3$

$\beta = 3.5 \text{ km/sec}$
 $\kappa_{\text{eff}} = 0.055 \text{ sec}$
 $\log f_a = 2.181 - 0.496$
 $\log f_b = 2.41 - 0.408 M$
 $\log \varepsilon = 0.605 - 0.255 M$
 $f < 1 \text{ Hz}, g(r) = r^{-1.2} \text{ for } r \leq 30 \text{ km}$
 $= r^{-0.7} \text{ for } 30 < r \leq 60 \text{ km}$
 $= r^{-1.4} \text{ for } 60 < r \leq 100 \text{ km}$
 $= r^{-0.1} \text{ for } r > 100 \text{ km}$
 $f \geq 1 \text{ Hz}, g(r) = r^{-1.0} \text{ for } r \leq 30 \text{ km}$
 $= r^{-0.6} \text{ for } 30 < r \leq 60 \text{ km}$
 $= r^{-0.9} \text{ for } 60 < r \leq 100 \text{ km}$
 $= r^{-0.1} \text{ for } r > 100 \text{ km}$
 $Q(f) = 180 (f / 1.0)^{0.45}$

Table 2.

High frequency ground motion model parameters
(one-corner frequency source model)

$\rho = 2.8 \text{ g/cm}^3$
 $\beta = 3.5 \text{ km/sec}$
 $\kappa_{\text{eff}} = 0.055 \text{ sec}$
 $\Delta\sigma = 80 \text{ bar}$
 $f_a = f_b$
 $f < 1 \text{ Hz}, g(r) = r^{-1.2} \text{ for } r \leq 30 \text{ km}$
 $= r^{-0.7} \text{ for } 30 < r \leq 60 \text{ km}$
 $= r^{-1.4} \text{ for } 60 < r \leq 100 \text{ km}$
 $= r^{-0.1} \text{ for } r > 100 \text{ km}$
 $f \geq 1 \text{ Hz}, g(r) = r^{-1.0} \text{ for } r \leq 30 \text{ km}$
 $= r^{-0.6} \text{ for } 30 < r \leq 60 \text{ km}$
 $= r^{-0.9} \text{ for } 60 < r \leq 100 \text{ km}$
 $= r^{-0.1} \text{ for } r > 100 \text{ km}$
 $Q(f) = 180 (f / 1.0)^{0.45}$

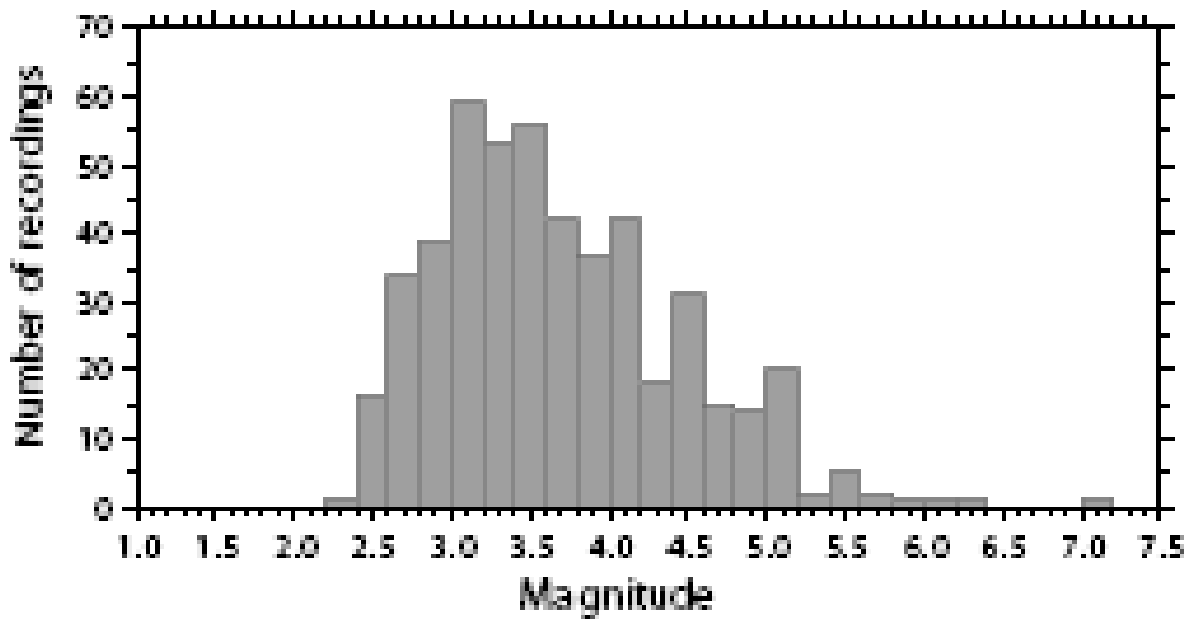
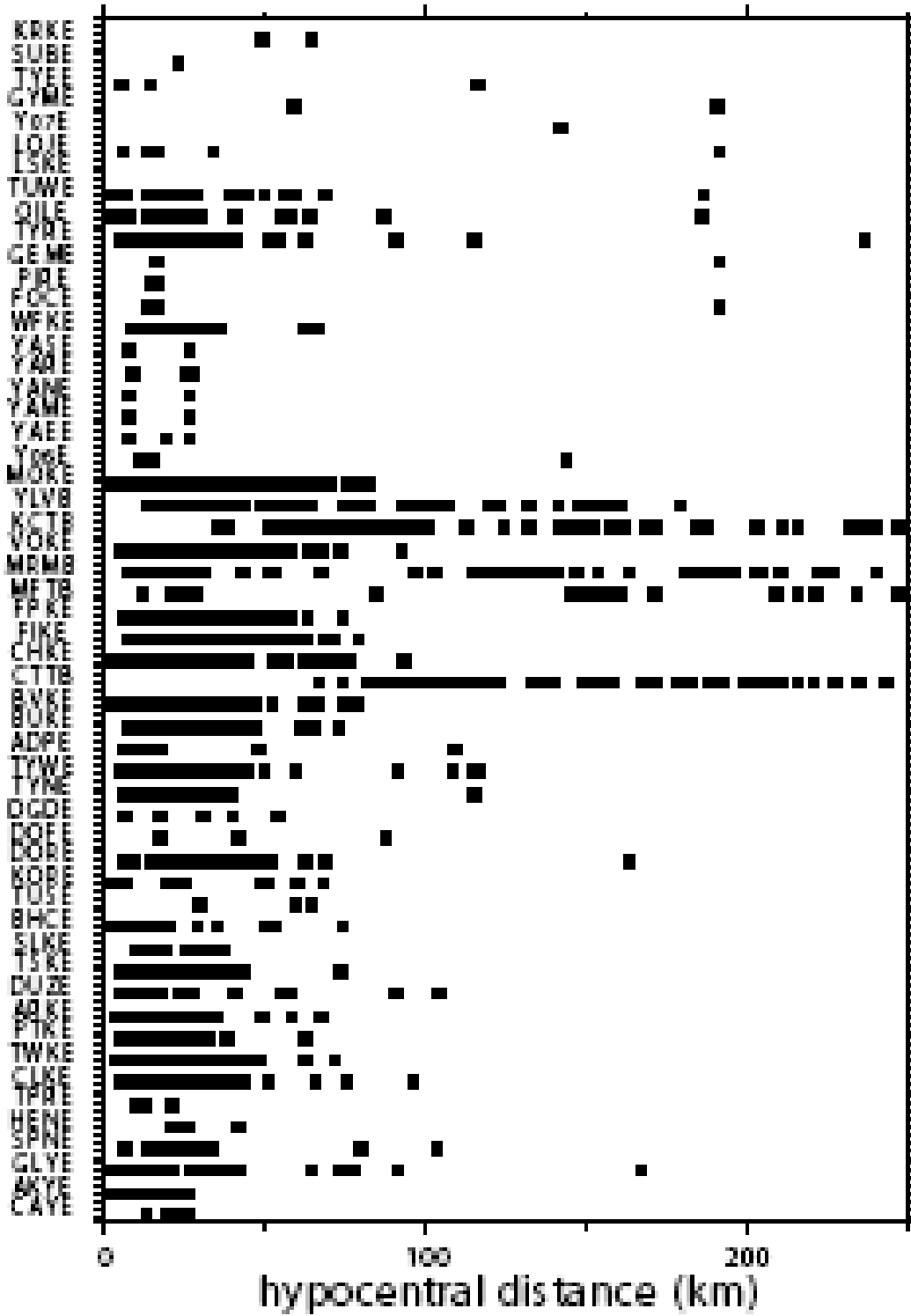


Figure 3



.Figure 4.

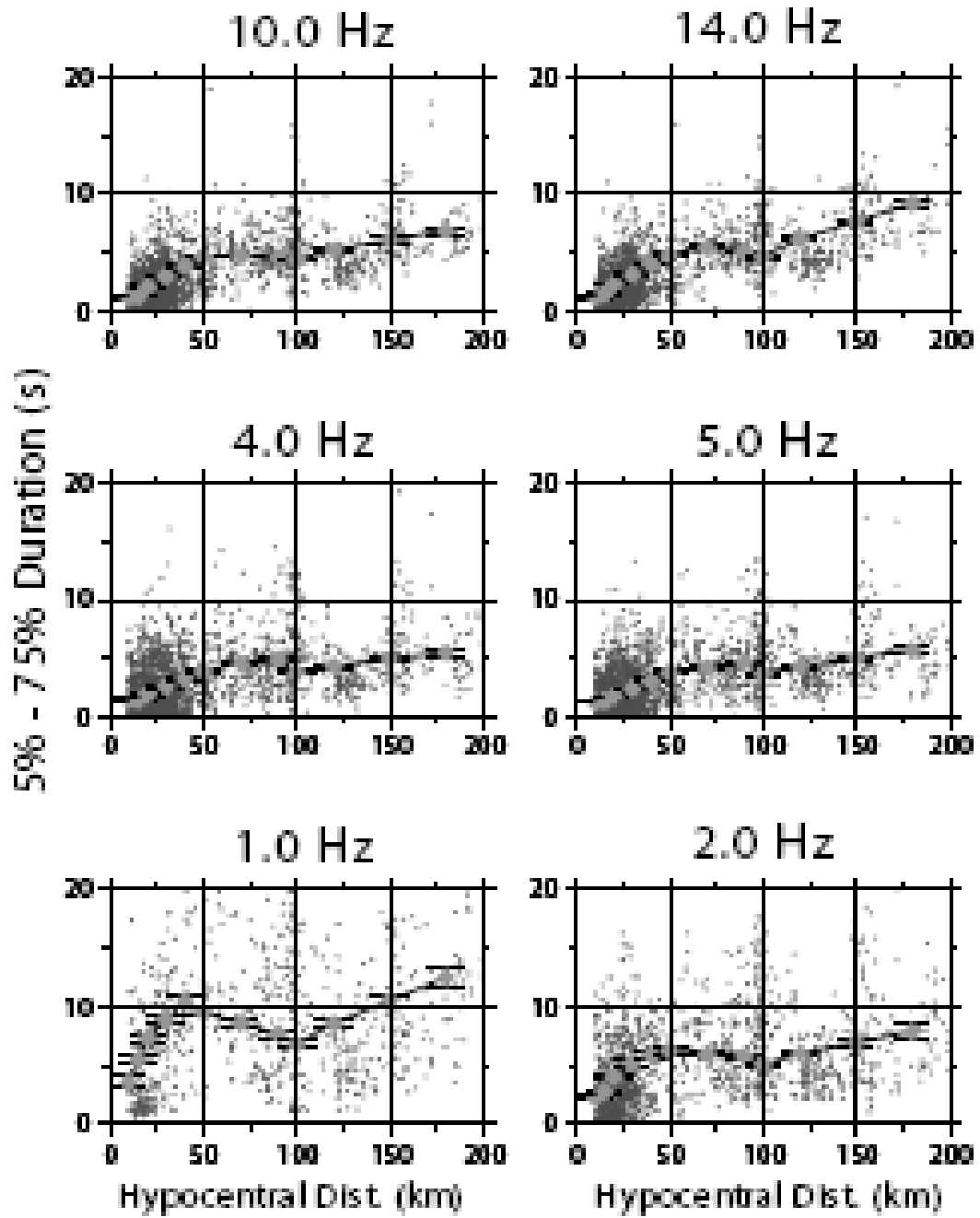


Figure 5.

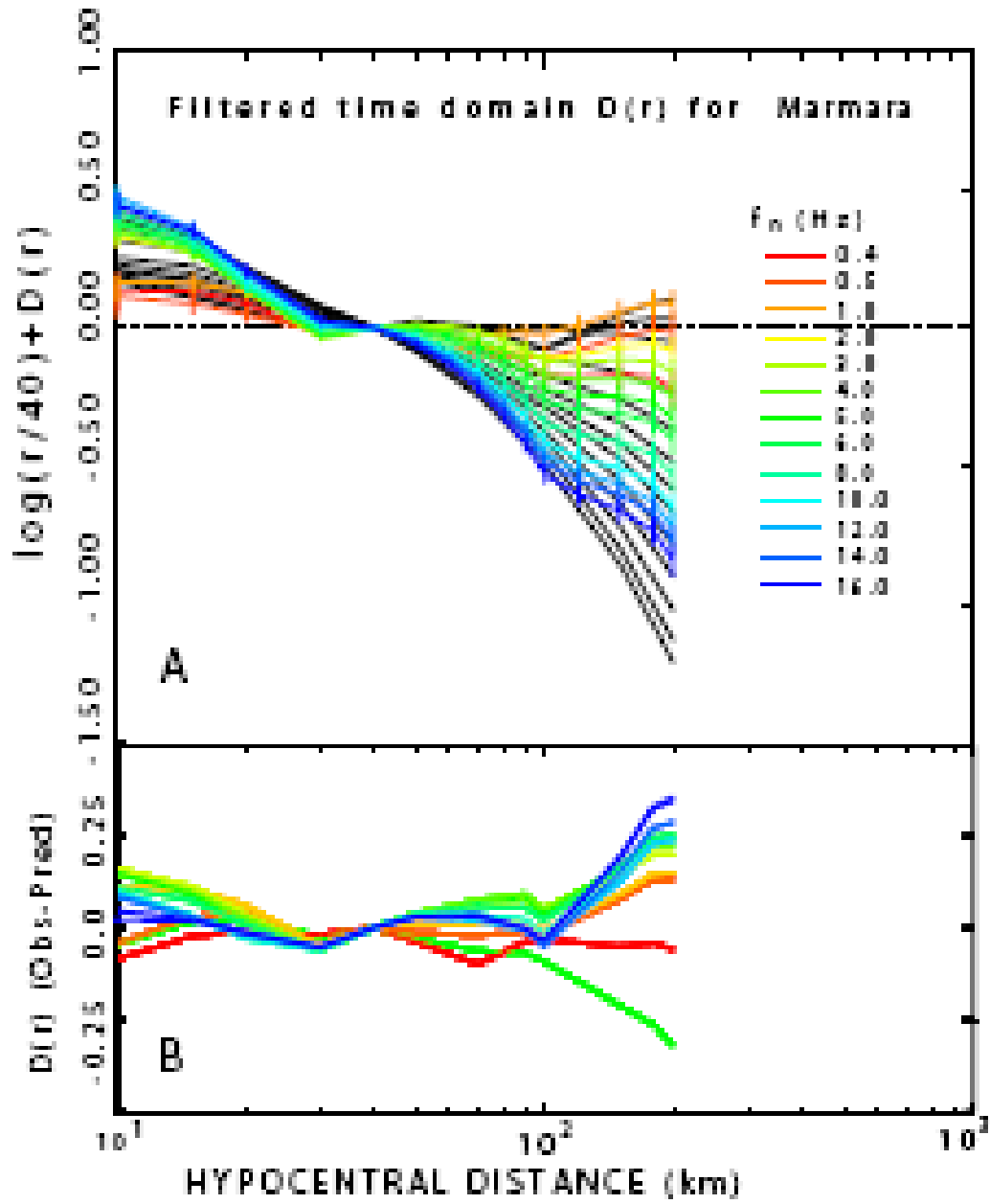


Figure 6.

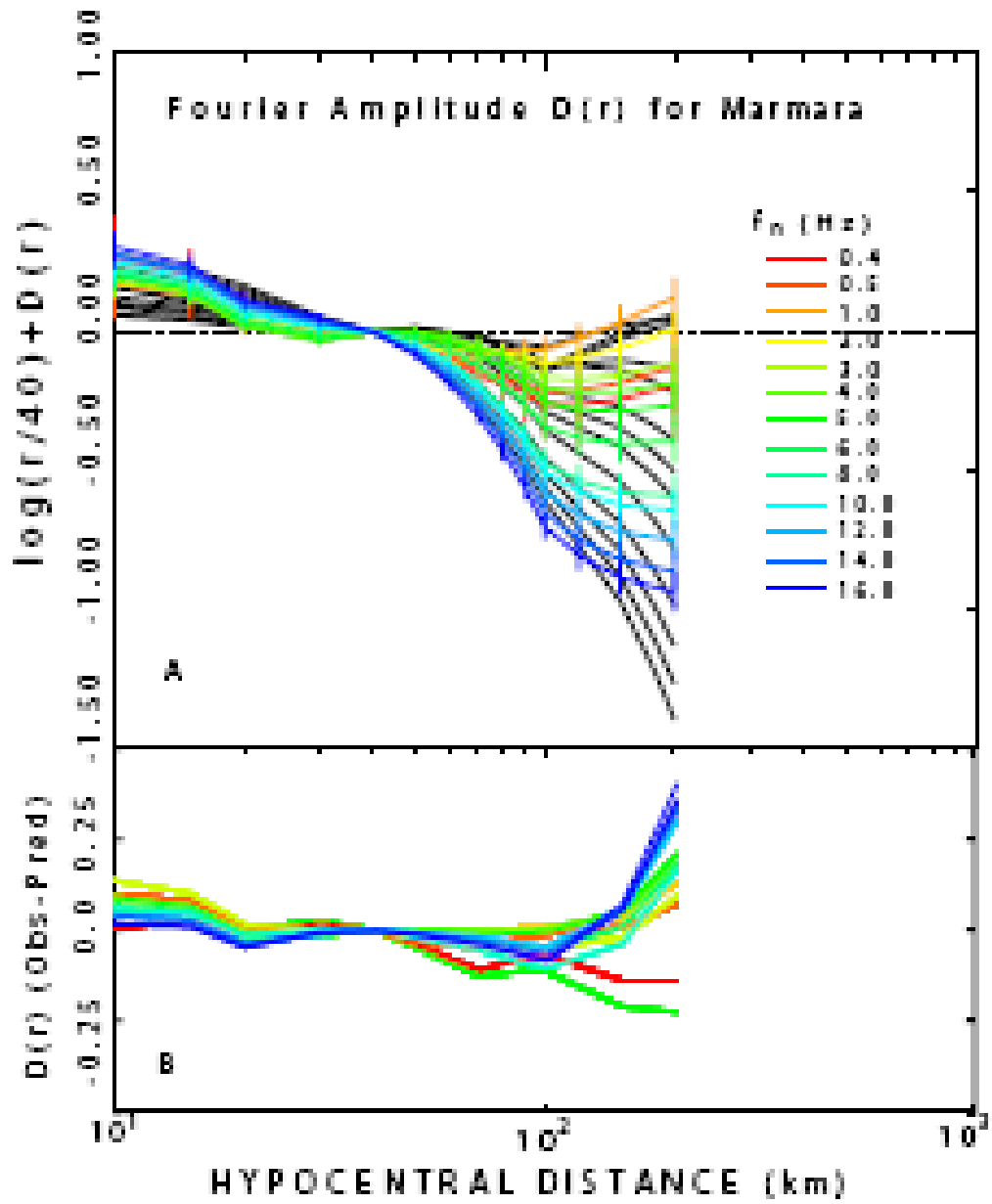


Figure 7.

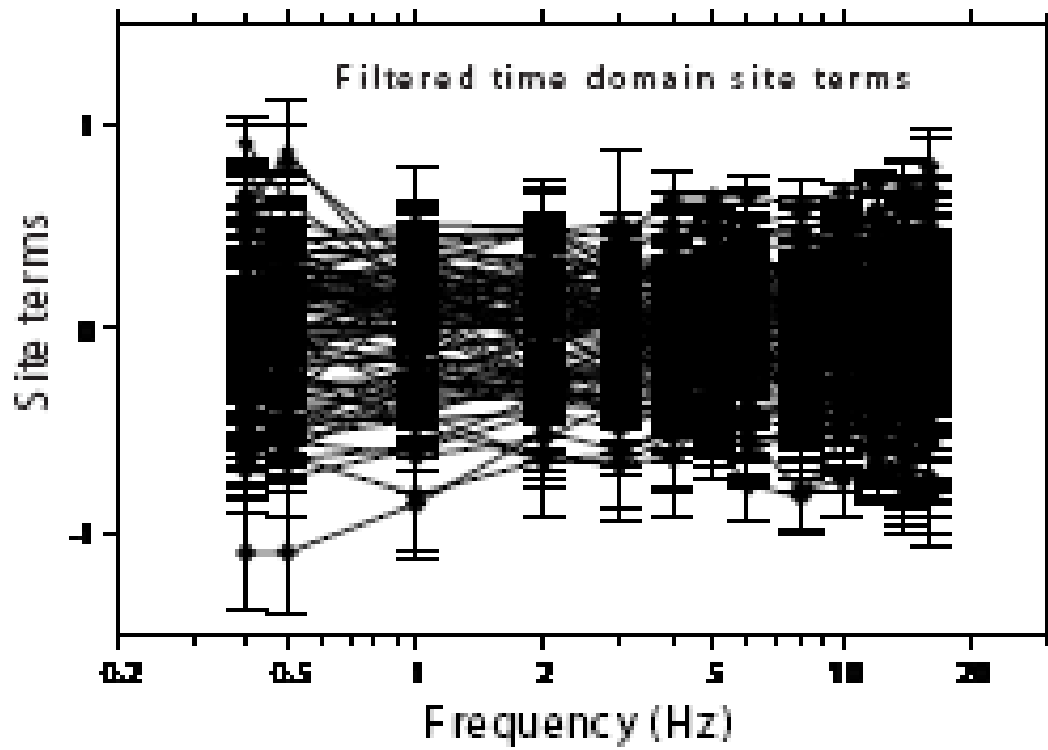


Figure 8.

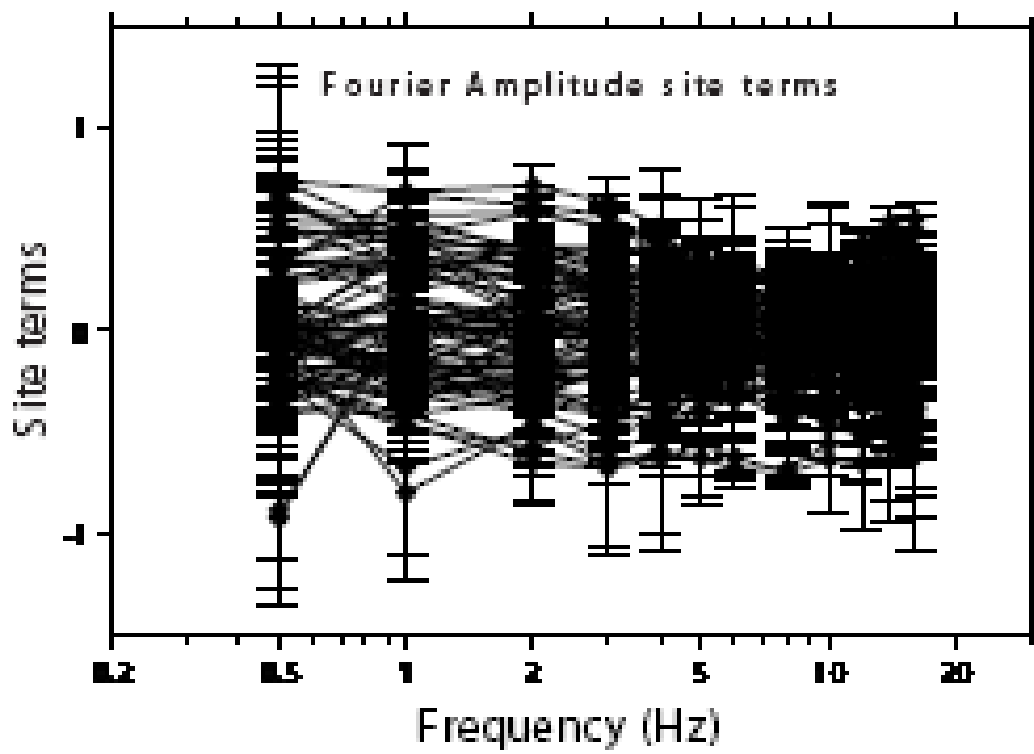


Figure 9.

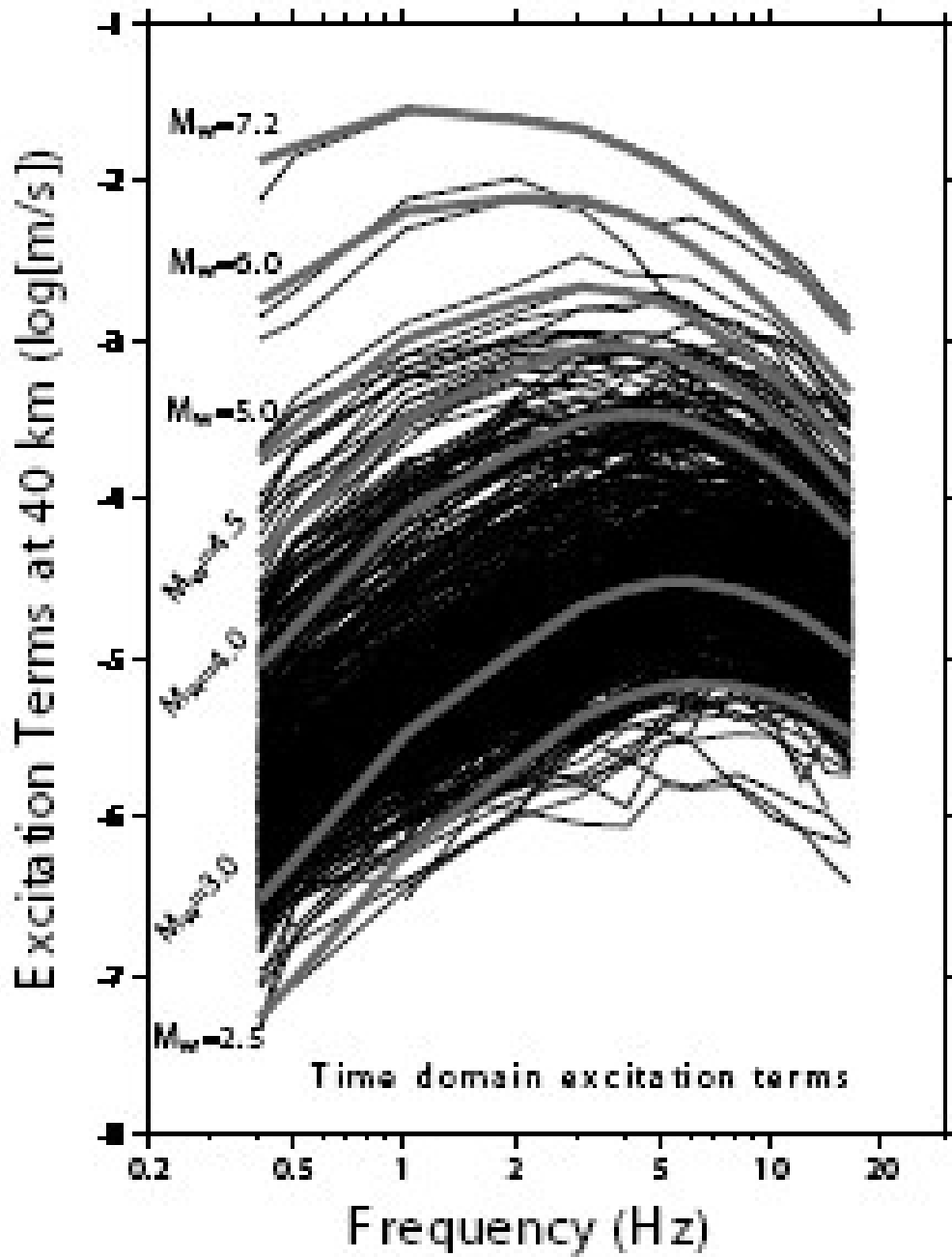


Figure 10.

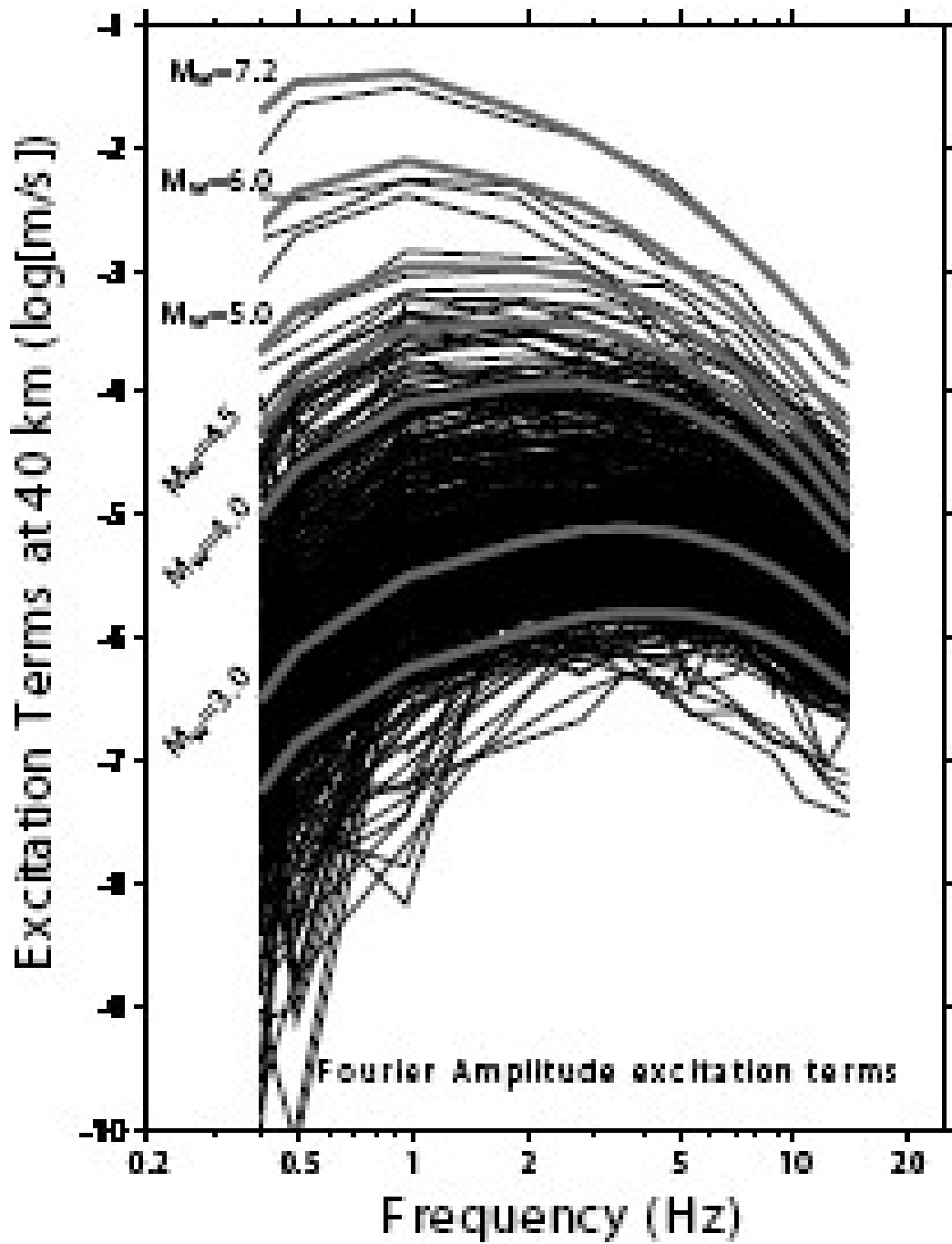


Figure 11.

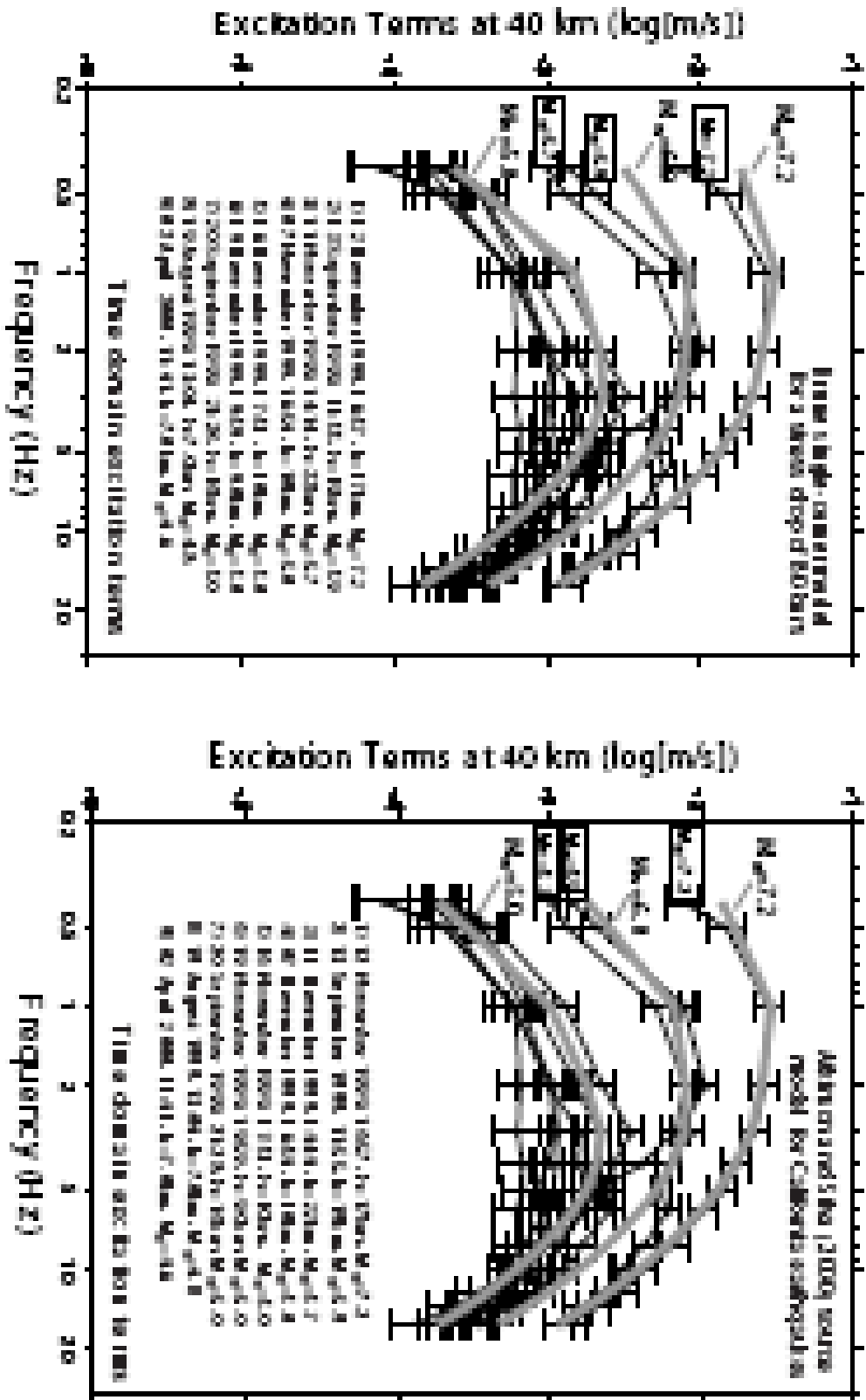


Figure 12.

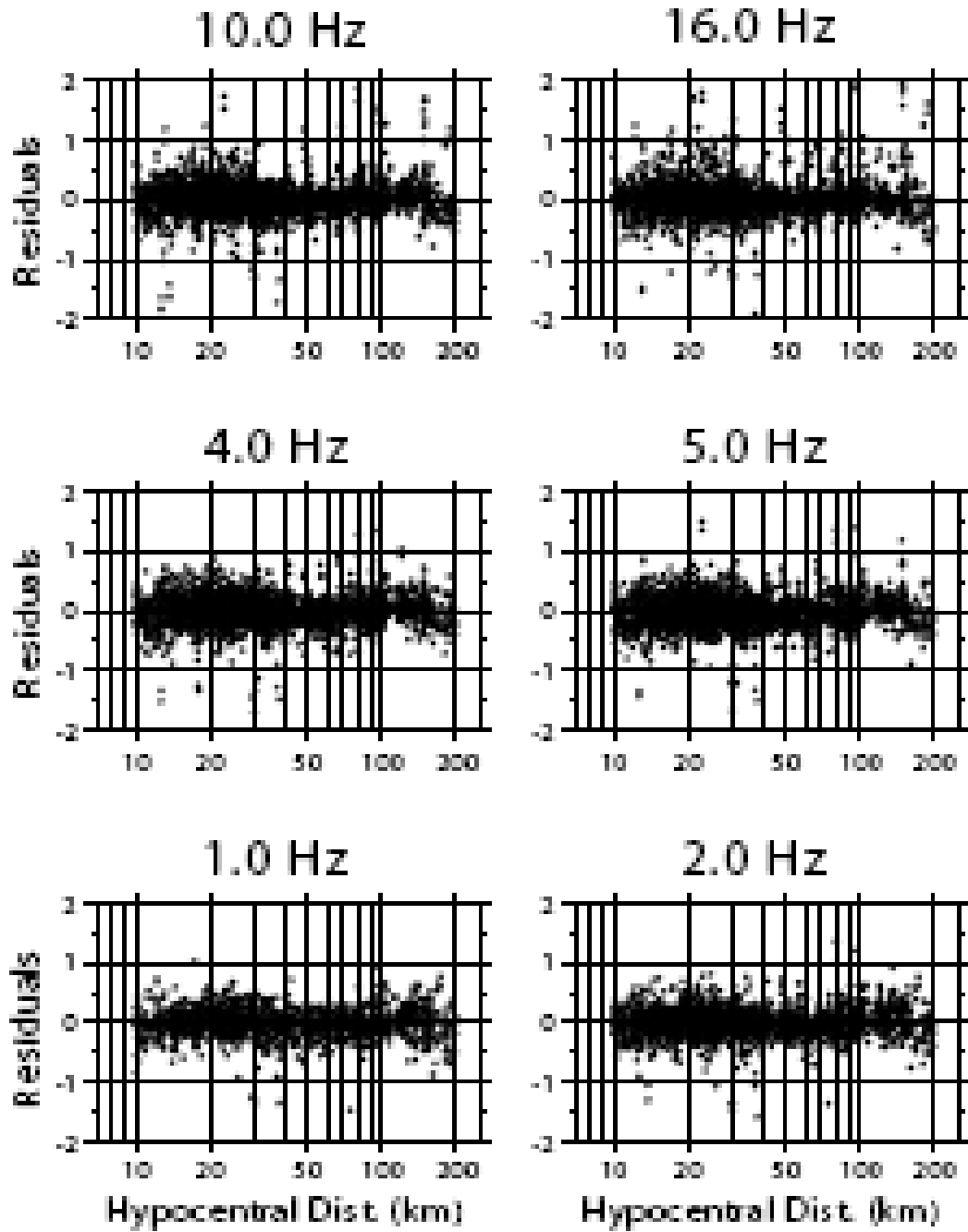


Figure 13.

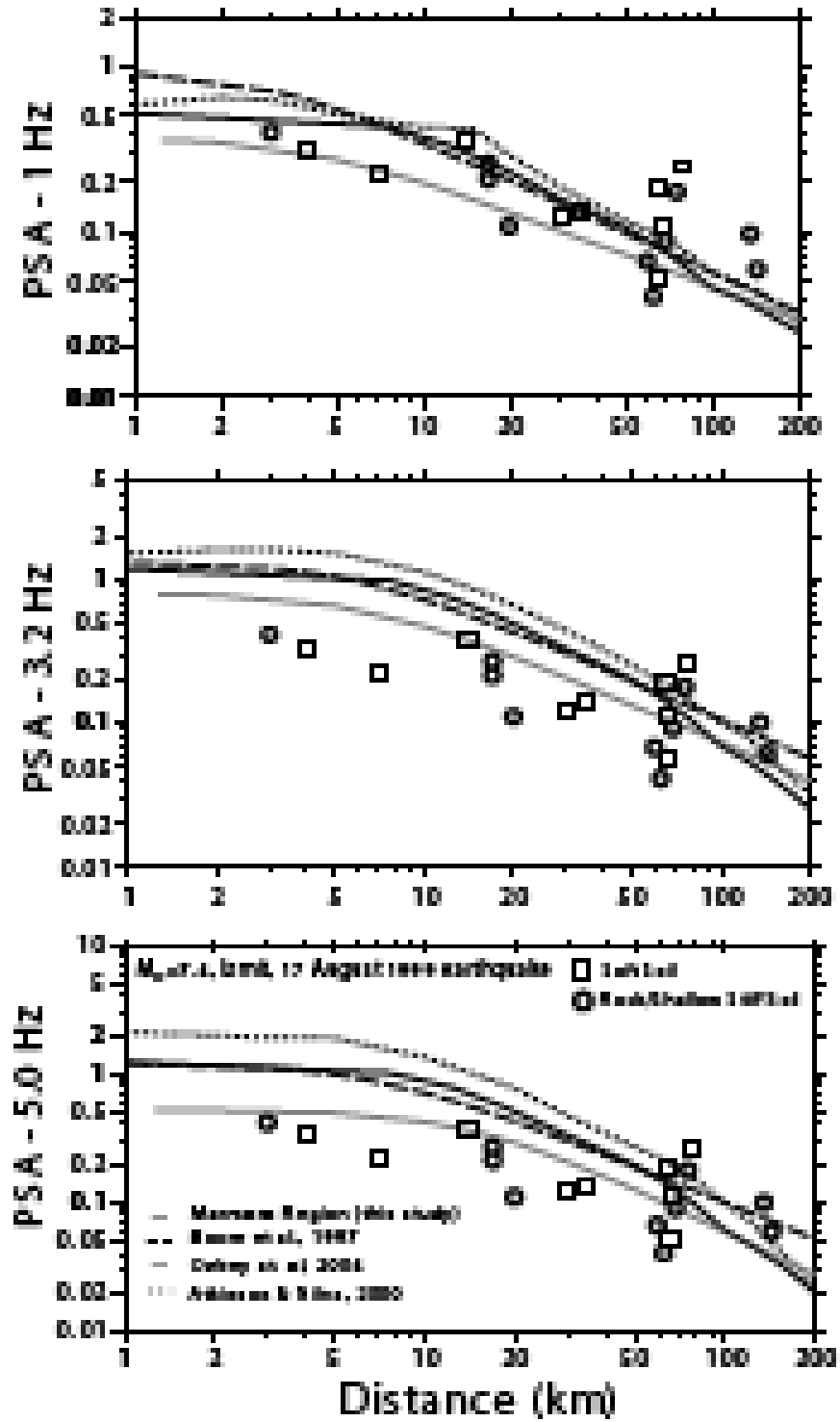


Figure 14.

APPENDIX III

Sørensen, M. B., Oprsal, I., Bonnefoy-Claudet, S., Atakan, K., Pulido, N., Mai, M. M, and Yalciner, C. (in review.): Local site effects in Ataköy area, Istanbul, Turkey, due to future large earthquake in the Marmara Sea. Submitted to the Geophysical Journal International.

Local site effects in Ataköy, Istanbul, Turkey, due to a future large earthquake in the Marmara Sea

Mathilde B. Sørensen¹, Ivo Oprsal^{2,3}, Sylvette Bonnefoy-Claudet^{4,5}, Kuvvet Atakan¹, P. Martin Mai², Nelson Pulido⁶ and Caglar Yalciner⁷

¹Department of Earth Science, University of Bergen, Norway,

²Institute of Geophysics, Swiss Federal Institute of Technology ETH, Zurich, Switzerland,

³Now at Charles University, Faculty of Mathematics and Physics, Department of Geophysics, Prague, Czech Republic,

⁴LGIT, Université Joseph Fourier, Grenoble, France,

⁵Now at Department of Astronomy, Physics of the Earth and Meteorology, Comenius University, Bratislava, Slovak Republic,

⁶Earthquake Disaster Mitigation Research Center EDM, NIED, Kobe, Japan,

⁷Osmangazi University, Eskisehir, Turkey.

Corresponding author: Mathilde Bøttger Sørensen, University of Bergen, Department of Earth Science, Allegt. 41, 5007 Bergen, Norway, Tel: +47 55583412, Fax: +47 55583660, e-mail: mathilde.sorensen@geo.uib.no.

Summary

Since the 1999 Izmit and Duzce earthquakes, many seismic hazard studies have focused on the city of Istanbul. An important issue in this respect is local site effects: strong amplifications are expected at a number of locations due to the local geological conditions. In this study we estimate the local site effects in the Ataköy area (southwestern Istanbul) by applying several techniques using synthetic data (hybrid 3D modelling and 1D modelling) and comparing to empirical data. We apply a hybrid 3D finite-difference (FD) method that combines a complex source and wave propagation for a regional 1D velocity model with site effects calculated for a local 3D velocity structure. The local velocity model is built from geological, geotechnical and geomorphological data. The results indicate that strongest spectral amplifications (SA) in the Ataköy area occur around 1 Hz and that amplification levels are largest for alluvial sites where SA reaching a factor of 2-2.5 can be expected in case of a large earthquake. We also compare our results to H/V spectral ratios calculated for microtremor data recorded at 30 sites as well as ambient noise synthetics simulated using a 1D approach. Because the applied methods complement each other, they provide comprehensive and reliable information about the local site effects in Ataköy. Added to that, our results have significant implications for the southwestern parts of Istanbul built on similar geological formations, for which therefore similar SA levels are expected.

Keywords: Earthquakes, Hybrid method, Strong ground motion, Istanbul, Fault model, Finite-difference methods

Introduction

Istanbul, with a population exceeding 12 millions, is considered one of the worlds mega-cities exposed to a large earthquake hazard. The catastrophic consequences of the two large earthquakes at Izmit and Düzce in 1999 have highlighted the need for careful analysis of seismic hazard including local site effects, although the earthquake hazard in this region has been a topic of considerable interest for a long time. Recent results from several studies (e.g. Atakan et al. 2002,

Erdik et al. 2003, Erdik et al. 2004, Pulido et al. 2004) emphasize the importance of earthquake preparedness and risk mitigation in the Istanbul metropolitan area and its rapidly growing surroundings. The present study addresses the issue of local site effects in this area.

Previous studies of local site effects, following the 1999 Izmit and Duzce earthquakes, have focused mainly on the Avcilar district of western Istanbul (e.g. Özel et al. 2002, Tezcan et al. 2002), and on the city of Adapazari in the east (e.g. Bakir et al. 2002, Komazawa et al. 2002, Sancio et al. 2002, Beyen & Erdik 2004 and Ansal et al. 2004), which experienced significant damage mainly due to site effects. In both areas, the presence of soft sediments in basin structures has caused strong amplifications of earthquake ground motions during past earthquakes.

As for the city of Istanbul, less attention has been paid to the possible effects of local geological variations. In a recent study, Birgören et al. (2004) found amplification levels up to a factor of 7 for some geological formations at 1 and 3 Hz frequencies, based on spectral ratios of records from a M=4.2 earthquake.

The main objective of this study is to estimate the local site effects in the Ataköy district of the Bakirköy Municipality, which lies to the east of the Atatürk international airport in southwestern Istanbul. In general, the area is geologically representative of the southwestern part of Istanbul (Figure 1), and the results therefore give an insight into the site conditions in this larger-scale area. An important argument for focusing on this area stems from recent results of ground motion modelling (Pulido et al. 2004) where the highest ground motions due to a scenario earthquake in the Marmara Sea are expected in the southwestern part of Istanbul (Figure 1b). This trend is also supported by probabilistic seismic hazard results for this area, predicting the highest seismic hazard in the southern parts of the city due to the close vicinity to the North Anatolian fault (Atakan et al. 2002). In addition to that, the area is densely populated, including critical facilities such as the Atatürk international airport and several industrial installations.

In this study, we apply three parallel approaches for assessing the local site effects in the Ataköy region. Since our final goal is to understand the site effects in three dimensions, we use a hybrid FD procedure to calculate spectral amplification due to a 3D velocity-density model representing of the Ataköy area. In order to improve this model and obtain further insight into the local variations of site effects, H/V spectral ratios are calculated for recorded microtremor data and compared to H/V spectral ratios for synthetic ambient noise data using 1D geological models.

The applied hybrid 3D FD procedure for calculating spectral amplifications (Opsal & Zahradnik 2002, Opsal et al. 2002) combines source, path and site effects in two consecutive steps. In the first step, input ground motions for bedrock conditions are modelled based on a target scenario earthquake for a regional 1D structure (Pulido et al. 2004). In the second step, a 3D FD scheme is used for calculating the spectral amplifications within the study area for a local 3D velocity structure. The procedure is capable of computing the full 3D wave field propagation. The resulting ground motion and corresponding SA factors (related to a bedrock site) cover the local area through surface receivers placed on a fine square grid. This kind of modelling and comparison provides a comprehensive picture of the site effects, although uncertainties in the input geological model may limit the final result.

The H/V spectral ratio method (or ‘Nakamura method’) (Nakamura 1989, Nakamura 2000) is a well-established method for fast and cost-efficient estimation of site effects. The limitations of the methodology are studied in detail in previous review papers (e.g. Lachet & Bard 1994, Atakan 1995, Kudo 1995, Mucciarelli 1998, Mucciarelli et al. 2003, Atakan et al. 2004a.). General consensus is that when the method is applied under careful experimental conditions (i.e. type of the

instruments used, measurement details with regard to the sensor coupling, surface conditions, external factors such as wind, rain etc., and the processing techniques used for analysis), fundamental frequencies on which the amplifications occur can be reliably assessed. However, the method is less reliable for the absolute amplification factors.

Synthetic noise data based on 1D models representative of the Ataköy area provide additional information about the effect of varying structures on the site amplification, and thus helps in interpreting the microtremor results. The method used to model the synthetic noise has recently been developed for more systematic investigation of the H/V spectral ratio method (Bonney-Claudet et al. 2004), however, the simulated noise also provides an input for studies of the effect of different velocity structures on the H/V ratio. As opposed to other analytical methods for estimating the ground response such as with one-dimensional layered damped soil on elastic bedrock using earthquake records (e.g. SHAKE, Schnabel et al. 1972), the method used in this study takes advantage of the noise wavefield and therefore provides a more appropriate basis for correlating the empirical results from the H/V spectral ratios.

Due to the differences in their uncertainties, the applied methods complement each other well, and in combination give a reliable estimate of the local site effects in the Ataköy area.

Geological setting and site selection

The metropolitan area of Istanbul is underlain by Paleozoic bedrock outcropping in the northern part of the city (north of Golden Horn) and alluvial systems of Quaternary age that dissect into the bedrock (Figure 1a). In the southwestern part of the city, on the other hand, weaker geological formations are dominating such as the Bakirköy and Güngören formations, with significant interplay of alluvial and delta systems. Taking into account this broad perspective, our attention is focused on the southwestern part of Istanbul, where the strongest local site effects are expected.

In general, dominating geological formations in southwestern Istanbul are the Bakirköy and Güngören formations, which are both of upper Miocene age. The Bakirköy formation is composed of alternating layers of limestone, marl and clay, whereas the Güngören formation consists of green coloured plastic clay, marl and clayey siltstone. These are also the dominating formations in the target area for this study, the Ataköy district. Figure 2 shows a detailed geological map of the Ataköy area. In addition to the Bakirköy and Güngören formations, the Kuldili formation of Quaternary age outcrops in a limited area and is composed of clay with molluscs, silt and mud. The overlying alluvial deposits (Quaternary) are the result of fluvial activity and consist of unconsolidated sediments composed of gravel, sand, silt and clay. In some parts of the area, construction material is dumped over the alluvium, overlain by a thin layer of gravel (20-30cm) and filled with soil on top (40-50 cm). The total thickness of these deposits is approximately 2-3 meters.

Our study focuses on the Bakirköy and Güngören formations because of their large spatial extent, as well as on the alluvium where strong site amplifications are expected to occur.

3D modelling of local site effects

The frequency-dependent ground response in the Ataköy area, due to a finite-extent source, regional-model path effects, and detailed local structure, is calculated using the hybrid FD procedure of Oprsäl & Zahradnik (2002) and Oprsäl et al. (2002). We use the hybrid formulation to model the complete wavefield because direct FD computations for a frequency range of engineering interest are too demanding in terms of computer memory and time. As for the methods used for the wave propagation modelling in complex 3D media, an FD method is considered one of the most

appropriate means for complete wave field simulation because of its simplicity, stability and relatively simple implementation. To decrease the time and memory demands, our hybrid method computes the wave field by FD in a local model containing complex 3D structure embedded in a (usually simpler and smoother) regional-structure medium. Combination of the source, path and local site effects in a two-step procedure (Figure 3), was first introduced by Alterman & Karal (1968) for representation of a seismic source in 2D simulation. The present method is a 3D/3D FD version, which is described in detail in Oprsal & Zahradnik (2002), Oprsal et al. (2002) and Oprsal et al. (2005). Here we only give a short summary.

In the first step, ground motion time series are calculated for receivers covering the surface of a double-planed box (called excitation box (EB)) surrounding the local site of interest. These calculations, for a seismic source placed outside the EB, are performed for a regional crustal velocity model with an outcrop V_s of 2.0 km/s, using the methodology of Pulido et al. (2004). This is based on a procedure combining a deterministic simulation at low frequencies (0.1-1 Hz) with a semi-stochastic simulation at high frequencies (1-10 Hz). A finite-extent scenario earthquake source embedded in a flat-layered 1D velocity structure is assumed. The source consists of a number of asperities, which are divided into subfaults assumed to be point sources. The total ground motion at a given site is obtained by summing the contributions from the different subfaults. For the low frequencies, subfault contributions are calculated using discrete wave number theory (Bouchon 1981) and summed assuming a given rupture velocity. At high frequencies, the subfault contributions are calculated using the stochastic method of Boore (1983) and summed using the empirical Greens function method of Irikura (1986). The radiation pattern is changed from a theoretical double-couple radiation pattern at low frequencies to a uniform radiation pattern at high frequencies following Pulido & Kubo (2004). The resulting wavefield for receivers on the EB is saved on disk.

In the second step, we perform a hybrid wave field injection of the excitation computed in the 1st step into the 2nd step 3D FD method. The 3D FD modelling now comprises detailed local structure and occupies only a small fraction of the model size considered in the first step. This approach benefits from the efficiency of the less demanding source-and-path-effects methods while exploiting the wave field completeness of the FD method. Thus final response contains the combined effects of source, path, and site effects while the memory and time requirements are still in realistic bounds.

The hybrid coupling keeps the excitation boundary fully transparent in the second step. The scattered wave field penetrates freely out of the EB and, if reflected by an inhomogeneity, it freely propagates through the EB back into the local structure. The same applies for possible new sources added in the second (FD) step (Oprsal & Zahradnik 2002, Oprsal et al. 2002, Oprsal et al. 2005).

The scenario earthquake used in the first step of the calculations is a slight modification of the worst-case scenario for the city of Istanbul defined by Pulido et al. (2004), which assumes a combined rupture of the two segments of the North Anatolian Fault in the Marmara Sea (total fault length 130 km) in a $M=7.5$ earthquake with rupture initiation in the westernmost end. Fault asperities are located in the central part of the rupturing fault, close to the boundary between the two fault segments, considering the seismicity in the area. Stress drop is calculated using the results of Das & Kostrov (1986) to 50 bar (background) and 100 bar (asperity), whereas rise time (3s) and rupture velocity (varying randomly between 2.8-3.2 km/s) are based on the values for the 1999 Izmit earthquake. We use the 1D regional crustal velocity model, which is used for routine earthquake location in the Marmara Sea region (Sarif Baris, personal communication, 2003). From this scenario earthquake, the ground motions were calculated on a coarse regular grid covering the Marmara Sea area.

As input for the second step of the computations, a densely sampled wavefield on the excitation box is needed. This was obtained by interpolating the above described coarse-grid regional simulation result. In order to avoid aliasing effects when creating the densely sampled wavefield (spacing 0.25 m) from the coarsely gridded input data (spacing 10 km) we used a Fourier-domain resampling approach. Waveforms were first aligned with respect to propagation direction using a cross-correlation approach, and then spatially interpolated on to the fine grid. The time-shifts for the input waveforms were interpolated to the fine grid as well, and then used to undo the waveform alignment.

The local 3D geological model is based on available geological, geotechnical and geomorphological data. The data sources are microtremor measurements, standard penetration test (SPT) data, cone penetration test (CPT) data, geological and geomorphological maps and empirical relations for rock characteristics (Schön 1996). The geometry of the model is determined from the geological and geomorphological maps of the area, and a number of assumptions have been made. The surface geometry is shown in Figure 4 together with the locations of recording sites and boreholes. The alluvial layer in the model is maximum 5 m thick in all places except under the sea where it reaches 10 m. The alluvium is assumed to be deposited in the depression caused by erosion of the Bakirköy formation due to fluvial activity (i.e. there is no change of the Bakirköy formation base under the alluvium). The Bakirköy formation is 20 m thick, thinning northwards as it erodes at the surface. In the eastern part of the model, the formation is slightly thicker in order to incorporate the increased elevation. The Güngören formation is 80 m thick, thinning in places where erosion occurs. A number of EW cross-sections of the resulting model are shown in Figure 5, and in Figure 6 is shown elevation maps of the different layers in the model.

The velocity model of the area is built on the geological model and gives V_p , V_s and density as a function of depth. Quantification of the velocities for the 3D grid is based on the formulae given in Table 1. For the alluvium, a low surface velocity and a low depth gradient is used. The chosen velocity is consistent with a NEHRP class E soil (soft soil) at the surface compacting to a class D soil (stiff soil) at 10 m depth. For the Bakirköy and Güngören formations, low surface velocities are chosen. For the upper 5 m there is a large velocity gradient for these formations, whereas the gradient is much lower for depths larger than 5 m. The low surface velocities and high gradient for the uppermost meters are included to take into account the strong weathering taking place at the surface. For the bedrock, the velocity structure is chosen in order to be consistent with the velocity model used in step 1 of the modelling (Pulido et al. 2004) at depths larger than 150 m.

The dimensions of the site of interest, given by the geological model, are 3360 m and 2219 m in the EW and NS directions, respectively, and approximately 180 m in depth. The S-wave velocities V_s are between 260 m/s and 2100 m/s, and maximum P-wave velocity $V_p = 3600$ m/s. These high variations in material parameters impose strong demands on the computational part of the FD problem. The influence of the water layer is neglected, which is supposed not to be playing a major role in the resulting wave field since it is only present in the very southernmost part of the model. Therefore FD computation of the site effects was performed on a vertically irregular grid with grid steps being 1.5 m in the vicinity of the free surface and 21 m in deeper parts of the model. The horizontal spacing of the grid is 2.5 m and remains unchanged through the whole visualized part of the model because of the spatial distribution of low-velocity riverbeds. However, to minimize the spurious reflections, the model was extended to each side and depth by 70 grid points where the grid step increases towards the edges of the computational model. At this part, where the known model is extended, we gradually decrease the depth of the interfaces and increase the grid step. To decrease spurious reflections, we apply tapers (Cerjan et al. 1985) at the strip of 50 grid points breadth around the edges, and non-reflecting boundaries at the edges of the computational model

(Emerman & Stephen 1983). The PML technique was taken into consideration in place of non-reflecting boundaries, however, these are too computationally demanding in our formulation. The frequency band is 0-8 Hz and the time step determined from the minimum ratio of $DX(x,y,z)/(1.6*Vp(x,y,z))$ is $DT= 4.0 \times 10^{-4}$ s. The computational model dimensions, further extended by the taper zones, are then 4600 m and 3500 m in the EW and NS directions, respectively, and approximately 1500 m in depth. The total number of the grid points is 1.5×10^8 , occupying approximately 5.9 GB of core memory, which is on the edge of reasonable time demand for a 2-processor PC. Because of very modest topography, the model in the computations has a flattened free surface. The flattening shifts the vertical structural profile under each point on the free surface so that such a profile remains unchanged.

To provide a more complete picture of the site ground motions on potential buildings, we give the results in the spectral amplification. The spectral amplification factors for pseudo acceleration response (PSA) depending on the frequency are shown in Figure 7a. Shown PSA factors cover the whole area and they are computed as ratio of 5%-damping spectral responses computed for the 3D and 1D (bedrock) models, respectively. The maximum PSA amplification for the alluvial sites is almost 2. For frequencies up to 1 Hz, there is a significant peak in the PSA amplification. A more pronounced amplification can be expected for frequencies between 10-20 Hz due to the shallow low-velocity deposits.

To compare the 3D FD modelling with a possibly more sophisticated 1D linear method, we performed a series of approximately 3×10^5 1D-structure-response computations (Mueller 1985) for points regularly distributed on the free surface. The 1D structure for each point was exactly the same as the vertical profile under such a point in the 3D model, hence pseudo 3D modelling. The code for 1D response computation in layered media was adopted after Bartak & Zahradnik (1991). The PSA factors are shown in Figure 7b. The maximum amplification for the alluvial systems is approximately 1.5. The significant amplification at these sites is well visible for all frequency bands, which is the main difference between the 1D and 3D response computation.

H/V spectral ratios of microtremor data

Recorded microtremor data give the opportunity of assessing the fundamental frequency at a given site based on the H/V (horizontal to vertical component of the recorded signal) spectral ratio technique (also known as "Nakamura method") (Nakamura 1989, Nakamura 2000, Lermo & Chávez-García 1993). The method is extensively used in microtremor studies throughout the world. The method is discussed in detail in previous studies and the reader is referred to the literature on this topic. Some recent discussions are given in Atakan et al. (2004a, 2004b), Guillier et al. (in prep.) and Chatelain et al. (in prep.).

The H/V spectral ratio method is based on the assumption that amplification of microtremor ground motion, mainly consisting of Rayleigh wave energy, due to the presence of a soft surface soil layer only occurs for the horizontal component of ground motion. Under this assumption, the vertical component of ground motion can be used to remove source and path effects from the signal and isolate the effect of the site (Lermo & Chávez-García 1993). The microtremor recordings are transformed into the frequency domain and the horizontal spectrum is divided by the vertical spectrum. The resulting spectral ratio gives frequency dependent amplification for the site.

In spite of the known limitations of the method, various sets of experimental data (e.g. Field & Jacob 1993, Duval et al. 1994, Duval et al. 1995, Field et al. 1995, Larchet et al. 1996, Gitterman et al. 1996, Fäh et al. 1997, Lebrun et al. 1997, Riepl et al. 1998) confirm that the spectral ratios are much more stable than the raw noise spectra and exhibit a clear peak at soft soil sites, which is well

correlated with the fundamental resonance frequency. These observations are supported by several theoretical investigations (Field & Jacob 1993, Lachet & Bard 1994, Lermo & Chavez-Garcia 1994, Bonnefoy-Claudet et al. 2004), showing that synthetics obtained with randomly distributed, near surface sources lead to H/V ratios sharply peaked around the fundamental S-wave frequency, whenever the surface layers exhibit a sharp impedance contrast with the underlying stiffer formations.

During a field campaign in the Ataköy area, microtremor data were collected at 30 sites (Figure 2). The sites were located mainly on the alluvium and the Bakirköy formation. Site selection was based on avoiding too much man-made noise and at the same time obtaining good coupling of the sensor to the ground. At each site, a minimum of 3 x 10 minutes of seismic noise was collected continuously using the GBV-316 (GeoSIG) portable digital seismographs. Each seismograph contains a 16-bit digitizer and a 4.5 Hz 3-component built-in sensor. The technical specifications of the instruments used were tested extensively through previous studies (Atakan et al. 2004a) and have a resolution down to 0.5 Hz (also down to 0.3 Hz under specific conditions). Communication was done using the Seislog data acquisition software developed for Pocket PC (Ojeda et al. 2004).

Data were processed using the recently available software J-SESAME (Atakan et al. 2004b), developed for calculation of H/V spectral ratios. An automatic window selection module is included, which filters out noisy time windows by applying an anti-trigger algorithm based on the STA/LTA ratio (short term average divided by the long term average of the signal amplitudes). The data are organized according to the recording sites and average H/V spectral ratios are computed using standard processing techniques (Atakan et al. 2004b).

The H/V spectral ratios calculated for sites on the Alluvium and Bakirköy formation are presented in Figures 8 and 9, respectively. For the alluvial sites (Figure 8), a strong peak is observed around 1 Hz. An additional, more diffuse peak is indicated around 3-6 Hz. For the Bakirköy formation (Figure 9), there is again a clear peak around 1 Hz whereas no peaks are observed for higher frequencies. This indicates that the 3-6 Hz peak observed for the alluvium is an effect of the alluvial layer, whereas the 1 Hz peak is caused by deeper lying formations.

In a previous study by Eyidogan et al. (2000), microtremor recordings were collected at a few sites in the Ataköy area (Figure 4). H/V ratios for these data, recorded mainly on alluvial deposits, are in agreement with the results obtained in the present study.

1D modelling of ambient noise

In order to check the H/V spectral ratio results for the recorded microtremors, ambient noise was simulated using 1D models representative of sites in Ataköy. H/V spectral ratios for the simulated noise were then calculated for comparison with the H/V spectral ratios of the recorded microtremors. The noise simulations were performed as described by Bonnefoy-Claudet et al. (2004), simulating noise originated by human activity for sites with heterogeneous subsurface structure. In this study, all sites are considered as 1D structures, and the Green's functions for the medium are calculated using the method of Hisada (1994). H/V spectral ratios for the synthetic noise were calculated using the J-SESAME software as described for the recorded microtremors.

Ambient noise was simulated for three sites representative of an alluvial site, a site on the Bakirköy formation and a site on the Güngören formation. The 1D structures of the sites are taken from the 3D model used for 3D FD simulations. The velocity profiles for the 1D sites were simplified so that each layer has a constant velocity to obtain reasonable computation times. The composition of these

sites is illustrated in Figure 10 and the velocities are given in Table 2.

For each site, noise sources were modelled as point forces with delta-like source time functions located at fixed depths (4 and 8 m) and distributed randomly in space, direction, amplitude and time. Convolving Green's functions calculated by the method of Hisada (1994) gave synthetic noise representative of the three sites.

The resulting H/V spectral ratios are shown in Figure 11. The significant peak around 1 Hz observed for the recorded microtremors is present also for the model results, however the amplitude of the peak is significantly smaller. In addition, a very significant peak is present for the alluvial site (site 1) at higher frequencies. This peak is probably related to the 3-6 Hz peak observed for the recorded microtremors, though shifted towards higher frequencies. Such a shift may be caused by the assumed shallow depth of the alluvial layer, which may be thicker in reality. Amplification levels are in agreement with those for the recorded microtremors, except for the mentioned reduction of the 1 Hz peak, which is probably due to the reduced complexity in the modelling.

Comparison and discussion

Individual results obtained from the empirical data and their comparison to 1D and 3D synthetic modelling show the following common features:

- 3D synthetic results give an insight to the complexity of the site response, especially for higher frequencies where lateral variations become more visible. In this respect the response of the alluvium is clearly visible at frequencies higher than 2 Hz.
- Regarding the frequency content of the site effects, the clear peaks observed in the microtremor data around 1 Hz are comparable to 1D and 3D synthetic results. This peak value is in good agreement with what might be expected from the soil thickness using the relation $f_{\text{peak}} = v_{s,\text{ave}}/4H$ where $v_{s,\text{ave}}$ is average S-wave velocity and H is thickness of the soil layer.
- The different methodologies predict different values for the amplification factors. The noise-based methodologies (recorded microtremors and 1D modelling) have significantly higher amplification levels when compared to the synthetic 3D data.
- Our results from the 3D modelling, based on a simulated strong ground motion (scenario earthquake of magnitude 7.5 in the Marmara Sea) predict amplification factors around 2. This is significantly lower than our results from microtremor data and previous results on weak motion data (Birgören et al. 2004).
- In addition, amplification factors are lower for the synthetic 3D data relative to the microtremor measurements since the real structure is definitely more complicated than our models, resulting in a poorer wavefield in terms of scattering for the modelling.
- Based on the above, it is recommended that site effects in the Ataköy area should be taken into account in any future application towards earthquake risk mitigation. Our results indicate that for a target earthquake of magnitude 7.5 in the Marmara Sea, a minimum amplification factor of 2 within the frequency band of 0.5-1.5 Hz is expected.

The study area is covered mainly by the Bakirköy formation, which consists of alternating layers of limestone, marl and clay of Upper Miocene age. This formation is quite fragmented and altered at the surface. The underlying Güngören formation has similar characteristics with respect to the lithology. The alluvium, on the other hand, represents the most critical unit in terms of site amplifications and is limited to the fluvial depositional centres. The vicinity to the coast of the area influences the lithological characteristics of both the sediments and sedimentary rocks. The gentle topography of the area, with shallow synclines and anticlines plunging towards the Marmara Sea in

the south, represents an environment, which is significantly different from classical alluvial valleys or closed sedimentary basins. In this respect, the expected site effects also differ significantly. Modelling such an environment in 3D presents several challenges with respect to the seismic velocities and their lateral variations. The 3D model outlined in this paper therefore introduces significant constraints in seismic wave propagation. In many respects the model resembles to a simplified 2D approximation due to the “open-ended architecture” of the system where the lateral extent of the sedimentary units are continuous over large distances. The 3D FD computation of PSA amplification shows a remarkable resemblance to the 1D pseudo 3D method.

Despite the uncertainties in the input 3D velocity model for the FD simulations, results are in good agreement with the H/V spectral ratio results based on recorded microtremor data. The fact that independent studies based on completely different data and methodologies give results in agreement supports the validity of conclusions drawn from these results.

Implications and conclusions

In this study, local site effects in the Ataköy district of western Istanbul have been studied using three different approaches. A hybrid FD method was applied to calculate amplification levels on a fine grid covering the entire Ataköy area based on a local geological model. This modelling indicates that amplification levels are highest for the alluvial sites, where amplification up to a factor of two is predicted. H/V spectral ratios of recorded microtremors were determined, and revealed a dominating peak of amplification around 1 Hz for the whole area. For the alluvial sites a more diffuse secondary peak was observed at 3-6 Hz frequencies. These ratios were compared to H/V ratios calculated for synthetic noise at three sites representative of Ataköy, and the dominant 1 Hz peak was confirmed.

Based on the above discussions it is clear that site effects in the Ataköy area will have significant consequences in case of future large earthquakes in the Marmara Sea. However, other factors such as construction practices, density of building stock and proximity to alluvial sediments will play an important role, especially when taking into account the frequency variations of the site effects. Our results are naturally valid only for the Ataköy area, however the similarity of the geological formations in the neighbouring Bakirköy and Zeytinburnu districts may give an insight to possible consequences in these highly populated areas in Istanbul. The similarity of the studied region to the surrounding areas makes it possible to use the present results in a broader context, concerning the importance of local site effects in southwestern Istanbul.

Acknowledgements

The present work was carried out as part of the EC project RELIEF (EVG1-CT-2002-00069). We are grateful to Serdar Akyuz and other staff and students at Istanbul Technical University (ITU) for their logistic help and housing during the field campaign. ITU kindly provided the geological, geotechnical and geomorphological data used in this study. This is contribution # 1386 of the Institute of Geophysics, ETH Zurich.

References

- Alterman Z. & Karal F.C., 1968. Propagation of elastic waves in layered media by finite-difference methods. *Bull. Seismol. Soc. Am.*, 58, 367-398.
- Ansal, A., Laue, J., Buchheister, J., Erdik, M., Springman, S.M., Studer, J. & Koksal, D., 2004. Site characterization and site amplification for a seismic microzonation study in Turkey, *Proceedings of the 11th Intl. Conf. on Soil Dyn. & Earthquake Engng. (11th ICSDEE) & the 3rd Intl. Conf. on Earthquake Geotech. Engng. (3rd ICEGE), January 7-9, Berkeley, CA*, pp. 53-60.
- Atakan, K., 1995. A review of the type of data and the techniques used in empirical estimation of local site response, *Proceedings of the "Fifth International Conference on Seismic Zonation", October 17-19, 1995, Nice, France, Ouest Éditions, Presses Académiques, Vol. II, 1451-1460.*
- Atakan, K., Ojeda, A., Meghraoui, M., Barka, A.A., Erdik, M. & Bodare, A., 2002. Seismic hazard in Istanbul following the 17 August 1999 Izmit and 12 November 1999 Düzce earthquakes, *Bull. Seismol. Soc. Am.*, 92, 466-482.
- Atakan, K., Duval, A.-M., Theodulidis, N., Guillier, B., Chatelain, J.-L., Bard, P.-Y. & the SESAME-team, 2004a. The H/V spectral ratio technique: Experimental conditions, data processing and empirical reliability assessment, *Proceedings of the 13th World Conference on Earthquake Engineering, Vancouver, Canada, 1-6 August, 2004*, paper no. 2268.
- Atakan, K., Bard, P.-Y., Kind, F., Moreno, B., Roquette, P. and Tiento, A. & the SESAME-team, 2004b. J-SESAME: a standardized software solution for the H/V spectral ratio technique, *Proceedings of the 13th World Conference on Earthquake Engineering, Vancouver, Canada, 1-6 August, 2004*, paper no. 2270.
- Bakir, B.S., Sucuoglu, H. & Yilmaz, T., 2002. An overview of local site effects and the associated building damage in Adapazari during the 17 August 1999 Izmit earthquake, *Bull. Seismol. Soc. Am.*, 92, 509-526.
- Bartak, V. & Zahradnik, J., 1991. PROGRAM SITEF, Seismic response analysis of horizontally layered sites, Charles University, Prague.
- Beyen, K. & Erdik, M., 2004. Two-dimensional nonlinear site response analysis of Adapazari plain and predictions inferred from aftershocks of the Kocaeli earthquake of 17 August 1999, *Soil Dynamics and Earthquake Engineering*, 24, 261-279.
- Birgören, G., Özel, O., Fahjan, Y. & Erdik, M., 2004. Determination of site effects in Istanbul area using a small earthquake record of the dense strong motion network, *XXIX General Assembly of the European Seismological Commission, Potsdam, Germany*, poster no. 249.
- Bonnefoy-Claudet, S., Cornou, C., Kristek, J., Ohrnberger, M., Wathelet, M., Bard, P.-Y., Moczo, P., Faeh, D. & Cotton, F., 2004. Simulation of seismic ambient noise: I. Results of H/V and array techniques on canonical models, *Proceedings of the 13th World Conference on Earthquake Engineering, Vancouver, Canada, 1-6 August, 2004*, paper no. 1120.
- Boore, D. M., 1983. Stochastic simulation of high frequency ground motions based on seismological models of the radiated spectra, *Bull. Seism. Soc. Am.*, 73, 1865-1894.
- Bouchon, M., 1981. A simple method to calculate Green's functions for elastic layered media, *Bull. Seism. Soc. Am.*, 71, 959-971.
- Cerjan C., Kosloff R. and Reshef M., 1985. A nonreflecting boundary condition for discrete acoustic and elastic wave equations, *Geophysics*, 50, 705-708.
- Chatelain, J.-L., Guillier, B., Duval, A.-M., Cultrera, G., Cara, F., Teves-Costa, P., Atakan, K., & Bard, P.-Y., in prep. Evaluation of the influence of experimental conditions on H/V results from ambient noise recordings. To be submitted to *Bulletin of Earthquake Engineering*.
- Duval, A.-M., Bard, P.-Y., Méneroud, J.-P. & Vidal, S., 1994. Usefulness of microtremor measurements for site effect studies, *proceedings of the 10th European Conference on Earthquake Engineering, Vienna, Austria*.
- Duval, A.-M., Bard, P.-Y., Méneroud, J.-P. & Vidal, S., 1995. Mapping of site effects with microtremors, *proceedings of the Fifth International Conference on Seismic Zonation, Nice, October 1995*.
- Emerman S.H. & Stephen R.A., 1983. Comment on Absorbing Boundary Conditions for Acoustic and Elastic wave Equations, by R. Clayton and B. Enquist, *Bull. seismol. Soc. Am.*, 73, 661-665.

- Erdik, M., Aydinoglu, N., Fahjan, Y., Sesetyan, K., Demircioglu, M., Siyahi, B., Durukal, E., Ozbey, C., Biro, Y., Akman, H. & Yuzugullu, O., 2003. Earthquake risk assessment for Istanbul metropolitan area, *Earthquake Engineering and Engineering Vibration*, Vol. 2, No. 1, 1-25.
- Erdik, M., Demircioglu, M., Sesetyan, K., Durukal, E. & Siyahi, B., 2004. Earthquake hazard in Marmar region, Turkey, *proceedings of the 11th SDEE/ 3rd ICEGE, California, USA*.
- Eyidogan, H., Ecevitoglu, B. & Caglar, I., 2000 (in Turkish). Bakirköy İlcesi 1. etap (Bakirköy-Ataköy) yerlesim alanlarinin jeolojik yapı ve deprensellik etüdü projesi, *Internal report*, part 6, TC. Bakirköy Belediyesi – ITÜ Gelistirme Vakfi. 55 p.
- Fäh, D., Rüttener, E., Noack, T. & Kruspan, P., 1997. Microzonation of the city of Basel, *Journal of Seismology*, 1, 87-102.
- Field, E.H. & Jacob, K., 1993. The theoretical response of sedimentary layers to ambient seismic noise, *Geophysical research letters*, 20(24), 2925-2928, 10.1029/93GL03054.
- Field, E.H., Clement, A.C., Jacob, K.H., Ahronian, V., Hough, S.E., Friberg, P.A., Babaian, T.O., Karapetian, S.S., Hovanessian, S.M. & Abramian, H.A., 1995. Earthquake site-response study in Giumri (formerly Leninakan), Armenia, using ambient noise observations, *Bull. seismol. Soc. Am.*, 85, 349-353.
- Gitterman, Y., Zaslavsky, Y., Shapira, A. & Shtivelman, V., 1996. Emperical site response evaluations: case studies in Israel, *Soil Dynamics and Earthquake Engineering*, 15, 447-463.
- Guillier, B., Atakan, K., Chatelain, J-L., Havskov, J., Duval, A-M., Ohrnberger, M., Cara, F., & Zacharapoulous, S., in prep. Influence of instruments on the H/V spectral ratios of ambient vibrations. To be submitted to *Bulletin of Earthquake Engineering*.
- Hisada, Y., 1994. An efficient method for computing Green's functions for a layered half-space with sources and receivers at close depths, *Bull. seismol. Soc. Am.*, 84, 1456-72.
- Irikura, K., 1986. Prediction of strong acceleration motion using empirical Green's function, *Proceedings of the 7th Japan. Earthq. Eng. Symp.*, 151-156
- Komazawa, M., Morikawa, H., Nakamura, K., Akamatsu, J., Nishimura, K., Sawada, S., Erken, A. & Onalp, A., 2002. Bedrock structure in Adapazari, Turkey – a possible cause of severe damage by the 1999 Kociaeli earthquake, *Soil Dynamics and Earthquake Engineering*, 22, 829-836.
- Kudo, K., 1995. Practical estimates of site response, State-of-the-art report, *proceedings of the Fifth International Conference on Seismic Zonation, Nice, October 1995*.
- Lachet, C., & P.-Y. Bard, 1994. Numerical and theoretical investigations on the possibilities and limitations of the "Nakamura's" technique, *Journal of Physics of the Earth*, 42-4, 377-397.
- Lachet, C., Hatzfeld, D., Bard, P.-Y., Theodulidis, N., Papaioannou, C. & Savvaidis, A., 1996. Site effects and microzonation in the city of Thessaloniki (Greece): comparison of different approaches, *Bull. seismol. Soc. Am.*, 86, 1692-1703.
- Lebrun, B., Bard, P.-Y. & Hatzfeld, D., 1997. Evidence for large, low frequency site effects in large alpine valleys: the example of Grenoble, France, *29th general assembly of IASPEI, Workshop W16, Thessaloniki, Greece*.
- Lermo, J. & Chávez-García, F.J., 1993. Site effect evaluation using spectral ratios with only one station. *Bull. seismol. Soc. Am.*, 83, 1574-1594.
- Lermo, J. & Chávez-García, F.J., 1994. Are microtremors useful in site response evaluation?, *Bull. seismol. Soc. Am.*, 84, 1350-1364.
- Mucciarelli, M., 1998. Reliability and applicability of Nakamura's technique using microtremors: An experimental approach, *J. Earthquake Eng.*, 2, 1-14.
- Mucciarelli, M., Gallipoli, M.R. & Arcieri, M., 2003. The stability of Horizontal-to-Vertical Spectral Ratio of triggered noise and earthquake recordings, *Bull. Seismol. Soc. Am.*, 93, 1407-1412.
- Mueller, G., 1985. The reflectivity method: a tutorial. *J. Geophys.*, 58, 153-174.
- Nakamura, Y., 1989. A method for dynamic characteristics estimation of subsurface using microtremors on the ground surface. *Q. Rep. Railway Tech. Res. Inst.*, 30, 1.
- Nakamura, Y., 2000. Clear identification of fundamental idea of Nakamura's technique and its applications, *proceedings of the 12th WCEE, New Zealand*, paper no. 2656.
- Ojeda, J. Å., Natvik, Ø., Berland, O. & Fjeldstad, F., 2004. SEISLOG CE (SEISLOG for Pocket PC), *29th general assembly of the European Seismological Commission, Potsdam, Germany 12-17 September 2004*, poster no. 77.

- Oprsal, I., Brokesova, J., Faeh, D., & Giardini, D., 2002. 3D Hybrid Ray-FD and DWN-FD Seismic Modeling For Simple Models Containing Complex Local Structures, *Stud. Geophys. Geod.*, 46, 711-730.
- Oprsal, I. & Zahradnik, J., 2002. Three-dimensional finite difference method and hybrid modeling of earthquake ground motion, *J. Geophys. Res.*, 107(B8), DOI 10.1029/2000JB000082.
- Oprsal, I., Faeh, D., Mai, M. & Giardini, D., 2005. Deterministic earthquake scenario for the Basel area - Simulating strong motion and site effects for Basel, Switzerland, *J. Geophys. Res.*, 110, doi:10.1029/2004JB003188.
- Özel, O., Cranswick, E., Meremonte, M., Erdik, M. & Safak, E., 2002. Site effects in Avcilar, west of Istanbul, Turkey, from strong- and weak-motion data, *Bull. Seismol. Soc. Am.*, 92, 499-508.
- Pulido, N. & Kubo, T., 2004. Near-fault strong motion complexity of the 2000 Tottori earthquake (Japan) from a broadband source asperity model, *Tectonophysics*, 390, 177-192.
- Pulido, N., Ojeda, A., Atakan, K. & Kubo, T., 2004. Strong ground motion estimation in the Marmara Sea region (Turkey) based on a scenario earthquake. *Tectonophysics*, 391, 357-374.
- Riepl, J., Bard, P.-Y., Hatzfeld, D., Papaioannou, C. & Nechtschein, S., 1998. Detailed evaluation of site response estimation methods across and along the sedimentary valley of Volvi (EURO-SEISTEST), *Bull. Seismol. Soc. Am.*, 88, 488-502.
- Sancio, R.B., Bray, J.D., Steward, J.P., Youd, T.L., Durgunoglu, H.T., Önalp, A., Seed, R.B., Christensen, C., Baturay, M.B. & Karasayilar, T., 2002. Correlation between ground failure and soil conditions in Adapazari, Turkey, *Soil Dynamics and Earthquake Engineering*, 22, 1093-1102.
- Schnabel, P.B., Lysmer, J. & Seed, H.B., 1972. SHAKE: a computer program for earthquake response analysis of horizontally layered sites, *Report EERC 72-12*, Earthquake Engineering Research Center, University of California, Berkeley.
- Schön, J. H., 1996. *Physical properties of rocks – Fundamentals and Principles of petrophysics*, Pergamon, 1996.
- Tezcan, S.S., Kaya, E., Bal, I.E. & Özdemir, Z., 2002. Seismic amplification at Avcilar, Istanbul, *Engineering Structures*, 24, 661-667.

Figure captions

Figure 1. a) Geological map of Istanbul. Redrawn from Oktay & Eren (Istanbul Metropolitan Municipality, Site Survey and Earthquake Department) b) Peak ground velocities (PGV) predicted by Pulido et al. (2004) for a $M=7.5$ scenario earthquake in the Marmara Sea. The star indicated the rupture initiation point, the thick white lines the extent of the rupturing fault and the blue lines the asperity locations.

Figure 2. Geological map of Ataköy and Bakirköy districts, western Istanbul. Ataköy is located between the two alluvial systems in the westernmost part of the map. Colours represent different geological formations. Numbered dots represent the microtremor recording sites used for calculating H/V spectral ratios. The map is provided by Istanbul Technical University.

Figure 3. Schematic illustration of the hybrid procedure used for modelling spectral amplification for a dense grid in Ataköy. a) In the first step, ground motions are calculated on the excitation box using a regional 1D velocity model. Dark grey fields within the fault plane are asperities. b) In the second step, surface ground motions are calculated using a 3D finite difference scheme and a local velocity model. Figure 3b corresponds to the stippled box in 3a.

Figure 4. Surface geometry of geological model of Ataköy, used in 3D FD model. The black square in the uppermost map shows the extent and location of the lowermost map. Symbols indicate borehole locations for SPT and CPT data and microtremor recording sites used by Istanbul Technical University (ITU, Eyidogan et al. 2000) and University of Bergen (UiB, this study). The four horizontal lines show the locations of the profiles in Figure 5.

Figure 5. EW cross-sections of geological model of the Ataköy area, used in the 3D FD model. The lowermost plot is in the southernmost part of the model, going northwards. Note the thinning of the Bakirköy formation towards north in most of the model due to erosion.

Figure 6. Elevation plots of top of the layers of the geological model of Ataköy, used in the 3D FD model.

Figure 7. a) Spectral amplification (pseudo-acceleration response PSA, damping 5%) with respect to a bedrock site for 3D FD modelling. The results are shown for a set of frequency bands; the left and right sides of the panel correspond to the maximum and mean PSA amplification. The amplified response of the southern part and of the two alluvial systems is apparent.

b) Spectral amplification (pseudo-acceleration response PSA, damping 5%) with respect to a bedrock site for the pseudo 3D (1D) modelling. The results are shown for a set of frequency bands; the left and right sides of the panel correspond to the maximum and mean PSA amplification. The amplified response of the southern part and of the two alluvial systems is apparent.

The geographical extent of the results shown corresponds to the same area as indicated in Figure 6.

Figure 8. Average H/V spectral ratios for sites located on alluvium.

Figure 9. Average H/V spectral ratios for sites located at Bakirköy formation.

Figure 10. 1D models used for simulating ambient noise. a) Alluvial site: 5 m alluvial layer, 8 m Bakirköy formation, 80 m Güngören formation and bedrock (half space). b) Bakirköy formation site: 11 m Bakirköy formation, 80 m Güngören formation and bedrock (half space). c) Güngören formation site: 77 m Güngören formation and bedrock (half space). Velocities of the different layers are given in Table 4.2.

Figure 11. H/V spectral ratios calculated for simulated ambient noise at 1D sites. a) Alluvial site, b) Bakirköy formation site, c) Güngören formation site.

Tables

Table 1. Formulae used for quantification of the velocities for the 3D model used for 3D FD modelling. V_s is S-wave velocity, V_p is P-wave velocity and ρ is density. $Z' = Z - Z_{\text{free surface}}$ is the depth relative to the free surface.

| Formation | V_s (m/s) | V_p/V_s | ρ (km/m ³) |
|-----------|--|-----------|---|
| Alluvium | $150 + 5 \cdot Z'$ | 1.732 | $1.7 - 1.224 \cdot \exp(-0.846 \cdot Z')$ |
| Bakirköy | $260 + 96 \cdot Z'$ for $Z' < 5$ m $685 + 11 \cdot Z'$ for $Z' > 5$ m | 1.8 | $2.2 - 1.224 \cdot \exp(-0.846 \cdot Z')$ |
| Güngören | $200 + 60 \cdot Z'$ for $Z' < 5$ m $445 + 11 \cdot Z'$ for $Z' > 5$ m | 1.8 | $2.0 - 1.224 \cdot \exp(-0.846 \cdot Z')$ |
| Bedrock | $450 + 11 \cdot Z'$ | 1.8 | $2.3 - 1.224 \cdot \exp(-0.846 \cdot Z')$ |

Table 2. Velocity model used for 1D modelling for alluvium, Bakirköy formation and Güngören formation sites. The sites are taken from the model used for 3D FD modelling, and average velocities are reported for each layer.

| Thickness (m) | V_s (m/s) | V_p (m/s) | Density (kg/m ³) | Formation |
|-------------------------|-------------|-------------|------------------------------|-----------|
| Alluvial site | | | | |
| 5 | 163 | 260 | 1.169 | Alluvium |
| 8 | 784 | 1406 | 2.691 | Bakirköy |
| 80 | 1028 | 1850 | 2.500 | Güngören |
| Half space | 1473 | 2799 | 2.700 | Bedrock |
| Bakirköy formation site | | | | |
| 11 | 533 | 960 | 2.078 | Bakirköy |
| 80 | 1006 | 1811 | 2.500 | Güngören |
| Half space | 1451 | 2757 | 2.700 | Bedrock |
| Güngören formation site | | | | |
| 77 | 748 | 1346 | 1.878 | Güngören |
| Half space | 1297 | 2464 | 2.700 | Bedrock |

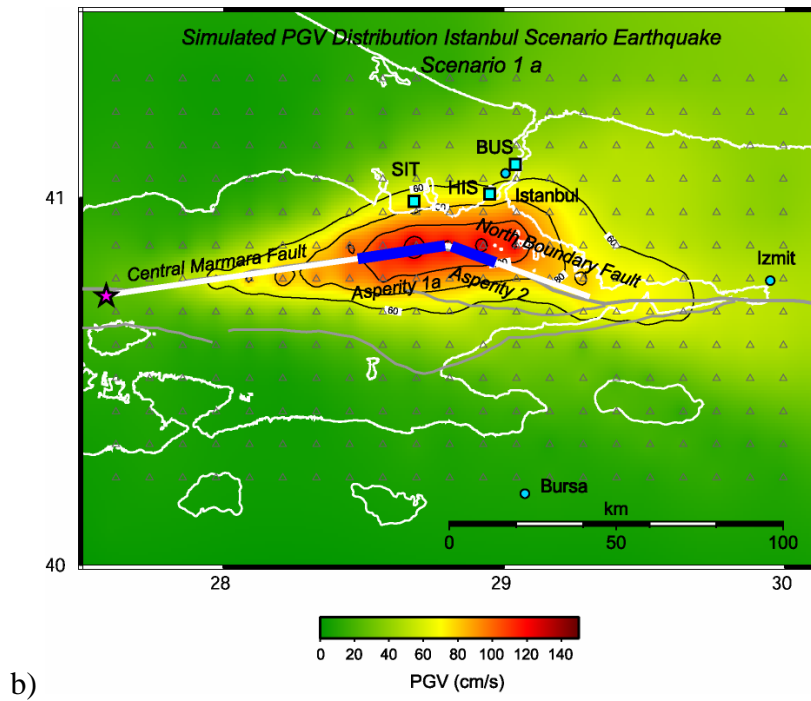
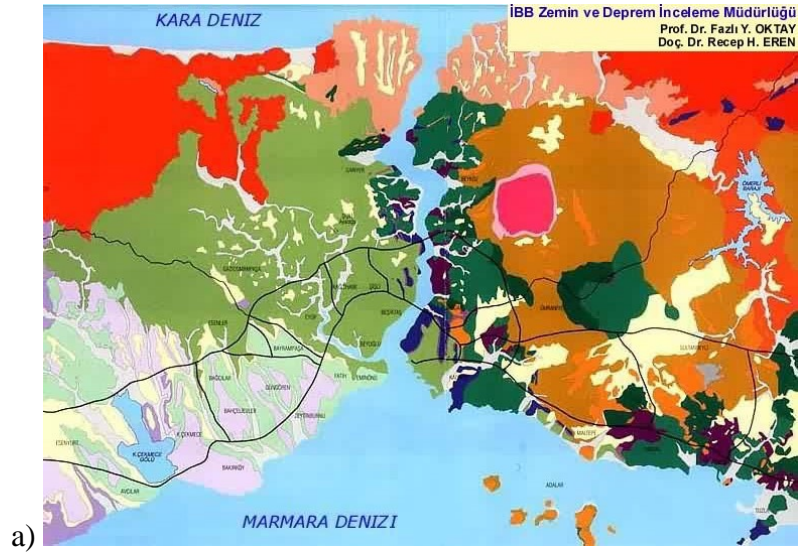


Figure 1

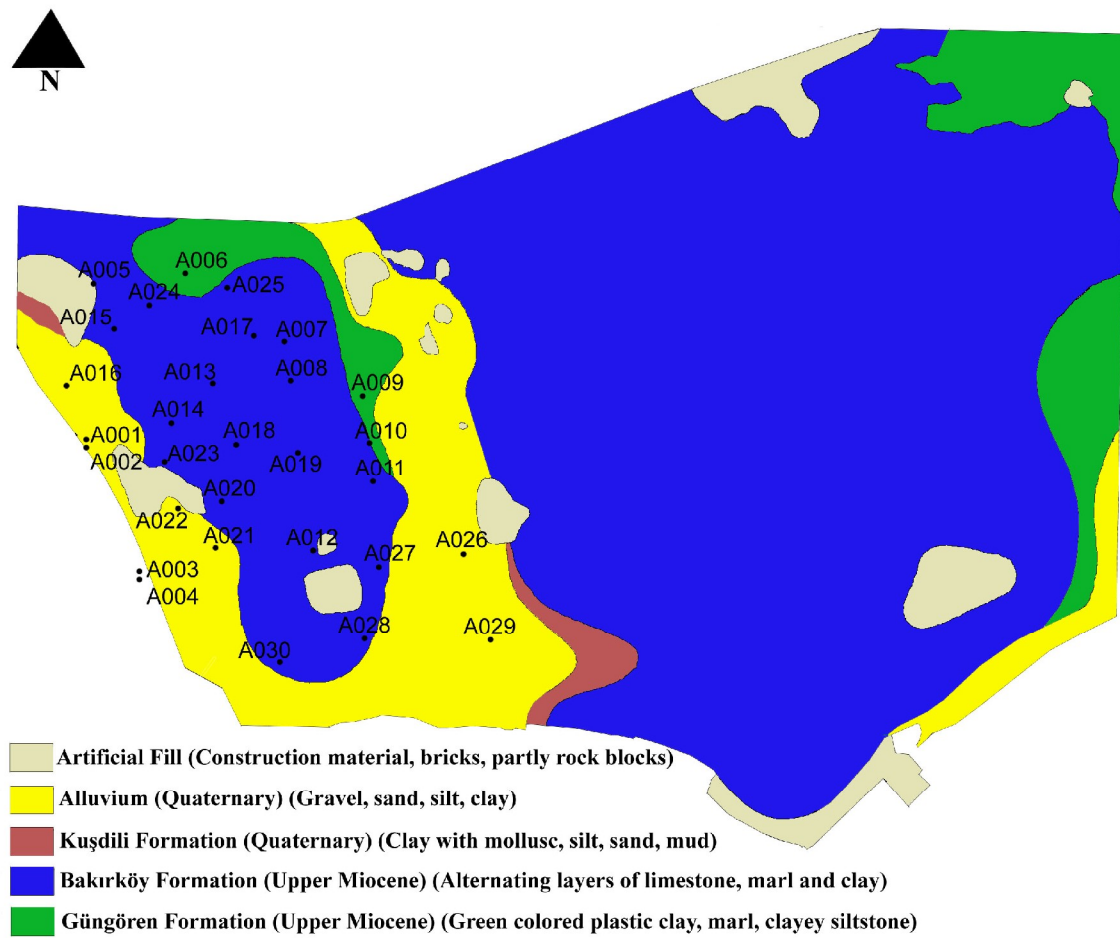


Figure 2.

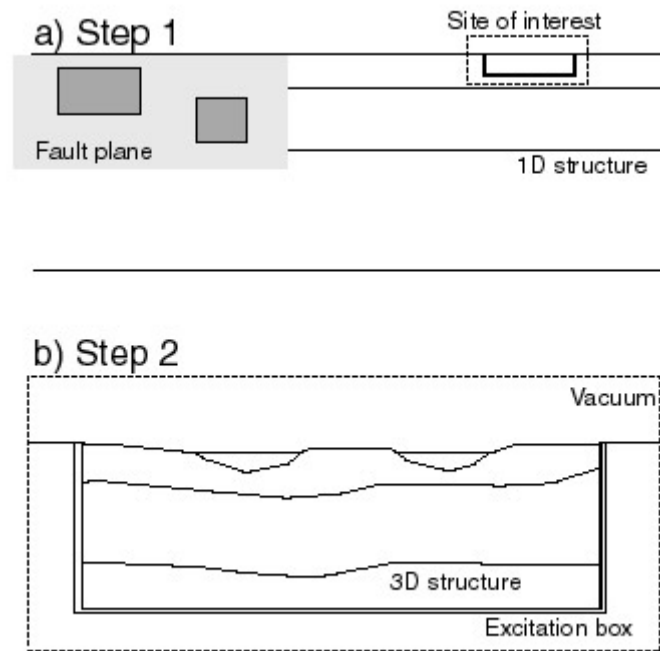


Figure 3.

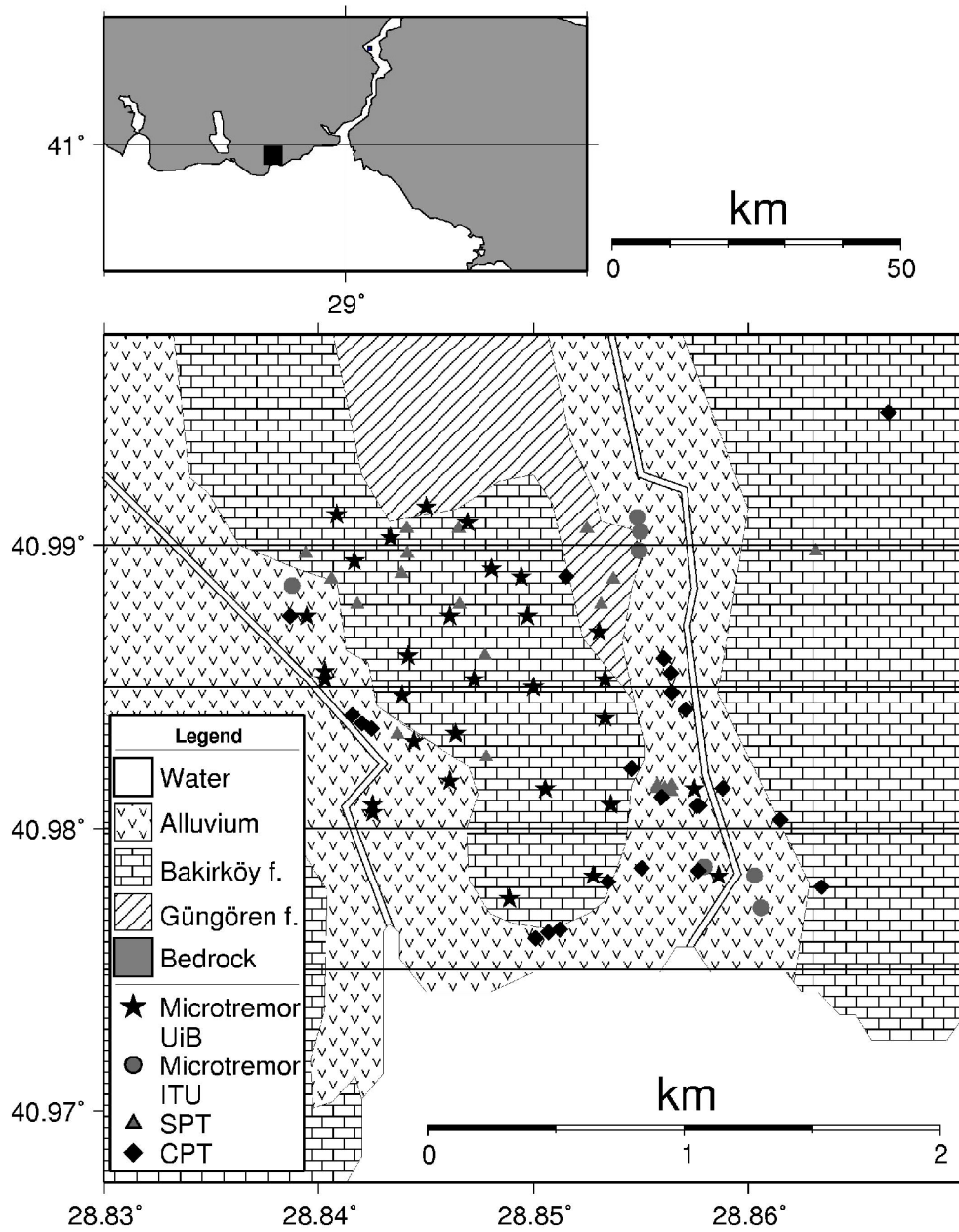


Figure 4.

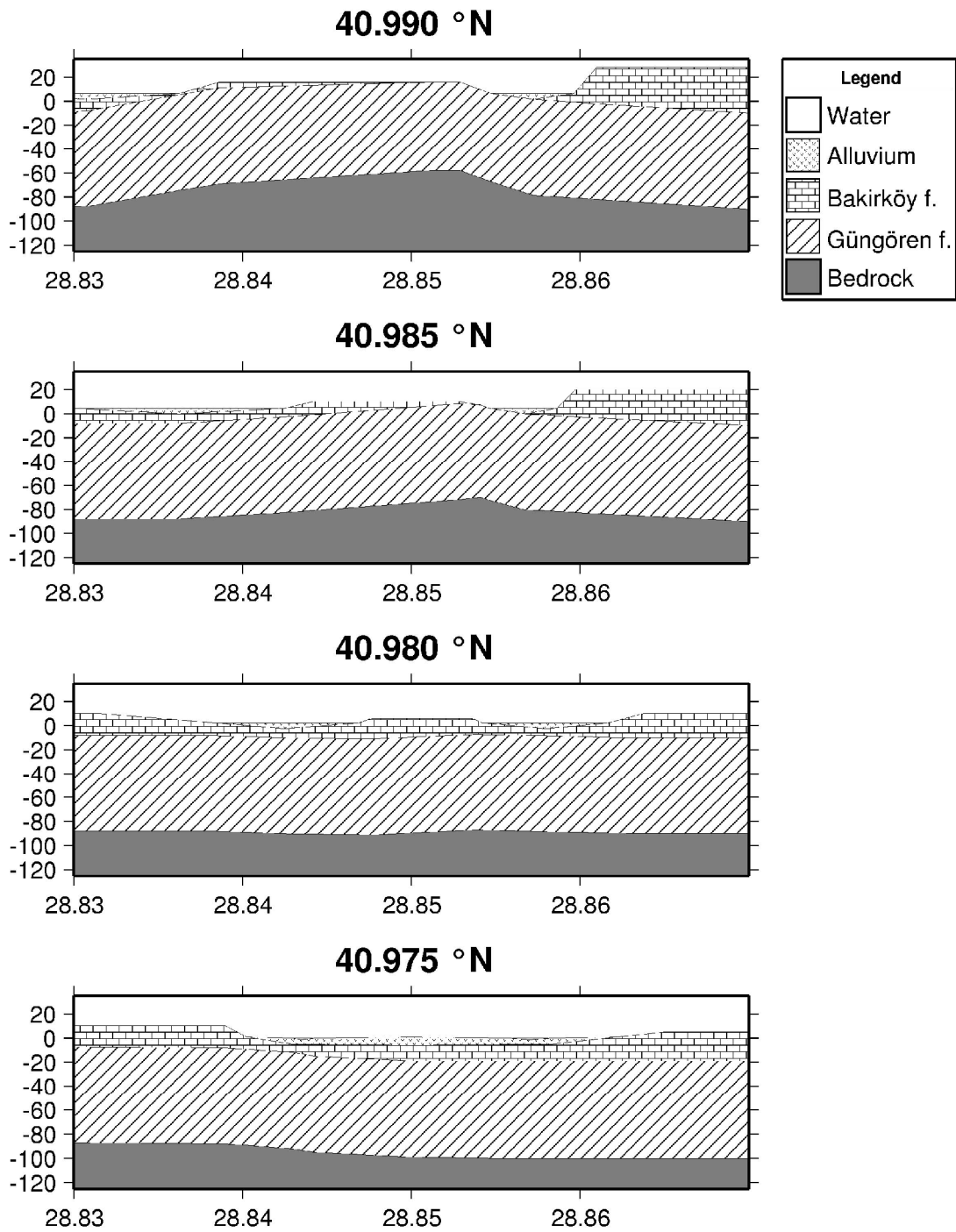


Figure 5.

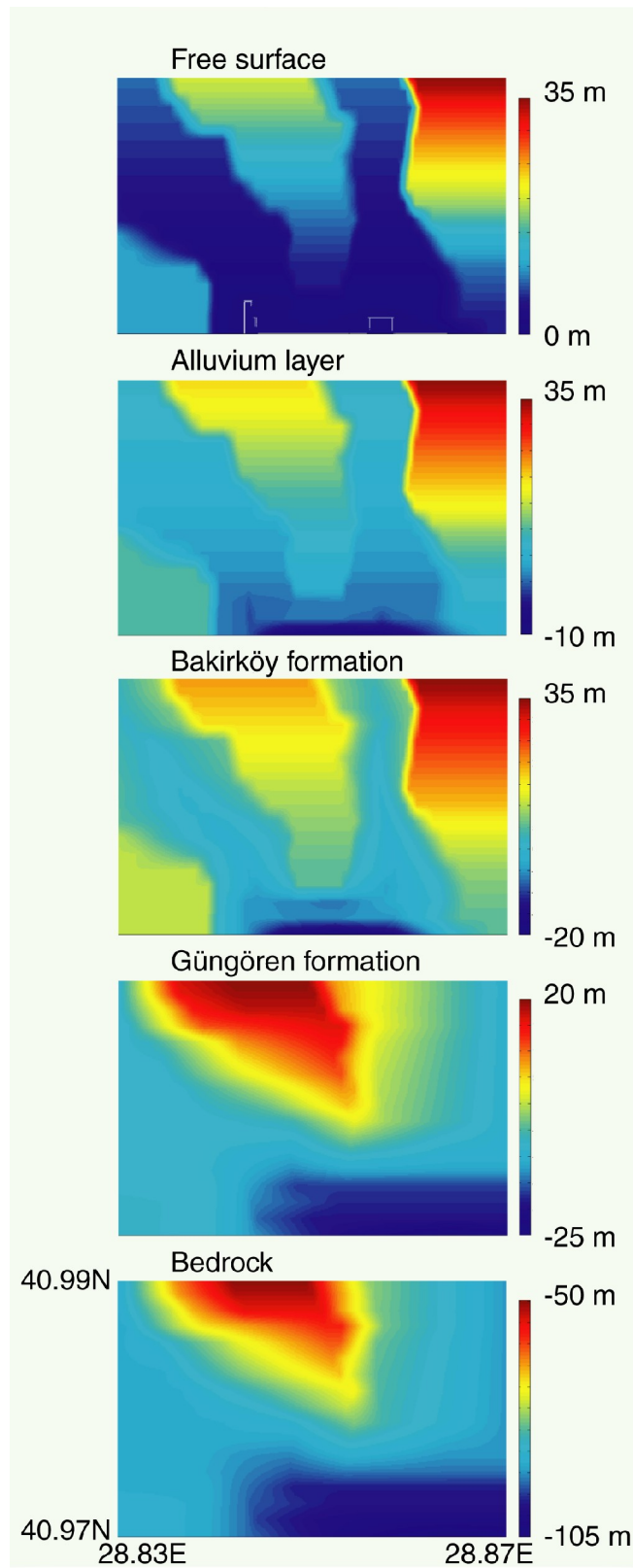


Figure 6

Spectral-acceleration amplification in Istanbul area

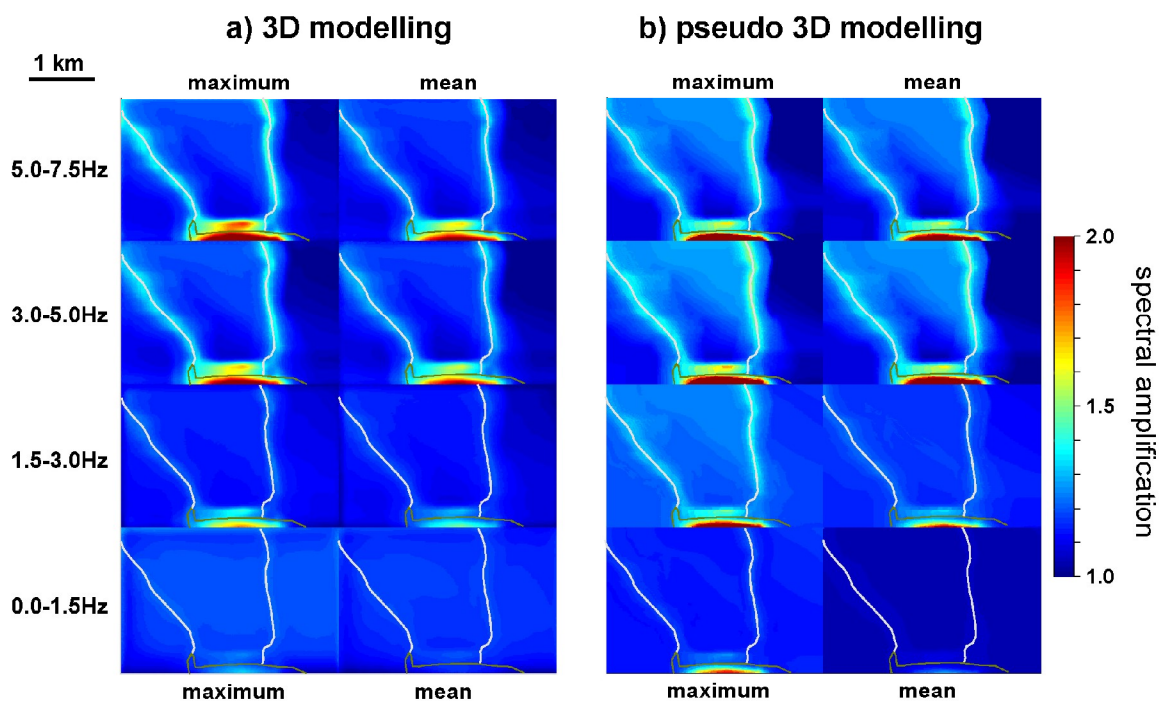


Figure 7

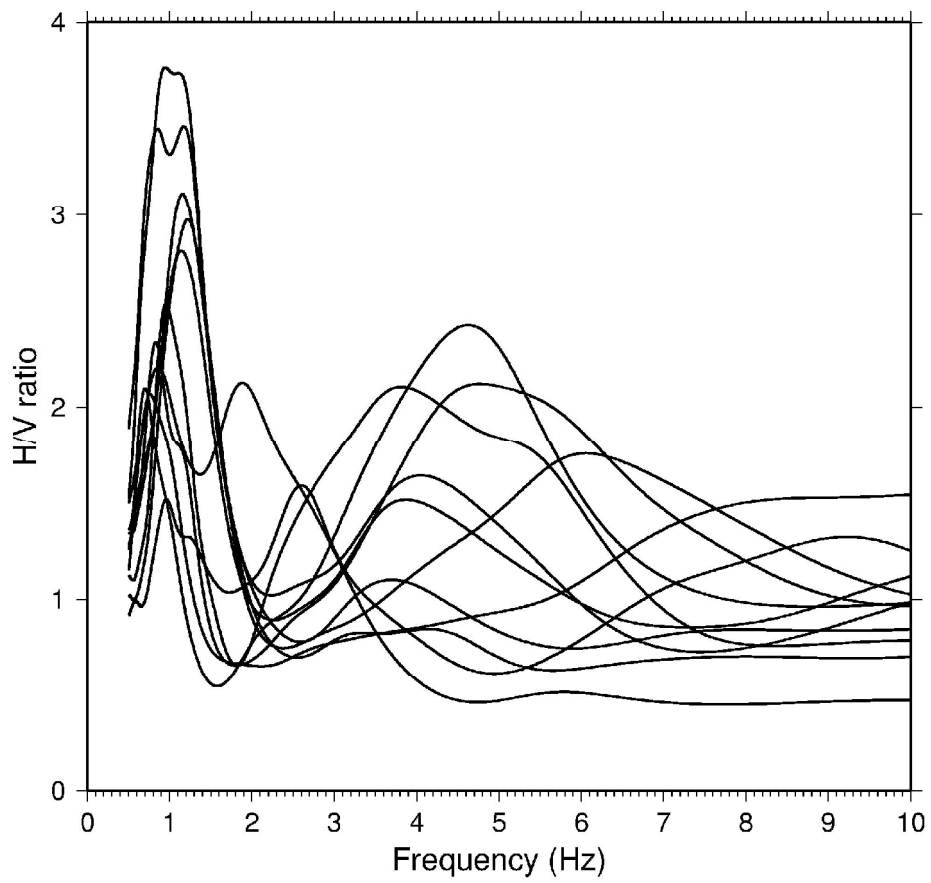


Figure 8.

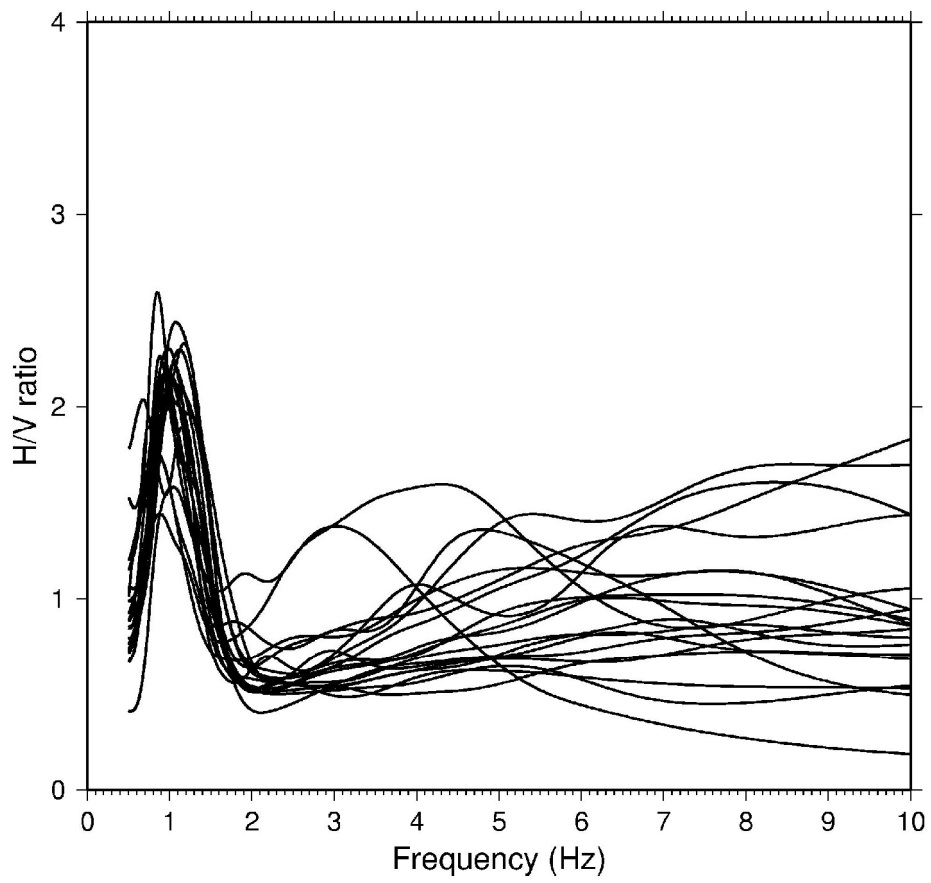


Figure 9.

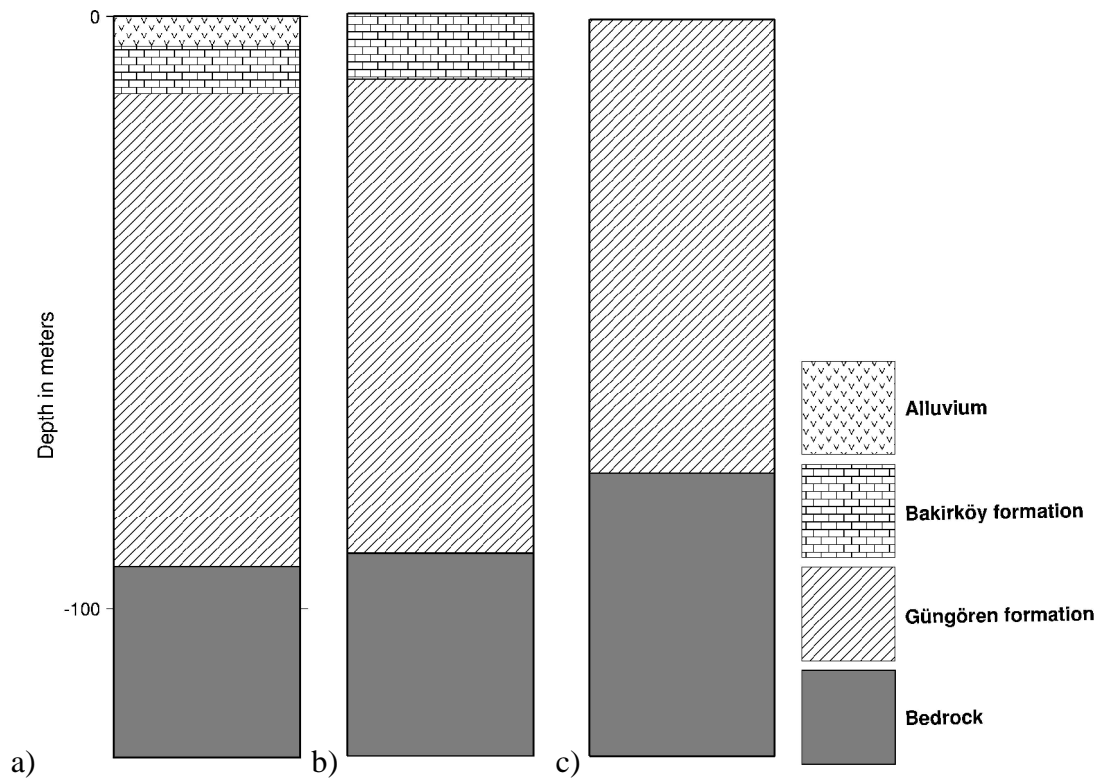


Figure 10.

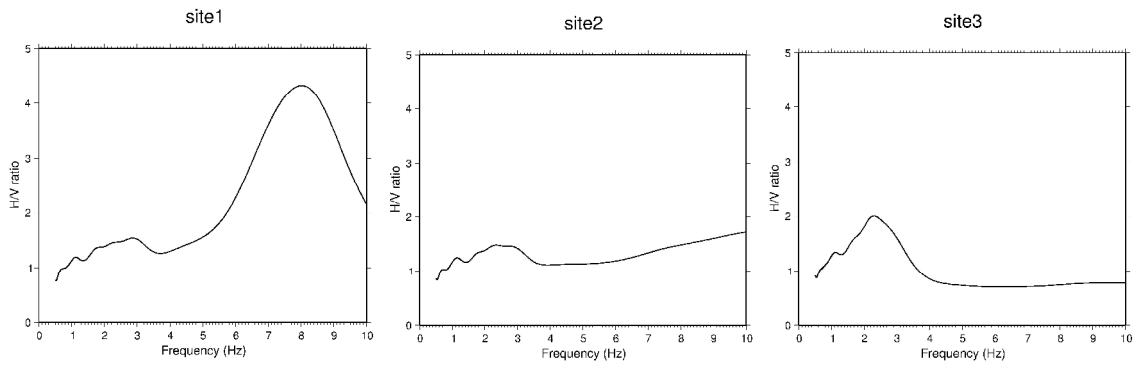


Figure 11.

This document was created with Win2PDF available at <http://www.daneprairie.com>.
The unregistered version of Win2PDF is for evaluation or non-commercial use only.